U.S. Department
of Transportation

**Federal Highway
Administration**

Publication No. FHWA-RD-03-083
June 2003

BRIDGE SCOUR IN NONUNIFORM SEDIMENT MIXTURES AND IN COHESIVE MATERIALS: SYNTHESIS REPORT

.

Federal Highway Administration
Office of Infrastructure Research and Development
Turner-Fairbank Highway Research Center
6300 Georgetown Pike
McLean, Virginia 22101

FOREWORD

This report is a summary of a six-volume series describing detailed laboratory experiments conducted at Colorado State University for the Federal Highway Administration as part of a study entitled "Effects of Sediment Gradation and Cohesion on Bridge Scour." This report will be of interest to hydraulic engineers and bridge engineers involved in bridge scour evaluations. It will be of special interest to other researchers conducting studies of the very complex problem of estimating scour in cohesive bed materials and to those involved in preparing guidelines for bridge scour evaluations. The six-volume series has been distributed to National Technical Information Service (NTIS) and to the National Transportation Library, but it will not be printed by FHWA. This summary report, which describes the key results from the six-volume series, will be published by FHWA.

T. Paul Teng, P.E.
Director, Office of Infrastructure
Research and Development

NOTICE

Technical Report Documentation Page

1. Report No.	2. Government Accession No.	3. Recipient's Catalog No.
FHWA-RD-03-083		

4. Title and Subtitle	5. Report Date
BRIDGE SCOUR IN NONUNIFORM SEDIMENT MIXTURES AND IN COHESIVE MATERIALS: SYNTHESIS REPORT	June 2003
	6. Performing Organization Code
7. Author(s) Albert Molinas	8. Performing Organization Report No.

9. Performance Organization Name and Address	10. Work Unit No. (TRAIS)
Colorado State University Engineering Research Center Fort Collins, CO	NCP# 3D3C1-582
	11. Contract or Grant No. DTFH61-91-C-00004
12. Sponsoring Agency and Address	13. Type of Report and Period Covered
Office of Infrastructure Research and Development Federal Highway Administration 6300 Georgetown Pike McLean, VA 22101	Laboratory Final Report Jan 1991 - Jan 1996
	14. Sponsoring Agency Code

15. Supplementary Notes

Contracting Officer's Technical Representative: J. Sterling Jones HRDI-07

16. Abstract

This report presents the summary and synthesis of the various components of the experimental study entitled "Effects of Gradation and Cohesion on Bridge Scour" conducted at Colorado State University between the dates 1991 through 1996.

As a result of this effort, in excess of 250 new pier scour data was collected and a new equation was developed expressing pier scour in terms of the dimensionless excess velocity factor, flow depth, pier diameter and a correction factor for the coarse fractions present in mixtures was derived. The new method was tested with available data from previous research. This equation shows that gradation effects are not constant through the entire range of flow conditions but vary with flow intensity. Additionally, a new method to adjust FHWA's Colorado State University pier scour equation for initiation of motion and sediment size was developed.

Abutment scour experiments resulted in over 384 new points and 2 new abutment scour equations. The first equation was derived from a 0.1 mm uniform sand mixture and defines an envelop relationship. The second equation applies to mixtures with coarse fractions. A coarse size fraction compensation factor W_g is presented to account for the presence of varying amounts of coarse material in sediment mixtures under different dimensionless flow intensities. These new equations represented the experimental data accurately but have not been tested with field data.

Effects of cohesion on pier and abutment scour was studied systematically, and in excess of 200 new data points were collected covering a range of flow and cohesive parameter values. Relationships were developed to explain the variability of bridge scour in cohesive materials for various cohesive material properties.

This report summarizes results from the following six-volume series, which was not printed but was distributed to the National Technical Information Service and the National Transportation Library:

FHWA-RD-99-183 Volume 1. Effect of Sediment Gradation and Coarse Material Fraction on Clear-Water Scour Around Bridge Piers.

FHWA-RD-99-184 Volume 2. Experimental Study of Sediment Gradation and Flow Hydrograph Effects on Clear Water Scour Around Circular Piers.

FHWA-RD-99-185 Volume 3. Abutment Scour for Nonuniform Mixtures.

FHWA-RD-99-186 Volume 4. Experimental Study of Scour Around Circular Piers in Cohesive Soils.

FHWA-RD-99-187 Volume 5. Effect of Cohesion on Bridge Abutment Scour.

FHWA-RD-99-188 Volume 6. Abutment Scour in Uniform and Stratified Sand Mixtures.

17. Key Words:	18. Distribution Statement
Bridge scour, Pier scour, Abutment scour, Local scour, Sand Mixtures, Gravel scour, Gradation, Cohesion, Clay, Montmorillonite, Kaolinite, Clear-water, Experimental study	No restrictions. This document is available to the public through the National Technical Information Service, Springfield, VA 22161

19. Security Classif. (of this report)	20. Security Classif. (of this page)	21. No. of Pages	22. Price
Unclassified	Unclassified	121	

Form DOT F 1700.7 (8-72) **Reproduction of completed page authorized**

SI* (MODERN METRIC) CONVERSION FACTORS

APPROXIMATE CONVERSIONS TO SI UNITS

Symbol	When You Know	Multiply By	To Find	Symbol
		LENGTH		
in	inches	25.4	millimeters	mm
ft	feet	0.305	meters	m
yd	yards	0.914	meters	m
mi	miles	1.61	kilometers	km
		AREA		
in^2	square inches	645.2	square millimeters	mm^2
ft^2	square feet	0.093	square meters	m^2
yd^2	square yard	0.836	square meters	m^2
ac	acres	0.405	hectares	ha
mi^2	square miles	2.59	square kilometers	km^2
		VOLUME		
fl oz	fluid ounces	29.57	milliliters	mL
gal	gallons	3.785	liters	L
ft^3	cubic feet	0.028	cubic meters	m^3
yd^3	cubic yards	0.765	cubic meters	m^3
		NOTE: volumes greater than 1000 L shall be shown in m^3		
		MASS		
oz	ounces	28.35	grams	g
lb	pounds	0.454	kilograms	kg
T	short tons (2000 lb)	0.907	megagrams (or "metric ton")	Mg (or "t")
		TEMPERATURE (exact degrees)		
^oF	Fahrenheit	5 (F-32)/9 or (F-32)/1.8	Celsius	^oC
		ILLUMINATION		
fc	foot-candles	10.76	lux	lx
fl	foot-Lamberts	3.426	$candela/m^2$	cd/m^2
		FORCE and PRESSURE or STRESS		
lbf	poundforce	4.45	newtons	N
lbf/in^2	poundforce per square inch	6.89	kilopascals	kPa

APPROXIMATE CONVERSIONS FROM SI UNITS

Symbol	When You Know	Multiply By	To Find	Symbol
		LENGTH		
mm	millimeters	0.039	inches	in
m	meters	3.28	feet	ft
m	meters	1.09	yards	yd
km	kilometers	0.621	miles	mi
		AREA		
mm^2	square millimeters	0.0016	square inches	in^2
m^2	square meters	10.764	square feet	ft^2
m^2	square meters	1.195	square yards	yd^2
ha	hectares	2.47	acres	ac
km^2	square kilometers	0.386	square miles	mi^2
		VOLUME		
mL	milliliters	0.034	fluid ounces	fl oz
L	liters	0.264	gallons	gal
m^3	cubic meters	35.314	cubic feet	ft^3
m^3	cubic meters	1.307	cubic yards	yd^3
		MASS		
g	grams	0.035	ounces	oz
kg	kilograms	2.202	pounds	lb
Mg (or "t")	megagrams (or "metric ton")	1.103	short tons (2000 lb)	T
		TEMPERATURE (exact degrees)		
^oC	Celsius	1.8C+32	Fahrenheit	^oF
		ILLUMINATION		
lx	lux	0.0929	foot-candles	fc
cd/m^2	$candela/m^2$	0.2919	foot-Lamberts	fl
		FORCE and PRESSURE or STRESS		
N	newtons	0.225	poundforce	lbf
kPa	kilopascals	0.145	poundforce per square inch	lbf/in^2

*SI is the symbol for the International System of Units. Appropriate rounding should be made to comply with Section 4 of ASTM E380.
(Revised March 2003)

BRIDGE SCOUR IN NONUNIFORM SEDIMENT MIXTURES AND COHESIVE MATERIALS: SYNTHESIS REPORT

TABLE OF CONTENTS

1. INTRODUCTION 1

2. EFFECTS OF GRADATION AND COARSE MATERIAL FRACTION ON PIER SCOUR 5

2.1 General 5
2.2 Experimental Setup and Measurements 5
2.3 Experimental Results 14
2.4 Analysis 24
2.5 Adjustment to FHWA's CSU Equation 29
2.6 Summary and Conclusions 31

3. EFFECTS OF GRADATION AND COARSE MATERIAL FRACTION ON ABUTMENT SCOUR 47

3.1 General 47
3.2 Experimental Setup and Measurements 48
3.3 Experimental Results 54
3.4 Analysis 75
3.5 Conclusions 80

4. BRIDGE SCOUR IN CLAYEY SANDS 81

4.1 General 81
4.2 Experimental Setup and Measurements 82
4.3 Experimental Results 83
4.4 Analysis 86
4.5 Conclusions 88

5. PIER SCOUR IN MONTMORILLONITE CLAY SOILS 89

5.1 General 89
5.2 Experimental Setup and Measurements 90
5.3 Experimental Results 91
5.4 Analysis 96
5.5 Conclusions 99

6. EFFECTS OF COHESION ON ABUTMENT SCOUR 101

6.1 General 101
6.2 Experimental Setup and Measurements 102

6.3 Experimental Results 103
6.4 Analysis.....108
6.5 Conclusions.....110

REFERENCES.....111

LIST OF FIGURES

Figure		Page
1	Variation of scour depth with velocity for sand mixtures used in sets 1 through 3	33
2	Comparison of FHWA's CSU equation with measured scour from sets 1 through 3	33
3	Velocity versus discrepancy ratio for set 1 through 3 experiments.	34
4	Flow velocity versus dimensionless scour for set 4 through 7 experiments	34
5	Dimensionless excess velocity factor, ψ, versus depth of scour for sets 1 through 3	35
6	Variation of dimensionless scour with excess velocity factor for various mixtures	35
7	Variation of dimensionless scour with excess velocity factor, ψ, for different coarse fraction sizes used in sets 4 through 7	36
8	Variation of dimensionless scour with excess velocity factor, ψ, for different coarse fraction sizes used in sets 8 and 9	36
9	Variation of scour depth with excess velocity factor, ψ, for different coarse fraction size ratios used in sets 4 through 7 experiments	37
10	Variation of measured coarse fraction reduction factor K_4 with excess velocity factor, ψ, for set 1 through 3 experiments	37
11	Variation of scour depth with pier size for the set 8 experiments	38
12	Relationship describing variation of pier scour with pier diameter	38
13	Computed versus measured pier scour depths for set 8 experiments	39
14	Variation of scour depth with excess velocity factor, ψ, for uniform sand and gravel	39
15	Computed versus measured pier scour depths using the uniform-mixture equation	40
16	Measured and computed scour for uniform sediment using FHWA's CSU equation	40
17	Computed scour for sets 1 through 3 experiments using equation 12 with K_4 from equation 14	41
18	Measured and computed scour for nonuniform-sand experiments in sets 1 through 3	41
19	Computed and measured scour for all data using equation 12 (uniform-mixture equation)	42

20 Computed and measured scour for all data using equation 12 with K_4 correction from equation 14 42

21 Computed scour using FHWA's CSU equation for uniform and nonuniform mixtures 43

22 Computed scour by using FHWA's CSU equation with and without K_4 correction from HEC 18, and by using the newly developed equation 12 with K_4 correction from equation 14. 43

23 Comparison of FHWA's CSU equation with K_4 correction (according to HEC 18) and the initiation of motion correction, K_i (according to equation 15) 44

24 FHWA's CSU equation adjusted with K_i and K_4 and with the HEC 18 correction for K_4 44

25 Comparison between computed and measured scour using K_i and K_4 corrections to the FHWA's CSU equation (equation 16) and by using equation 12 with K_4 correction from equation 14 45

26 Variation of dimensionless abutment scour with Froude number: (a) abutment protrusion length, a, as characteristic length; (b) $L_c = (a\ Y)^{0.5}$ as characteristic length. 47

27 Variation of dimensionless abutment scour with deflected flow excess velocity 75

28 Adjustment factors for gradation and coarse material fraction: (a) Gradation reduction factor, K_s; (b) Coarse fraction adjustment, K_{15} 78

29 Measured and computed abutment scour for hydrodynamics flume experiments: (a) For uniform mixtures; (b) All mixtures 79

30 Effect of clay content on abutment scour 81

31 Pier scour reduction factor for Montmorillonite clay mixtures 86

32 Abutment scour reduction factor for Montmorillonite clay mixtures 87

33 Abutment scour reduction factor for Kaolinite mixtures 88

34 Computed and measured dimensionless pier scour depth for unsaturated Montmorillonite clay 98

35 Computed and measured dimensionless pier scour depth for saturated Montmorillonite clay 98

36 Computed and measured relative abutment scour for Montmorillonite clay 109

37 Computed and measured relative abutment scour for Kaolinite clay 110

LIST OF TABLES

Table		Page
1	Properties of sediment mixtures used in pier scour experiments	16
2	Summary of sand-scour experiments in the sedimentation flume for set 1	17
3	Summary of sand-scour experiments in sedimentation flume for set 2	18
4	Summary of sand-scour experiments in sedimentation flume for set 3	19
5	Summary of sand-scour experiments in hydrodynamics flume for sets 4 through 7	20
6	Summary of river mechanics flume experiments to study pier width effects for set 8	22
7	Summary of gravel-scour experiments in sedimentation flume for sets 9 and 10	23
8	Experimental conditions for set A runs for abutment scour	58
9	Experimental conditions for set B runs for abutment scour	60
10	Experimental conditions for set C runs for abutment scour	62
11	Experimental conditions for set G runs for abutment scour	63
12	Experimental conditions for set H runs for abutment scour	64
13	Experimental conditions for set I runs for abutment scour	65
14	Experimental conditions for set J runs for abutment scour	66
15	Experimental conditions for set K runs for abutment scour	67
16	Experimental conditions for set L runs for abutment scour	68
17	Experimental conditions for set M runs for abutment scour	69
18	Experimental conditions for set N runs for abutment scour	70
19	Experimental conditions for set D runs for abutment scour	71
20	Experimental conditions for set E runs for abutment scour	72
21	Experimental conditions for set F runs for abutment scour	73
22	Properties of sediment mixture types used in abutment scour experiments	74
23	Summary of pier scour experiments in clayey sands	84
24	Summary of abutment scour experiments in clayey sands	85

25 Results of set 1 experiments to study effects of clay content 92

26 Summary of experimental conditions and results for set 2 (effect of compaction on pier scour in cohesive soils) 93

27 Summary of experimental conditions and results for set 3 (effect of IWC on pier scour in cohesive soils) 94

28 Summary of experimental conditions and results for set 3 (effects of initial water content on pier scour for saturated clay) 95

29 Results of Montmorillonite clay experiments conducted in the 2.44-m wide sedimentation flume using 0.22 m abutment protrusion length 104

30 Results of Montmorillonite clay experiments conducted in the 1.22-m wide flume using 0.11 m abutment protrusion length 105

31 Results of Montmorillonite clay experiments conducted in the 2.44-m wide flume using 0.11 m abutment protrusion length 106

32 Results of Kaolonite clay experiments in the 2.44-m wide flume with 0.22 m abutment width 107

1. INTRODUCTION

This report presents the summary and synthesis of the various components of the experimental study entitled "Effects of Gradation and Cohesion on Bridge Scour" conducted at Colorado State University (CSU) from 1991 through 1996. This study encompassed experiments conducted under four major categories:

1. Effects of gradation and coarse material fraction on pier scour experiments.
2. Effects of gradation and coarse material fraction on abutment scour experiments.
3. Effects of cohesion on pier scour experiments.
4. Effects of cohesion on abutment scour experiments.

During this 5-year study, 5 different experimental flumes of varying sizes with 20 noncohesive and 10 cohesive sediment mixtures were utilized. In pier scour experiments, nine different pier sizes were tested; in abutment scour experiments, seven different abutment protrusion lengths were utilized. Depending on the purpose and scale of the experiments, varying degrees of data collection programs were implemented. The measurements utilized various levels of sophistication and collected detailed flow and sediment data in the vicinity of pier and abutment models. These experimental results were then utilized to quantify effects of coarse material fraction and cohesion on bridge scour. The details of the study were presented in a separate, six-volume set. These reports are:

Vol. 1.	*Effect of Sediment Gradation and Coarse Material Fraction on Clear Water Scour Around Bridge Piers*[1]
Vol. 2.	*Experimental Study of Sediment Gradation and Flow Hydrograph Effects on Clear Water Scour Around Circular Piers* [2]
Vol. 3.	*Abutment Scour for Nonuniform Mixtures* [3]
Vol. 4.	*Experimental Study of Scour Around Circular Piers in Cohesive Soils* [4]
Vol. 5.	*Effect of Cohesion on Bridge Abutment Scour* [5]
Vol. 6.	*Abutment Scour in Uniform and Stratified Sand Mixtures* [6]

In this synthesis report, the experimental facilities, experimental equipment and measurements, results, and analysis and conclusions for each of the components of the experimental study are presented individually in chapters 2 through 6. Each chapter tabulates the properties of the materials used, the approaching flow conditions, and the resulting scour measurements. The results from the various components of the study are also presented in terms of unified relationships and equations.

In chapter 2, results of experiments to study the effects of gradation and coarse bed material fraction on pier scour are presented. In the first phase of the study, effects of gradation and coarse bed material fraction were investigated experimentally in the 2.44-meter (m) wide by 60-m long tilting flume at the Engineering Research Center, CSU. Six different sand mixtures with the same median diameter, D_{50}, of 0.75 millimeter (mm), but with gradation coefficients ranging from 1.38 to 3.4 were used in the experiments. To study the coarse material fraction effects, mixtures with the same median diameter, D_{50}, and gradation coefficient, σ_g, but with varying D_{90} and D_{95} sizes were subjected to the same scour conditions. Experiments revealed that the coarse material fraction, rather than the gradation coefficient, is the controlling factor in pier scour. This set of experiments was limited to clear water scour around a circular pier with a diameter of 0.178 m. Flow intensities starting with incipient conditions were increased in the experiments until live-bed conditions were encountered. Extensive bed material samples from the scour hole and the approach were obtained and analyzed. Also, in chapter 2, the results of a smaller scale study for quantifying the effects of gradation on pier scour are presented using six sand mixtures with the same median sizes of 1.8 mm and 0.78 mm, but with different gradation coefficients. These smaller scale experiments, conducted in a 0.61-m wide by 18-m long experimental flume using circular piers with a diameter of 0.076 m, examined the effects of model scaling. These experiments, along with additional experiments conducted in the 5.1-m wide river mechanics flume, were used in defining the dependence of scour on pier diameter. It was found that local scour, D_s, varied with pier diameter, b, according to a simple power relationship: $D_s \sim b^{0.6}$. Finally, the study was extended to larger sediment sizes by conducting experiments using uniform and coarse fraction enriched gravel mixtures. As a result of this effort, a new equation was developed expressing pier scour in terms of the dimensionless excess velocity factor, flow depth, pier diameter, and a correction factor for the coarse fractions present in mixtures was derived. The new method was tested with available data from previous research. This equation shows that gradation effects are not constant through the entire range of flow conditions but vary with flow intensity.

In chapter 3, effects of size fraction on clear water abutment scour was studied using 16 different sediment mixtures ranging from very fine sand to gravel sizes. Experiments were conducted in 0.61-m, 2.44-m, and 5.18-m wide flumes to cover a range of geometrically similar flow conditions to analyze scale effects in physical modeling of abutment scour. In the experiments, for mixtures with median (D_{50}) sediment sizes of 0.1 mm, 0.55 mm, 0.78 mm, and 1.8 mm, the coarse size fractions present in mixtures corresponding to D_{90} and D_{95} sizes were varied while keeping the median size and

sediment gradation constant. Results of abutment scour experiments were normalized using corresponding abutment scour values for uniform mixtures with the same median D_{50} sediment sizes. Similar to pier scour analysis, a coarse fraction reduction factor for graded mixtures was derived for different gradation coefficients. It was found that, for very low flow intensities and for intensities approaching live-bed conditions, the coarse material fractions have little effect. However, for a wide range of intermediate dimensionless flow intensities, abutment scour is very much dependent on the coarse material fraction and can be as low as 15 percent of scour in uniform material with the same D_{50} size. As a result of abutment scour experiments, two new equations were developed. The first equation was derived from a 0.1 mm uniform sand mixture and defines an envelope relationship. The second equation applies to mixtures with coarse fractions. A coarse size fraction compensation factor W_g is presented to account for the presence of varying amounts of coarse material in sediment mixtures under different dimensionless flow intensities. These new equations represent the experimental data very accurately but have not been tested with field data.

In chapter 4, effects of clay content on bridge scour are presented. For both pier and abutment scour experiments, clayey sand mixtures with varying amounts of clay were subjected to different approach flow conditions. The resulting scour values from these experiments were normalized with the corresponding scour experienced in pure sand used as the base material. In pier scour experiments, for Montmorillonitic clay mixtures, results showed that for sandy clays, increasing the clay content to up to 30 percent may reduce scour by up to 40 percent. Beyond a certain clay content (30 to 40 percent for the present mixture) parameters such as compaction, initial water content, degree of saturation, shear strength, etc., dominated the pier scour. Similarly, in abutment scour experiments, for Montmorillonitic clay mixtures, experimental results showed that for clayey sands, increasing the clay content up to 30 percent may reduce scour by up to 40 percent. For Kaolinitic clay mixtures the results are more dramatic; for the clear water scour range, scour reduction can be up to 80 percent of that observed in pure sands. Beyond a certain percentage of clay content (30 to 40 percent for the present mixture) parameters such as compaction, initial water content, degree of saturation, shear strength, etc., dominate the cohesive material scour. These experiments were conducted for the range of flows that represented clear-water scour conditions for the base material. However, it is expected that for velocities much in excess of those that could mobilize the base material, ultimate scour would be reached.

In chapter 5, effects of cohesion on pier scour are investigated experimentally using 1.22-m, 2.44-m, and 5.18-m wide test flumes at the Engineering Research Center, CSU. In these experiments, flows with corresponding Froude numbers ranging from 0.2 to 1.4 were used to investigate scour taking place in saturated and unsaturated Montmorillonitic sandy clay mixtures. Regression equations relating flow and selected cohesive soil parameters to pier scour were derived for a fixed circular pier geometry and a constant flow depth. These experiments showed that pier scour in cohesive material can be expressed in terms of cohesive soil parameters that can be obtained in the field.

The equations derived from this study do not attempt to relate effects due to pier geometry, size, flow depth, gradation of sand in the mixtures, etc., and therefore are not intended for general application. These relationships are derived to explain the variability of pier scour with cohesive properties.

In chapter 6, effects of cohesion on abutment scour were investigated experimentally using 1.22-m and 2.44-m wide test flumes. In abutment scour experiments, Montmorillonitic and Kaolinitic sandy clay mixtures were used to examine clay mineralogy effects as well as effects due to compaction, initial water content, and soil shear strength. Froude numbers in these experiments varied between 0.2 and 0.6 to cover a wider range of hydraulic conditions. Regression equations relating flow and clay properties to abutment scour express scour in terms of sands scour and were therefore developed for the range of flows that represented clear water scour conditions for the base material.

The data resulting from the experimental study are presented in chapters 2 through 6 in tabulated, consistent units. The majority of these data were derived from the six-volume report mentioned above. The results of pier scour experiments in gravel and the results of pier scour experiments to study effects of pier width were conducted beyond the initial set of experiments and are included in this report in chapter 2.

2. EFFECTS OF GRADATION AND COARSE MATERIAL FRACTION ON PIER SCOUR

2.1 GENERAL

Pier scour has been extensively studied in the past for uniform and graded sediment mixtures. In general, pier scour equations account for the variation in sediment properties by either including a correction factor for sediment gradation or by using median size and the gradation coefficient in developing the experimental regression equations. In this study, a new governing sediment parameter was brought to attention. This parameter, which describes the characteristics of the coarse fraction available in mixtures, accounts for the wide variation in scour depth for mixtures with the same median size and size gradation factor. Along with a dimensionless flow intensity parameter, a new pier scour equation was developed to account for the sediment properties in clear-water scour range. This equation was shown to be applicable to a wide range of sediment sizes ranging all the way from 0.1 mm to 40 mm. Pier scour experiments conducted in noncohesive materials in this study were aimed at identifying the effects of sediment properties on the resulting scour. For this purpose 10 sets of experiments were designed to vary sediment size, gradation, and other size distribution properties. Pier scour experiments for each sediment mixture were conducted by varying the approach flow conditions. Since the primary goal of the study was to define effects of gradation and coarse material fraction on pier scour, other flow variables such as depth, flow angle of attack, pier shape, etc., were kept constant.

2.2 EXPERIMENTAL SETUP AND MEASUREMENTS

This section presents experimental flumes, sediment mixtures used as bed materials, piers, experimental procedures, as well as the individual measurements employed in quantifying effects of gradation and coarse material fraction on pier scour.

LABORATORY FLUMES

Three laboratory flumes, designated as the hydrodynamics flume, sedimentation flume, and the river mechanics flume, were simultaneously utilized for conducting the pier scour experiments in noncohesive sediment mixtures. The first two flumes are sediment recirculating facilities, while the latter does not recirculate sediment. All flumes are housed at the Hydraulics Laboratory of the Engineering Research Center at CSU. The water supply to these flumes is from the nearby Horsetooth Reservoir. The temperature of the water in the laboratory is controlled through a heating pipe system.

Hydrodynamics Flume

The hydrodynamics flume is a tilting, water and sediment recirculating laboratory facility. The flume is 0.6-m wide, 0.75-m deep, and 18-m long and is made of a steel bottom and Plexiglas side walls to facilitate visual observations. The facility is rigidly supported on U-shaped steel frames located every 1.2 m and is equipped with angled upper and lower flange stiffeners. The bottom flanges are supported on two I-beams spanning the full length of the flume and ground supported at the far upstream, the middle, and far downstream. Two carefully leveled guide rails are mounted on the top flanges to provide an escorting track for the measuring carriage. The flume can be tilted around its middle lateral axis through the synchronized operation of two mechanical jacks located at the upstream and downstream ends. Flow is supplied to the flume from a ground sump via a 0.3-m diameter steel pipe line, equipped with a 0.15-m diameter bypass for fine tuning of the flow, and a 20-horsepower (HP) centrifugal pump. The flow is first introduced to an upstream head box equipped with a multi-layer screen containing gravel at its outlet to serve as a flow guide to provide uniform velocities and turbulence characteristics at the entrance of the flume. A wave suppressor is then introduced to ensure accomplishment of the previous concerns. The flow depth is controlled by a downstream rotating gate hinged across the bottom of the flume, spanning the full width, and operated by a system of pulleys. Because of the tail gate control and the nature of the flume, a back water effect is sometimes noticed, causing the water depth to increase as the gate is approached. A uniform sediment layer 23 centimeters (cm) thick is prepared from the tested mixture and is spread along the full length of the flume with provisions made for a downstream 1.8-m long sediment trap and an upstream 1.8-m long transition zone. The upstream transition zone is composed of coarser sediments, with a sloping profile carefully designed to provide excess friction to ensure the existence of fully developed turbulent flow, with a boundary layer hitting the free surface, far upstream of the study reaches for all flow conditions.

Sedimentation Flume

The sedimentation flume is an elevated sediment transport testing facility that provides for both longitudinal tilting and sediment recirculation. The flume is 60-m long, 2.4-m wide, 1.2-m deep, and allows for slope adjustments up to 3 percent through a system of hydraulic jacks. The flume is constructed from steel plates at the bottom and sides, with provisions for Plexiglas windows along specific locations at its side. The structure's skeleton is composed of U-shaped lateral steel frames supported on box-sectioned longitudinal girders. A walkway is cantilevered from the lateral frames on each side of the structure. The upper flanges house guide rails for an electrically motorized measuring carriage that can virtually move to any point in the flume. Three different pumps (125, 150, and 250 HP), with a maximum combined capacity of 3 cubic meters per second (m^3/s), can be simultaneously operated to supply water to the flume from a reservoir sump via three separate steel pipe lines. The flow is first introduced to the upstream head box, which contains several guide vanes and flow straighteners followed

by a honeycomb mesh. It then passes through a gravel-filled screen succeeded by a wave suppressor. Rapid development of the fully turbulent boundary layer is achieved through an upstream concrete ramp and/or artificial roughening of the entrance zone. The flow depth is regulated through a manually operated downstream adjustable tail gate. The sediment bed is built to a thickness of about 0.4 m, with provisions made for a downstream sediment trap that extends for 6 m. To facilitate drainage of the flume after the experiments, a perforated 10-cm diameter poly vinyl chloride (PVC) pipe was embedded in the bed material and spanned the full length of the study reach. A motorized instrument carriage runs longitudinally on rails mounted on the side walls of the flume.

River Mechanics Flume

The river mechanics flume is a fixed-slope facility. The flume is 6-m wide, 0.9-m deep, and around 30-m long. The test section, however, was 24-m long, 5.1-m wide, and 0.9-m deep, providing for two Plexiglass viewing sections along one side of the flume and a large upstream reservoir to create uniform entrance conditions. I-beam rails are mounted on the side walls to provide a track for the measuring carriage. A 75-HP axial pump of maximum capacity around 0.6 m^3/s supplies water to the flume through a 0.6-m diameter pipeline. The upstream main ends in a similar size diffuser located orthogonal to the main flow direction to distribute the flow uniformly across the flume width. The flow then passes through a gravel-filled screen followed by an artificially coarsened concrete ramp that joins the main sediment bed. The setup also provides for a downstream sediment trap and a downstream sill for depth regulation.

PIERS

For the pier scour experiments conducted in the sedimentation flume, three identical 1.22-m high clear Plexiglas cylindrical piers with an outside diameter of 0.18 m were utilized. Circular piers were used because of their symmetry and the abundance of data available for comparative purposes. All three piers were placed at the center line of the flume for each run. In the longitudinal direction, the leading pier was 13.7 m from the head box of the flume, the second one was 24.4 m from the head of the flume, and the third one was 36.6 m from the head of the flume. To keep side-wall effects insignificant, the maximum pier size (for use in the 2.4-m wide flume) was kept at 0.18 m resulting in a flume width-to-pier ratio of 13.7. The depth measurements for pier scour with time were achieved utilizing visual techniques. For this purpose, the piers were constructed of transparent Plexiglas material, and three measuring scales were glued to the front, side, and back of each pier, in addition to a mirror with handle angled at 45^o placed at the base of the pier. The base of the scour hole and the deepest point of the scour hole at any time could be easily identified and recorded by sliding the mirror within the Plexiglas pier and reading the corresponding measurement on the scale. In this way, scour depth with elapsed time could be obtained up to an accuracy of ±0.0015 m. A bright light located above the water surface was used to improve the visibility of the scour region under clear

water-scour conditions. For the hydrodynamics flume experiments, three Plexiglas piers with outside diameters of 0.051 m, 0.051 m, and 0.07 m were installed in the flume, equidistant from the walls. Pier scour experiments in the river mechanics flume investigated the effects of pier width on the resulting scour. For this purpose six additional pier diameters including 0.019 m, 0.032 m, 0.057 m, 0.089 m, 0.165 m, and 0.216 m were tested.

SEDIMENT MIXTURES

Previous researchers have indicated that there is a very strong tendency for alluvial sediments to follow the log-normal size distribution. Such size distribution can be represented by a straight line on plots using logarithmic-normal probability scales. In this case the median sediment size D_{50} is also the geometric mean diameter, D_g of the sediment mixture, where D_{50} is the sediment diameter for which 50 percent of the sediment material is finer by weight. The geometric standard deviation σ_g is given by:

$$\sigma_g = \frac{D_{84}}{D_{50}} = \frac{D_{50}}{D_{16}} \tag{1}$$

or

$$\sigma_g = \frac{1}{2}\left(\frac{D_{84}}{D_{50}} + \frac{D_{50}}{D_{16}}\right) \tag{2}$$

or

$$\sigma_g = \sqrt{\frac{D_{84}}{D_{16}}} \tag{3}$$

where: D_{16} , D_{50} , and D_{84} are the sediment diameters for which 16, 50, and 84 percent of the sediment material is finer by weight, respectively. The log-normal distribution function is a two-parameter distribution and is completely defined by D_{50} and σ_g. However, most natural sediments show an approximate log-normal distribution only through the mid part of the distribution, say $D_{50} \pm \sigma_g$, but they usually have long tails in both the coarse and fine fractions. Thus, equations 1 through 3 are for gradation coefficients that measure the spread of the distribution only between D_{84} and D_{16} in most natural sediments. The presence of coarse material in sediment mixtures is better defined by sizes of different quantities, such as D_{98}, D_{95}, D_{90}, etc. For the work here, D_{50} and σ_g were held constant and sizes of D_{90}, D_{95}, D_{98}, etc., were changed since armoring in the scour hole involves mostly the coarser fractions of the mixture.

There is a specific requirement that needs to be met in determining the gradation of the initial grain size distribution for the sediment mixtures. This requirement is to keep the median size diameter constant throughout the study. In the sedimentation flume sand-scour experiments, the median diameter was chosen to be 0.75 mm, with gradation coefficients

varying between 1.3 and 4.0. In the hydrodynamics flume sand-scour experiments, the median diameter was chosen to be 1.8 mm, with gradation coefficients varying between 1.1 and 4. Additional runs using 0.75-mm diameter uniform sand were conducted to study scaling effects. In the river mechanics flume sand-scour experiments, 0.45-mm diameter sand with a gradation coefficient of 2.3 was used. Finally, in the gravel-scour experiments conducted in the sedimentation flume, the median diameter was chosen to be 18 mm, with gradation coefficients varying between 1.4 and 2.3.

The properties of the sediment mixtures used in the pier-scour experiments are given in table 1.

MEASUREMENTS

A series of measurements is needed to define the relationship between local pier scour and the various hydraulic, geometric, and sediment parameters. These measurements are presented below.

Flow Discharge

The water discharge in all three test flumes was measured through a system of orifice-meter and a differential manometer. For the hydrodynamics flume, two orifice plates were available: one mounted on the 0.3-m diameter main, and the other attached to the 0.15-m diameter bypass line. Both orifice plates are connected to a dual water-mercury manometer for detecting the pressure drop across the ends of the plate. The flow discharge was then computed from the calibration curves for the orifices. The pressure tapping across the orifice plate is connected to the manometer through hard vinyl tubing provided with bleeding valves for drainage and for ensuring an air-free environment. The sedimentation flume is equipped with three similar setups for measuring the discharge, each attached to a different pump. Extreme care was taken to ensure the release of air bubbles entrapped in all manometer lines. Flow discharges were also estimated by integrating the vertical velocity profiles over the entire cross section of the flume at several locations. The error in measuring the discharge in the hydrodynamics flume is around 3 percent, in the sedimentation flume around 4 percent, and in the river mechanics flume around 5 percent. These error estimates are due to the calibration errors of orifice plates, unsteadiness in the pump discharge, and fluctuations in manometer readings.

Flow Velocity

In the hydrodynamics flume, velocities were measured utilizing a two-dimensional electromagnetic Marsh McBirney, Model 523 velocity meter attached to a point gauge to measure velocity components in two orthogonal directions in a plane parallel to the bottom of the flume. The meter consists of a spherical electromagnetic probe with cable and signal processor powered by 6-volts direct current (V DC) externally charged with 110-volts alternating current (V AC). The probe has a diameter of 12 mm and is mounted on a 6-mm diameter vertical standing rod. The analog signals corresponding to the two orthogonal velocities sensed by the probe are intercepted by a

multichannel data acquisition board connected to a personal computer. The sampling duration was 30 s, with a frequency of 50 Hertz (Hz). Overall accuracy of the latter setup is around 3.5 percent.

In the river mechanics and sedimentation flumes, velocities were measured with a one-dimensional Marsh McBirney, Model 2000 electromagnetic flow meter with a 2.54-cm elliptic probe and a digital display conversion voltmeter. The accuracy of the flow meter is reported to be ±2 percent by the manufacturer, and its operating range is from -0.015 m/s to +6.1 m/s within temperature extremes of 0 ^{o}C to 71 ^{o}C. Overall accuracy of the velocity measuring setup is estimated to be 5 percent.

Flow Depth and Hydraulic Grade Line

In the case of nonuniform material, bed irregularities affect the accuracy of bed elevation measurements. Theoretically, during experiments the bed surface is not known and the bed elevation measurement at any section depends on the position of the tip of the point gauge relative to the larger grains on the bed. To reduce such errors, during the sedimentation flume experiments three different point gauge readings utilizing a flat tip were taken across each of the test sections. The bed elevation was accepted as the average of these three values. Using a pointed point-gauge tip, the corresponding water surface elevations were also measured. At specified test sections the depth of flow was then calculated as the average difference between the water surface and the bed surface elevations. For all experimental runs a uniform flow depth over the entire flume length was maintained at 0.3 m ±0.03 m by regulating the tail gate at the flume exit. However, the local flow depth varied along the flume length during runs No. MA-12, MA-19, and MA-27, in response to the presence of bed features.

Slope in laboratory flumes is one of the most difficult quantities to measure. Special attention was devoted to reduce the error in slope measurements as much as possible. For this reason bed levels were measured using the point gauge, then corrected through conversion factors obtained from a careful leveling of the carriage along the entire flume using a surveyor's level and rod. The bed slope was then computed as the slope of the line of best fit based on least square-criteria. The water surface slope was calculated in a similar manner.

In the hydrodynamics flume, the water surface elevations were measured using point gauges with a resolution of ±0.3 mm. Water surface elevation measurements were conducted at a minimum of three approach cross sections per pier and at a minimum of four locations across the flume width at each cross section. At every location in the cross section, the water level was considered to be the average of detected values, to account for any residual fluctuations in the supply discharge and any surface waves induced by the setup. This tedious procedure assumes an accuracy of 2 percent in the computed water depth. The hydraulic grade line is identified through regressing the measured water surface values after being adjusted with the level correction factors. The regression results in high correlation coefficients (R^2 = 0.95). The velocity head was then added to the hydraulic grade line to define the total energy line.

Free Stream Bed and Scour Hole Topographies

The bed topographies for the scour holes and the free stream approaches are measured using point gauges. In all flumes, the standard topography measurement procedure started with the leveling of instrumentation carriages at each measurement location along and across the flume to account for the potential unevenness of tracks. Choosing an arbitrary fixed level, every location in the flume, as identified by its Cartesian coordinates, was assigned a correction factor reflecting its elevation relative to the fixed level. In the hydrodynamics flume, point gauges with flat/pointed tips were utilized for measuring purposes depending on the location and accuracy desired. The bed topographies at four different approach sections were measured for each pier model to define the upstream bed elevation. At each cross section, the bed level was considered to be the average of 10 measurements evenly distributed across the flume's width. To define bed topography in the vicinity of local scour requires more intensive measurements. An intensive measuring grid was adopted to describe the scour hole region for each pier. A similar procedure was followed for the other two flumes, with provisions made for measuring the initial as well as the final levels. The raw measurements are adjusted with the leveling correction factors for each location and then regressed together to yield the value of the bed slope. Approximately 300 topography measurements were performed for each pier model per experiment. Due to the large sampling size, the error in bed elevation measurements is considered to be equal to 0.25 of the D_{90} grain size. The maximum scour depth value for each run was calculated as the difference between the mean initial bed elevation and the lowest measured point of scour around each pier.

Scour versus Time Measurements

The measurement of the scour hole development for piers utilized visual techniques. As mentioned earlier, piers were made out of transparent Plexiglas. Measuring grid tapes were pasted on the interior wall at the front, side, and back of each pier. Using a simple periscope manufactured by an inclined-mirror, the development of scour with time was recorded without interference with the flow. A series of lights was used to facilitate the observation of the scour hole development. The depth of scour was recorded at regular intervals as the scour hole formed. The frequency of scour depth measurements decreased as the rate of scouring decreased. The experiments were stopped when no change occurred to the maximum depth of the scour hole over a minimum period of 4 hours.

Sampling of the Armor Layer

At the end of each experiment, the particle size distribution of the armor layers formed around each pier in the scour hole, approach bed to each pier, and downstream of the pier were measured from samples obtained by the flour paste technique described by Abdou[7]. Sieve analysis was then performed on the samples using U.S. standard sieves and the available shaker in the Sediment Laboratory of the Engineering Research Center, CSU.

To determine the grain size distribution of the armor layer, it was required to collect all grains in the top layer only. The most common method used by previous

researchers for such a purpose is the wax method. Gessler[8] used molten resin at 200 °C, Little and Mayer[9] used purified bee's wax at 65 °C to 68 °C, Davies[10] used molten petroleum wax at 76 °C to 78 °C, and Proffitt[11] used paraffin wax at 55 °C to 57 °C. In previous work, the measured grain size distribution of the armor layers was found to be highly affected by the temperature at which the wax was poured onto the bed. If the temperature is outside the narrow ranges specified above, the wax either permeates down before solidifying or solidifies before all grains in the top layer adhere to it.

Day[12] used the paint method to identify grains in the top layer but still used the wax method to lift it up. This method predicted a coarser grain size distribution of the armor layer than the wax method. Day explained this to be caused by the penetration of the wax below the armor layer.

In the present study, the flour paste technique developed by Abdou[7] was used. The procedure proved to be much easier than the wax method in terms of preparation, use, time elapsed, and separation of the grains adhering to the paste. The paste was sticky enough for all grain sizes to adhere easily and thickly enough so that it did not penetrate further than the surface layer.

After the bed was allowed to dry, the paste was placed on the surface of the bed. A gentle uniform pressure was applied downward on the paste to pick up all the grain sizes on the surface layer. The paste was then lifted up bringing with it the grains that had been the surface layer. Washing the surface of the paste with warm water and then gently brushing by hand achieved the separation of grains from the paste. A visual observation of the paste surface clearly indicated that all grains, even the finest, were separated from the paste. The material was then dried, weighed, sieved, and the grain size distribution of the armor layer at a specific area for a given flow condition was obtained.

Grain Size Distribution

Mechanical (or sieve) analysis was used to determine the particle sizes and their relative distribution for particles greater than 0.074 mm. The smallest sieve size used in this analysis was the U.S. No. 200. The sieve number corresponds to the number of openings per linear inch; for example, the U.S. Bureau of Standards No. 8 sieve has eight openings per inch.

To accomplish the mechanical analysis, sieves were stacked one on top of the other in the shape of a nest of sieves, in which the largest screen opening (smallest sieve number) was on top, progressing to the sieve with the smallest screen openings (largest sieve number) on the bottom of the nest. A lid was placed on top of the nest and a pan was placed below the bottom sieve to catch any sediment that passed through the smallest opening. A 10-minute shaking period was used in this procedure. A larger sample required a longer shaking period. Similarly, a sample composed primarily of fine-grained material requires a longer shaking period than a coarse-grained sample of equal weight.

EXPERIMENTAL PROCEDURE

Preparation for the scour test was initiated by leveling the bed. Prior to each run, the sediment bed was leveled with the aid of a flat plate that was of the same width as the flume and was connected vertically to the instrument carriage by clamps. By employing the point gauge mounted on the carriage, initial bed elevations were taken to check the leveling of the flume and calculate the average initial bed elevation around each pier.

The gate was kept closed until the flume was filled with water. Then the gate was adjusted to get the desired depth, and the valves of the pump were adjusted to get the desired discharge, which was determined with an orifice inserted in the recirculating pipeline. Flow depth in the sedimentation flume experiments was maintained around 0.3 m; water surface and bed slopes were almost parallel. For the hydrodynamics flume experiments flow depth was kept around 0.08 m.

Once the requested flow conditions were verified, the carriage and the point gauge were moved along the flume in such a way that any point in the study area could be reached with the measuring devices. Water surface profile was measured along the length of the flume to calculate the water surface slope. Vertical velocity profiles and development of scour with time were recorded during each experiment. In the sedimentation flume experiments, the duration of runs was selected to be 16 hours (h) to allow maximum scour to be reached and the final scour hole geometry to be established. This period was long enough to maintain the maximum scour depth constant for at least 3 to 4 h. For the hydrodynamics flume experiments longer experiment durations were tested. Test runs up to 56 h showed that, for the ranges of sediment sizes and gradation used in the experiments, the longer experiment durations did not alter maximum scour. For a given discharge, once the surface armor layer was formed, bed profiles remained virtually constant. At the end of each run, the tail gate was slowly closed and the pump stopped to drain the flume without any disturbance. Then the flume was slowly drained with the aid of an efficient drainage system on the floor of the flume with its end open toward the tail gate.

The bed was then allowed to dry over a 24-h period, photos of scour holes around each pier were taken, and measurements of the final bed elevations were recorded to determine the maximum scour depth around each pier and the final bed slope. The bed was allowed to dry another 24 h, and then the armored layers around each pier and different areas in the approach and downstream of the piers were sampled using the flour paste technique described by Abdou[7]. Sieve analysis was then performed on the samples using U.S. standard sieves (the sieving of the sediment samples was completed by using a series of sieves at intervals of $\sqrt{2}$ times sieve diameter).

This procedure was repeated for each run. In the sedimentation flume experiments, the area around each pier within 6.1 m had to be refilled with the proper mixtures, leveled, and saturated with water. Flow conditions were verified, and velocity was measured at the approach of each pier in addition to the water surface profile measurements and scour depth with time. After the scour depth became constant with time for at least 3.0 to 4.0 h, the flow was stopped to let the bed dry, then the final bed

elevations were taken. Finally, the surface layer around each pier as well as the approach and downstream of each pier was sampled to determine the size distribution of the armored layers.

2.3 EXPERIMENTAL RESULTS

A comprehensive experimental program was designed to investigate the different aspects of gradation and coarse material fraction effects on local pier scour. These experiments are categorized into 10 different sets of runs labeled 1 through 10. The experimental program was carried out concurrently in three different laboratory facilities. Sets 1 through 3, 9, and 10 were conducted in the sedimentation flume; sets 4 through 7 were performed in the hydrodynamics flume; and set 8 experiments were carried out in the mechanics flume. Thirteen different sediment mixtures and 10 different pier models were subjected to a range of flow conditions, resulting in a total of 188 different pier scour case studies.

Set 1 experiments were conducted by subjecting three identical piers to specified flow conditions. The purpose of this set of runs was to check the repeatability of results for scour depth at the three piers subjected to the same flow conditions. This first set (runs MA-1 through MA-12) was performed using a graded sand mixture with a geometric standard deviation, σ_g of 2.43, and D_{50} of 0.75 mm. Set 2 experiments (runs MA-13 through MA-19) were conducted using the same sand with σ_g of 2.43 and D_{50} of 0.75 mm as the bed material around pier 1. Around piers 2 and 3 the size of coarse material fraction in the original sediment mixture corresponding to 10 percent (around pier 2) and to 5 percent (around pier 3) was increased. The gradation coefficient, σ_g, and D_{50} were kept constant at 2.43 and 0.75 mm, respectively. The purpose of this second set of runs was to examine the behavior of the scour depth with increasing the sizes of sediments for the fraction above D_{90} and D_{95} in the original sediment mixture without changing the gradation coefficient. Set 3 experiments (runs MA-20 through MA-27) used a sediment mixture with σ_g of 3.4 and D_{50} of 0.75 mm as the bed material around pier 2 and increasing the coarse fraction above D_{90} in the same sediment mixture as the bed material around pier 1. For pier 3, a uniform sand with σ_g of 1.38 and D_{50} of 0.75 mm was used. The purpose of set 2 and 3 experiments was to investigate the effect of increasing coarse material fraction and gradation of bed materials on local pier scour depth.

Sets 4 through 7 were conducted in a smaller flume with scaled down (1:4) flume width, flow depth, and pier width. In sets 4 through 6, a coarse sand mixture with the same median diameter, D_{50}, of 1.8 mm, but different gradation coefficients were subjected to a range of approach flow conditions. In set 4, a uniform mixture with σ_g of 1.15 was used; whereas in sets 5 and 6, σ_g was 2.43 and 3.4, respectively. Finally, in set 7 the same sediment used in set 1 (with D_{50} of 0.75 mm and σ_g of 2.43) was used to study scaling effects.

Set 8 experiments were conducted in the 5.18-m wide river mechanics flume to examine and verify pier size effects. For this purpose, a series of circular piers with

varying diameters was subjected to the same oncoming flows. The sediment used for these experiments was medium sand with a median diameter of 0.55 mm and gradation coefficient of 2.43. The results of these experiments were used to establish scaling parameters for pier widths. In general terms, it is found that pier scour is a function of $b^{2/3}$.

Sets 9 and 10 were conducted in the sedimentation flume and examined the effects of coarse fraction on gravel scour. The two sediment mixtures used in these experiments had both a median diameter of 18 mm and gradation coefficient of 1.45. However, the gravel mixture used in set 9 experiments contained larger coarse fractions. The D_{90} for the mixtures used in sets 9 and 10 was 40 mm and 22 mm, respectively. The purpose of these experiments was to investigate the range of applicability of the theory developed from the study.

A summary table of the sediment characteristics associated with the different mixtures utilized in the study is given in table 1. Tables 2 through 7 present these cases. In the pier scour experiments presented in this section, the effects of the following parameters were investigated:

- Effect of mean sediment size, D_{50} (all sets).
- Effect of sediment gradation, σ_g (all sets).
- Effect of the coarsest 10th percentile of the sediment size gradation (sets 1-3; 9-10).
- Effect of flow depth, Y (all sets).
- Effect of pier diameter, b (set 8).

The following sections present results of experiments. References to related summary tables are given whenever applicable.

Table 1. Properties of sediment mixtures used in pier scour experiments.

Mixture No. (1)	Mixture ID (2)	σ_g (3)	D_m (mm) (4)	D_{16} (mm) (5)	D_{35} (mm) (6)	D_{50} (mm) (7)	D_{65} (mm) (8)	$D_{84.6}$ (mm) (9)	D_{85} (mm) (10)	D_{90} (mm) (11)	D_{95} (mm) (12)	D_{99} (mm) (13)	D_{cfm} (mm) (14)	D_{cfm}/D_{50} (15)
1	MA-1A	2.43	0.75	0.31	0.50	0.75	1.11	1.83	1.83	2.10	2.36	4.80	2.59	3.46
2	MA-1B	2.43	0.75	0.31	0.50	0.75	1.11	1.83	1.83	2.80	5.00	8.00	4.24	5.65
3	MA-1C	2.43	0.75	0.31	0.50	0.75	1.11	1.83	1.83	2.00	2.36	8.00	3.09	4.12
4	MA-2E	3.40	0.75	0.23	0.45	0.75	1.31	2.65	2.65	4.76	6.40	8.00	5.50	7.33
5	MA-2D	3.40	0.75	0.23	0.45	0.75	1.31	2.65	2.65	3.20	4.20	8.00	4.24	5.66
6	MA-3	1.38	0.75	0.55	0.65	0.75	0.87	1.05	1.05	1.18	1.22	1.30	1.19	1.59
7	HN-1	3.70	1.87	0.40	1.02	1.87	3.00	5.47	5.47	6.30	8.04	10.00	7.36	3.93
8	HN-2	1.15	1.87	1.56	1.74	1.87	2.01	2.21	2.21	2.26	2.32	2.38	2.29	1.23
9	HN-3	2.17	1.80	1.10	1.29	1.80	2.53	3.89	3.89	4.39	4.93	5.60	4.69	2.61
10	HN-4	1.28	0.76	0.63	0.66	0.76	0.87	1.03	1.03	1.08	1.14	1.19	1.11	1.46
11	MH-1	2.24	0.55	0.22	0.40	0.55	0.75	1.10	1.10	1.30	1.60	2.30	1.53	3.40
12	MH-2	1.28	16.90	11.50	16.10	16.90	17.84	19.10	38.10	40.00	42.40	45.00	41.30	2.44
13	MH-3	1.30	16.70	13.00	15.20	16.70	18.16	20.20	20.20	20.90	21.70	22.40	21.30	1.28

Table 2. Summary of sand-scour experiments in sedimentation flume for set 1 (runs 1 through 12).

Run ID	Mixture ID	Median Diameter D_{50} (mm)	Gradation Coefficient σ_g	Flow Discharge Q (l/s)	Approach Depth Y (m)	Approach Velocity V (m/s)	Energy Slope S_e	Froude Number Fr	Scour Depth D_s (m)	Flow Duration t (h)
MA-1-1	MA-1	0.75	2.43	206.43	0.384	0.213	0.00020	0.11	0.037	8
MA-1-2	MA-1	0.75	2.43	206.43	0.396	0.204	0.00020	0.10	0.037	8
MA-1-3	MA-1	0.75	2.43	206.43	0.399	0.201	0.00020	0.10	0.034	8
MA-2-1	MA-1	0.75	2.43	246.07	0.287	0.347	0.00040	0.21	0.076	8
MA-2-2	MA-1	0.75	2.43	246.07	0.293	0.341	0.00040	0.20	0.067	8
MA-2-3	MA-1	0.75	2.43	246.07	0.293	0.338	0.00040	0.20	0.067	8
MA-3-1	MA-1	0.75	2.43	300.16	0.287	0.421	0.00060	0.25	0.168	19
MA-3-2	MA-1	0.75	2.43	300.16	0.290	0.405	0.00060	0.24	0.143	19
MA-3-3	MA-1	0.75	2.43	300.16	0.293	0.405	0.00060	0.24	0.143	19
MA-4-1	MA-1	0.75	2.43	300.16	0.381	0.302	0.00040	0.16	0.049	12
MA-4-2	MA-1	0.75	2.43	300.16	0.375	0.302	0.00040	0.16	0.049	12
MA-4-3	MA-1	0.75	2.43	300.16	0.378	0.290	0.00040	0.15	0.046	12
MA-5-1	MA-1	0.75	2.43	263.63	0.354	0.296	0.00042	0.16	0.046	8
MA-5-2	MA-1	0.75	2.43	263.63	0.344	0.293	0.00042	0.16	0.046	8
MA-5-3	MA-1	0.75	2.43	263.63	0.341	0.296	0.00042	0.16	0.040	8
MA-6-1	MA-1	0.75	2.43	280.34	0.335	0.332	0.00045	0.18	0.088	12
MA-6-2	MA-1	0.75	2.43	280.34	0.335	0.332	0.00045	0.18	0.082	12
MA-6-3	MA-1	0.75	2.43	280.34	0.335	0.329	0.00045	0.18	0.079	12
MA-7-1	MA-1	0.75	2.43	323.10	0.323	0.396	0.00060	0.22	0.146	16
MA-7-2	MA-1	0.75	2.43	323.10	0.326	0.390	0.00060	0.22	0.134	16
MA-7-3	MA-1	0.75	2.43	323.10	0.326	0.387	0.00060	0.22	0.134	16
MA-8-1	MA-1	0.75	2.43	360.76	0.320	0.442	0.00065	0.25	0.186	12
MA-8-2	MA-1	0.75	2.43	360.76	0.326	0.411	0.00065	0.23	0.183	12
MA-8-3	MA-1	0.75	2.43	360.76	0.323	0.421	0.00065	0.24	0.183	12
MA-9-1	MA-1	0.75	2.43	267.03	0.320	0.335	0.00043	0.19	0.091	16
MA-9-2	MA-1	0.75	2.43	267.03	0.311	0.335	0.00043	0.19	0.079	16
MA-9-3	MA-1	0.75	2.43	267.03	0.305	0.341	0.00043	0.20	0.079	16
MA-10-1	MA-1	0.75	2.43	390.49	0.332	0.469	0.00070	0.26	0.195	10
MA-10-2	MA-1	0.75	2.43	390.49	0.326	0.457	0.00070	0.26	0.186	10
MA-10-3	MA-1	0.75	2.43	390.49	0.317	0.460	0.00070	0.26	0.183	10
MA-11-1	MA-1	0.75	2.43	429.00	0.335	0.491	0.00073	0.27	0.207	14
MA-11-2	MA-1	0.75	2.43	429.00	0.329	0.479	0.00073	0.27	0.198	14
MA-11-3	MA-1	0.75	2.43	429.00	0.320	0.494	0.00073	0.28	0.207	14
MA-12-1	MA-1	0.75	2.43	473.74	0.363	0.503	0.00085	0.27	0.198	16
MA-12-2	MA-1	0.75	2.43	473.74	0.363	0.524	0.00085	0.28	0.195	16
MA-12-3	MA-1	0.75	2.43	473.74	0.384	0.482	0.00085	0.25	0.201	16

Table 3. Summary of sand-scour experiments in sedimentation flume for set 2 (runs 13 through 19).

Run ID	Mixture ID	Median Diameter D_{50} (mm)	Gradation Coefficient σ_g	Flow Discharge Q (l/s)	Approach Depth Y (m)	Approach Velocity V (m/s)	Energy Slope S_e	Froude Number Fr	Scour Depth D_s (m)	Flow Duration t (h)
MA- 13-1	MA-1A	0.75	2.43	314.32	0.323	0.390	0.00055	0.22	0.155	16
MA- 13-2	MA-1B	0.75	2.43	314.32	0.323	0.366	0.00055	0.19	0.049	16
MA- 13-3	MA-1C	0.75	2.43	314.32	0.323	0.372	0.00055	0.21	0.067	16
MA- 14-1	MA-1A	0.75	2.43	206.43	0.311	0.256	0.00029	0.15	0.049	16
MA- 14-2	MA-1B	0.75	2.43	206.43	0.314	0.250	0.00029	0.14	0.012	16
MA- 14-3	MA-1C	0.75	2.43	206.43	0.314	0.250	0.00029	0.14	0.027	16
MA- 15-1	MA-1A	0.75	2.43	146.11	0.305	0.250	0.00022	0.11	0.009	16
MA- 15-2	MA-1B	0.75	2.43	146.11	0.308	0.183	0.00022	0.11	0.003	16
MA- 15-3	MA-1C	0.75	2.43	146.11	0.305	0.186	0.00022	0.11	0.006	16
MA- 16-1	MA-1A	0.75	2.43	236.73	0.329	0.280	0.00045	0.16	0.082	16
MA- 16-2	MA-1B	0.75	2.43	236.73	0.335	0.265	0.00045	0.15	0.027	16
MA- 16-3	MA-1C	0.75	2.43	236.73	0.338	0.259	0.00045	0.14	0.046	16
MA- 17-1	MA-1A	0.75	2.43	259.38	0.329	0.302	0.00050	0.17	0.091	16
MA- 17-2	MA-1B	0.75	2.43	259.38	0.332	0.293	0.00050	0.16	0.030	16
MA- 17-3	MA-1C	0.75	2.43	259.38	0.332	0.290	0.00050	0.16	0.049	16
MA- 18-1	MA-1A	0.75	2.43	380.30	0.329	0.451	0.00062	0.25	0.213	16
MA- 18-2	MA-1B	0.75	2.43	380.30	0.329	0.427	0.00062	0.24	0.085	16
MA- 18-3	MA-1C	0.75	2.43	380.30	0.335	0.433	0.00062	0.24	0.128	16
MA- 19-1	MA-1A	0.75	2.43	477.14	0.335	0.549	0.00098	0.30	0.226	16
MA- 19-2	MA-1B	0.75	2.43	477.14	0.335	0.558	0.00098	0.31	0.180	16
MA- 19-3	MA-1C	0.75	2.43	477.14	0.305	0.646	0.00098	0.37	0.201	16

Table 4. Summary of sand-scour experiments in sedimentation flume for set 3 (runs 20 through 27).

Run ID	Mixture ID	Median Diameter D_{50} (mm)	Gradation Coefficient σ_g	Flow Discharge Q (l/s)	Approach Depth Y (m)	Approach Velocity V (m/s)	Energy Slope S_e	Froude Number Fr	Scour Depth D_s (m)	Flow Duration t (h)
MA-20-1	MA-2E	0.75	3.40	147.25	0.305	0.195	0.00047	0.11	0.003	16
MA-20-2	MA-2D	0.75	3.40	147.25	0.308	0.189	0.00047	0.11	0.003	16
MA-20-3	MA-3	0.75	1.38	147.25	0.308	0.186	0.00047	0.11	0.009	16
MA-21-1	MA-2E	0.75	3.40	184.06	0.341	0.207	0.00050	0.11	0.009	16
MA-21-2	MA-2D	0.75	3.40	184.06	0.338	0.210	0.00050	0.12	0.012	16
MA-21-3	MA-3	0.75	1.38	184.06	0.338	0.213	0.00050	0.12	0.040	16
MA-22-1	MA-2E	0.75	3.40	206.71	0.323	0.250	0.00054	0.14	0.012	16
MA-22-2	MA-2D	0.75	3.40	206.71	0.329	0.241	0.00054	0.13	0.015	16
MA-22-3	MA-3	0.75	1.38	206.71	0.332	0.238	0.00054	0.13	0.064	16
MA-23-1	MA-2E	0.75	3.40	259.38	0.335	0.305	0.00062	0.17	0.018	16
MA-23-2	MA-2D	0.75	3.40	259.38	0.335	0.299	0.00062	0.16	0.021	16
MA-23-3	MA-3	0.75	1.38	259.38	0.338	0.293	0.00062	0.16	0.128	16
MA-24-1	MA-2E	0.75	3.40	314.32	0.326	0.387	0.00070	0.22	0.030	16
MA-24-2	MA-2D	0.75	3.40	314.32	0.329	0.378	0.00070	0.21	0.052	16
MA-24-3	MA-3	0.75	1.38	314.32	0.326	0.381	0.00070	0.21	0.213	16
MA-25-1	MA-2E	0.75	3.40	379.45	0.332	0.451	0.00090	0.25	0.070	16
MA-25-2	MA-2D	0.75	3.40	379.45	0.332	0.436	0.00090	0.24	0.085	16
MA-25-3	MA-3	0.75	1.38	379.45	0.335	0.430	0.00090	0.24	0.250	16
MA-26-1	MA-2E	0.75	3.40	478.55	0.317	0.591	0.00150	0.34	0.189	16
MA-26-2	MA-2D	0.75	3.40	478.55	0.317	0.582	0.00150	0.33	0.189	16
MA-27-1	MA-2E	0.75	3.40	518.20	0.299	0.674	0.00200	0.39	0.219	16
MA-27-2	MA-2D	0.75	3.40	518.20	0.299	0.652	0.00200	0.38	0.201	16

Table 5. Summary of sand-scour experiments in hydrodynamics flume for sets 4 through 7.

Run ID	Mixture ID	Median Diameter D_{50} (mm)	Gradation Coefficient σ_g	Pier Diameter b (m)	Flow Discharge Q (l/s)	Approach Depth Y (m)	Approach Velocity V (m/s)	Froude Number Fr	Bed Slope S_o	Scour Depth D_s (m)	Flow Duration t (h)
HN-01-1	HN-1	1.87	3.70	0.051	6.91	0.040	0.207	0.33	0.00418	0.010	8
HN-01-2	HN-1	1.87	3.70	0.051	6.91	0.050	0.165	0.23	0.00418	0.003	8
HN-01-3	HN-1	1.87	3.70	0.070	6.91	0.056	0.143	0.19	0.00418	0.004	8
HN-02-1	HN-1	1.87	3.70	0.051	13.79	0.065	0.436	0.54	0.00418	0.025	8
HN-02-2	HN-1	1.87	3.70	0.051	13.79	0.073	0.351	0.41	0.00418	0.009	8
HN-02-3	HN-1	1.87	3.70	0.070	13.79	0.080	0.314	0.35	0.00418	0.013	8
HN-03-1	HN-1	1.87	3.70	0.051	10.90	0.061	0.354	0.46	0.00363	0.015	8
HN-03-2	HN-1	1.87	3.70	0.051	10.90	0.071	0.271	0.32	0.00363	0.008	8
HN-03-3	HN-1	1.87	3.70	0.070	10.90	0.074	0.235	0.28	0.00363	0.008	8
HN-04-1	HN-1	1.87	3.70	0.051	17.58	0.075	0.488	0.57	0.00336	0.028	10
HN-04-2	HN-1	1.87	3.70	0.051	17.58	0.079	0.399	0.45	0.00336	0.012	10
HN-04-3	HN-1	1.87	3.70	0.070	17.58	0.081	0.354	0.40	0.00336	0.014	10
HN-05-1	HN-1	1.87	3.70	0.051	20.67	0.075	0.521	0.61	0.00368	0.032	10
HN-05-2	HN-1	1.87	3.70	0.051	20.67	0.078	0.451	0.52	0.00368	0.027	10
HN-05-3	HN-1	1.87	3.70	0.070	20.67	0.078	0.421	0.48	0.00368	0.036	10
HN-10-1	HN-2	1.87	1.15	0.051	6.91	0.075	0.162	0.19	0.00375	0.002	11
HN-10-2	HN-2	1.87	1.15	0.051	6.91	0.088	0.128	0.14	0.00375	0.000	11
HN-10-3	HN-2	1.87	1.15	0.070	6.91	0.101	0.110	0.11	0.00375	0.000	11
HN-11-1	HN-2	1.87	1.15	0.051	9.00	0.077	0.216	0.25	0.00375	0.007	9
HN-11-2	HN-2	1.87	1.15	0.051	9.00	0.087	0.158	0.17	0.00375	0.000	9
HN-11-3	HN-2	1.87	1.15	0.070	9.00	0.101	0.140	0.14	0.00375	0.000	9
HN-12-1	HN-2	1.87	1.15	0.051	10.90	0.075	0.256	0.30	0.00391	0.048	14
HN-12-2	HN-2	1.87	1.15	0.051	10.90	0.085	0.189	0.21	0.00391	0.009	14
HN-12-3	HN-2	1.87	1.15	0.070	10.90	0.098	0.158	0.16	0.00391	0.014	14
HN-13-1	HN-2	1.87	1.15	0.051	12.35	0.078	0.274	0.31	0.00418	0.058	21
HN-13-2	HN-2	1.87	1.15	0.051	12.35	0.088	0.204	0.22	0.00418	0.012	21
HN-13-3	HN-2	1.87	1.15	0.070	12.35	0.101	0.180	0.18	0.00418	0.017	21
HN-14-1	HN-2	1.87	1.15	0.051	13.79	0.077	0.387	0.44	0.00417	0.077	19
HN-14-2	HN-2	1.87	1.15	0.051	13.79	0.088	0.296	0.32	0.00417	0.042	19
HN-14-3	HN-2	1.87	1.15	0.070	13.79	0.100	0.247	0.25	0.00417	0.018	19
HN-20-1	HN-2	1.87	1.15	0.051	16.88	0.073	0.445	0.53	0.00417	0.078	30
HN-20-2	HN-2	1.87	1.15	0.051	16.88	0.089	0.344	0.37	0.00417	0.066	30
HN-20-3	HN-2	1.87	1.15	0.070	16.88	0.097	0.290	0.30	0.00417	0.061	30
HN-21-1	HN-3	1.8	2.17	0.051	10.90	0.085	0.212	0.23	0.00341	0.012	17
HN-21-2	HN-3	1.8	2.17	0.051	10.90	0.091	0.189	0.20	0.00341	0.003	17
HN-21-3	HN-3	1.8	2.17	0.070	10.90	0.097	0.149	0.15	0.00341	0.007	17
HN-22-1	HN-3	1.8	2.17	0.051	13.79	0.087	0.273	0.30	0.00341	0.014	22
HN-22-2	HN-3	1.8	2.17	0.051	13.79	0.094	0.244	0.25	0.00341	0.012	22
HN-22-3	HN-3	1.8	2.17	0.070	13.79	0.097	0.213	0.22	0.00341	0.012	22
HN-23-1	HN-3	1.8	2.17	0.051	16.88	0.088	0.342	0.37	0.00341	0.031	25

Table 5. Summary of sand-scour experiments in hydrodynamics flume (continued).

Run ID	Mixture ID	Median Diameter D_{50} (mm)	Gradation Coefficient σ_g	Pier Diameter b (m)	Flow Discharge Q (l/s)	Approach Depth Y (m)	Approach Velocity V (m/s)	Froude Number Fr	Bed Slope S_o	Scour Depth D_s (m)	Flow Duration t (h)
HN-23-3	HN-3	1.80	2.17	0.070	16.88	0.095	0.258	0.27	0.00341	0.020	25
HN-24-1	HN-3	1.80	2.17	0.051	20.70	0.088	0.410	0.44	0.00323	0.048	24
HN-24-2	HN-3	1.80	2.17	0.051	20.70	0.087	0.377	0.41	0.00323	0.042	24
HN-29-3	HN-4	0.76	1.28	0.070	7.56	0.098	0.122	0.12	0.00000	0.002	8
HN-30-1	HN-4	0.76	1.28	0.051	9.74	0.076	0.232	0.27	0.00000	0.062	20
HN-30-2	HN-4	0.76	1.28	0.051	9.74	0.086	0.170	0.19	0.00000	0.024	20
HN-30-3	HN-4	0.76	1.28	0.070	9.74	0.096	0.152	0.16	0.00000	0.017	20
HN-31-1	HN-4	0.76	1.28	0.051	11.95	0.079	0.261	0.30	0.00000	0.081	21
HN-31-2	HN-4	0.76	1.28	0.051	11.95	0.091	0.191	0.20	0.00000	0.058	21
HN-31-3	HN-4	0.76	1.28	0.070	11.95	0.101	0.174	0.18	0.00000	0.047	21
HN-32-1	HN-4	0.76	1.28	0.051	13.79	0.079	0.298	0.34	0.00000	0.085	23
HN-32-2	HN-4	0.76	1.28	0.051	13.79	0.091	0.255	0.27	0.00000	0.066	23
HN-32-3	HN-4	0.76	1.28	0.070	13.79	0.101	0.205	0.21	0.00000	0.083	23

Table 6. Summary of river mechanics flume experiments to study pier width effects for set 8.

Run ID	Mixture ID	Median Diameter D_{50} (mm)	Gradation Coeficient σ_g	Pier Diameter b (m)	Approach Depth Y (m)	Approach Velocity V (m/s)	Bed Slope S_o (m/m)	Froude Number Fr	Scour Depth D_s (m)	Flow Duration t (h)
MH 11-1	MH-1	0.55	2.24	0.216	0.238	0.244	0.001	0.160	0.045	16
MH 10-1	MH-1	0.55	2.24	0.216	0.157	0.448	0.001	0.361	0.196	16
MH 9-1	MH-1	0.55	2.24	0.216	0.198	0.371	0.001	0.266	0.153	16
MH 8-1	MH-1	0.55	2.24	0.216	0.212	0.255	0.001	0.177	0.060	16
MH 7-1	MH-1	0.55	2.24	0.216	0.255	0.272	0.001	0.172	0.079	16
MH 6-1	MH-1	0.55	2.24	0.216	0.239	0.257	0.001	0.168	0.072	16
MH 5-1	MH-1	0.55	2.24	0.216	0.246	0.290	0.001	0.187	0.120	16
MH 12-1	MH-1	0.55	2.24	0.152	0.237	0.280	0.001	0.184	0.088	16
MH 13-1	MH-1	0.55	2.24	0.152	0.210	0.253	0.001	0.176	0.069	16
MH 14-1	MH-1	0.55	2.24	0.152	0.224	0.274	0.001	0.185	0.089	16
MH 15-1	MH-1	0.55	2.24	0.152	0.244	0.316	0.001	0.205	0.116	16
MH 16-1	MH-1	0.55	2.24	0.152	0.214	0.282	0.001	0.195	0.081	16
MH 17-1	MH-1	0.55	2.24	0.152	0.290	0.517	0.001	0.307	0.248	16
MH 18-1	MH-1	0.55	2.24	0.152	0.247	0.361	0.001	0.232	0.191	16
MH 19-1	MH-1	0.55	2.24	0.152	0.224	0.307	0.001	0.207	0.111	16
MH 11-3	MH-1	0.55	2.24	0.165	0.219	0.246	0.001	0.168	0.049	16
MH 10-3	MH-1	0.55	2.24	0.165	0.138	0.465	0.001	0.400	0.143	16
MH 9-3	MH-1	0.55	2.24	0.165	0.182	0.408	0.001	0.305	0.158	16
MH 8-3	MH-1	0.55	2.24	0.165	0.194	0.265	0.001	0.192	0.065	16
MH 7-3	MH-1	0.55	2.24	0.165	0.237	0.307	0.001	0.201	0.088	16
MH 11-2	MH-1	0.55	2.24	0.089	0.238	0.240	0.001	0.157	0.037	16
MH 10-2	MH-1	0.55	2.24	0.089	0.157	0.479	0.001	0.385	0.117	16
MH 9-2	MH-1	0.55	2.24	0.089	0.198	0.349	0.001	0.250	0.111	16
MH 8-2	MH-1	0.55	2.24	0.089	0.212	0.238	0.001	0.165	0.066	16
MH 7-2	MH-1	0.55	2.24	0.089	0.255	0.270	0.001	0.171	0.077	16
MH 6-2	MH-1	0.55	2.24	0.089	0.239	0.276	0.001	0.180	0.073	16
MH 11-4	MH-1	0.55	2.24	0.057	0.219	0.235	0.001	0.160	0.035	16
MH 10-4	MH-1	0.55	2.24	0.057	0.138	0.436	0.001	0.374	0.057	16
MH 9-4	MH-1	0.55	2.24	0.057	0.182	0.378	0.001	0.283	0.068	16
MH 8-4	MH-1	0.55	2.24	0.057	0.194	0.250	0.001	0.181	0.036	16
MH 7-4	MH-1	0.55	2.24	0.057	0.237	0.276	0.001	0.181	0.032	16
MH 10-5	MH-1	0.55	2.24	0.032	0.138	0.463	0.001	0.398	0.029	16
MH 9-5	MH-1	0.55	2.24	0.032	0.182	0.413	0.001	0.309	0.037	16
MH 8-5	MH-1	0.55	2.24	0.032	0.194	0.266	0.001	0.193	0.022	16
MH 7-5	MH-1	0.55	2.24	0.032	0.237	0.305	0.001	0.200	0.038	16
MH 10-6	MH-1	0.55	2.24	0.019	0.157	0.437	0.001	0.352	0.014	16
MH 9-6	MH-1	0.55	2.24	0.019	0.198	0.339	0.001	0.243	0.034	16
MH 8-6	MH-1	0.55	2.24	0.019	0.212	0.219	0.001	0.152	0.018	16

Table 7. Summary of gravel-scour experiments in sedimentation flume for sets 9 and 10.

Run ID	Mixture ID	Median Diameter D_{50} (mm)	Gradation Coefficient σ_g	Pier Diameter b (m)	Approach Depth Y (m)	Approach Velocity V (m/s)	Bed Slope S_o (m/m)	Froude Number F_r	Scour Depth D_s (m)	Flow Duration t (h)
MHG1-1	MH-2	16.90	1.28	0.178	0.296	0.850	0.0007	0.499	0.049	16
MHG2-1	MH-2	16.90	1.28	0.178	0.320	1.073	0.0007	0.605	0.073	16
MHG3-1	MH-2	16.90	1.28	0.178	0.338	1.192	0.0007	0.654	0.110	16
MHG4-1	MH-2	16.90	1.28	0.178	0.354	1.228	0.0007	0.659	0.113	16
MHG5-1	MH-2	16.90	1.28	0.178	0.372	1.384	0.0007	0.724	0.113	16
MHG6-1	MH-2	16.90	1.28	0.178	0.290	1.859	0.0007	1.103	0.110	16
MHG7-1	MH-2	16.90	1.28	0.178	0.238	2.286	0.0007	1.497	0.271	16
MHG1-2	MH-3	16.70	1.30	0.178	0.335	0.771	0.0007	0.425	0.073	16
MHG2-2	MH-3	16.70	1.30	0.178	0.357	0.969	0.0007	0.518	0.085	16
MHG3-2	MH-3	16.70	1.30	0.178	0.381	1.079	0.0007	0.558	0.119	16
MHG4-2	MH-3	16.70	1.30	0.178	0.357	1.186	0.0007	0.634	0.152	16
MHG5-2	MH-3	16.70	1.30	0.178	0.375	1.320	0.0007	0.688	0.183	16
MHG6-2	MH-3	16.70	1.30	0.178	0.250	2.018	0.0007	1.288	0.235	16
MHG7-2	MH-3	16.70	1.30	0.178	0.219	2.478	0.0007	1.688	0.305	16

2.4 ANALYSIS

This section presents the parameters affecting the pier scour in nonuniform mixtures and derives relationships to quantify their effects on the resulting scour depths. The equations derived from this analysis are then tested with the data from the experimental study and with data from earlier studies.

GOVERNING PARAMETERS

Experiments conducted for sets 1 through 3 varied the size gradation and coarse material fraction of six sand mixtures while keeping their median diameter constant. In these experiments, the flow depth was kept relatively constant, and the pier diameter remained 0.18 m while the discharge into the flume was incremented. Since the channel width and flow depth remained constant, this discharge variation in the experiments corresponded to varying velocity while keeping all other flow parameters constant. Figure 1 shows the variation of dimensionless scour depth in sets 1 through 3 experiments with approach velocity. By keeping all other variables constant, these experiments isolate the effects of gradation and coarse material fraction on pier scour. As shown in figure 1, the initiation of pier scour takes place independent of the size of coarse material fractions for approach velocities of about 0.18 m/s. This velocity is termed as the scour initiation velocity, V_i, and marks the threshold condition for clear-water scour. For approach velocities greater than V_i , the largest scour depth in figure 1 takes place in uniform sediment mixtures (gradation coefficient , σ_g = 1.38). As the size gradation coefficient increases from 1.38 to 2.43 to 3.4, the depth of scour decreases. This finding is in agreement with previous research. However, the reduction of scour is not a constant factor as suggested by earlier studies, but is a function of flow intensity. While the largest scour reduction takes place for an intermediate velocity value, for velocities slightly greater than 0.18 m/s and for velocities greater than 0.6 m/s, the scour reduction remains small. Figure 1 also shows two mixtures with the same median sediment sizes and gradation coefficients but with enlarged coarse fractions. In mixtures identified as 2.38A and 2.38B, while D_{50} and σ_g were kept at 0.75 mm and 2.43, respectively, the coarsest 5-percent and 10-percent fractions were enlarged by replacing these size groups with coarser sediments. As a result, as shown in figure 1, the scour depths corresponding to these mixtures are smaller. In fact, the scour observed for the mixture with enlarged coarsest 10-percent fraction (mixture 2.43 A) is the same as the scour observed in mixture 3.4A with a gradation coefficient of 3.4. Similarly, introducing larger coarse fractions to mixture 3.4A results in further reduction in scour depth.

Figure 2 compares the results of sets 1 through 3 experiments with the computed scour values from the CSU equation given in Federal Highway Administration's (FHWA) HEC-18[13]. In figure 2 several observations can be made: 1) As the intensity of flow increases (indicated by larger scour depth) the computed scour depths approach the measured values; 2) For larger gradation factors and for mixtures with larger coarse fractions, the convergence of computed and measured values takes place at higher flow intensities; and 3) At low flow intensities the computed values are in the order of 8 to 10

times the measured values. In figure 3, the ratio of measured to computed scour depth is plotted against the flow velocity for sets 1 through 3 experiments. For these data, this ratio approaches 1 (perfect agreement) as the flow velocity (or intensity) increases. For a given flow velocity, the ratio is closer to 1 for uniform mixtures (illustrated in the figure by the 1.38 gradation coefficient above the plot points) than for mixtures with large size variations (illustrated by the 3.40 gradation coefficient above the plot points). A general conclusion from figures 2 and 3 is that the discrepancy between measured and computed scour depths, using the current CSU equation, becomes worse as the gradation coefficient increases and as the velocity (or flow intensity) decreases.

Figure 4 shows results from set 4 through 7 experiments conducted using coarser sediment mixtures and compares these results with the finer uniform sand mixture used in sets 1 through 3. In these experiments smaller depths and pier diameters were used; without applying proper modeling scale ratios for flow depth and pier diameter the results cannot be superimposed on the previous results. However, the pattern of scour depth variation with flow intensity remains identical. Both in figures 1 and 4 the relationship between velocity and D_s /b shows that for uniform material, the variation of scour with velocity is almost linear. For graded material, and material with larger coarse fractions, this relationship assumes the characteristics of 2nd or 3rd degree polynomial (concave). At high flow velocities, both figures show that scour values tend to converge to an "ultimate" value. The velocity at which maximum clear-water scour takes place is a function of the size of coarsest size fractions present in mixtures. This velocity is identified as the critical velocity, V_c, at which the entire bed is mobilized (live-bed conditions).

It is possible to define a dimensionless excess velocity, ψ, which is a relative velocity with respect to the critical velocity that fully mobilizes the bed given by:

$$\psi = \frac{V - V_i}{V_c - V_i}; \qquad 0 \le \psi \le 1 \tag{4}$$

The value of ψ varies between 0 and 1; the 0 corresponding to initiation of scour and 1 corresponding to the condition of fully mobilized bed. The values of V_i and V_c can be determined by relating these velocities to critical flow conditions corresponding to initiation of motion. Using Shields' relationship for critical shear

$$\tau_c = K\gamma_s^{'} D_r \tag{5}$$

or

$$\gamma R S = K\gamma_s^{'} D_r \tag{6}$$

where τ_c = critical shear; K = experimental constant (≈ 0.047); γ_s' = submerged specific weight of sediment ($\approx 1.65\gamma$); R = hydraulic radius; S = slope of the energy grade line; and D_r = characteristic sediment size. For critical conditions, using Manning-Strickler equation to express the slope of the energy line in terms of approach velocity ($S = V_c^2 n^2 / R^{2/3}$, where V_c and R are in metric units) and using a relationship expressing the roughness coefficient, n, in terms of the characteristic sediment size ($n = D_r^{1/6}$ /26.1, where D_r is in meters) it is possible to obtain:

$$\gamma \frac{V_c^2 D_r^{1/3}}{26.1^2 R^{1/3}} = 0.047\, \gamma_s' D_r \tag{7}$$

or

$$V_c = 26.1 \sqrt{\frac{0.047\, \gamma_s'}{\gamma}}\, D_r^{1/3} R^{1/6} = K_* \; D_r^{1/3} R^{1/6} \tag{8}$$

where V_c , R, and D_r are in SI units. Replacing γ_s'/γ with 1.65 and after simplifications, equation 8 reduces to $V_c(\text{m/s}) \approx 7.27 D_r(\text{m})^{1/3} Y(\text{m})^{1/6}$. In English units, the critical velocity expression becomes V_r (ft/sec) ≈ 13.16 D_r (ft)$^{1/3}$ Y (ft)$^{1/6}$. For the purposes of this study, however, the constant K_* in equation 8 is left to be an experimentally determined value. Using results of pier scour experiments, K_* was found to be 6.625 for SI units (using D_r in meters) and 12 for English units (using D_r in feet). To reflect the characteristics of the coarse material fractions, the representative sediment size, D_r, is defined by the median size of the coarse material fraction, D_{cfm}, given by:

$$D_{cfm} = \frac{D_{85} + 2D_{90} + 2D_{95} + D_{99}}{6} \tag{9}$$

The parameter D_{cfm} is a representative size (in meters for SI units and in feet for English units) for the coarse fractions present in sediment mixtures. Experimental evidence in figures 1 and 4 indicate that fully mobilized bed cannot be achieved without mobilizing coarser sizes. In the absence of extensive size information, or in cases where there are no discontinuities in the size gradation curves, it is possible to utilize D_{90} to represent coarse fractions.

Velocities in the vicinity of piers are amplified. From potential flow theory, this amplification is in the order of 1.7 times the approach velocity. The scour initiation takes place when the accelerated flows past the pier are capable of removing the bed material from the pier region. Experimental evidence indicates that these velocities are dependent on the finer size fractions that are significantly available in the bed. For this study, the representative size for initiation of motion was determined to be D_{35}. This size was used

in the sedimentation literature by Einstein and Chien[14], Ackers and White[15] to account for the gradation effects in the transport of bed material. The expression for the initiation of pier scour can be derived from the critical velocity relationship and can be expressed as:

$$V_i = K'' D_{35}^{1/3} Y^{1/6} \quad (10)$$

where K'' is an experimental coefficient. From the pier scour experiments, the value of K'' was found to be 2.65 for SI units using D_{35} in meters (4.8 for English units using D_{35} in feet).

Using the dimensionless velocity factor ψ, the data presented earlier in figure 1 are expressed in figure 5. Figure 5 shows that while maximum scour depth is reached at $\psi = 0.6$ for the uniform mixture, for graded sediments higher flow intensities may be needed. This figure also shows that for mixtures with coarse fractions, low relative flow intensities produce significantly smaller scour depths. For these mixtures, ultimate scour is produced sharply beyond a threshold intensity. Figure 5 indicates that even though the ultimate scour might be the same, for intermediate flows, different mixtures exhibit different scour patterns. The information in figure 5 is reproduced in figure 6 in nondimensional form.

Figures 7 and 8 present dimensionless velocity versus depth of scour for sets 4 through 7, 8, and 9. In these figures the parameter D_{cfm} is used to differentiate between mixtures with the same median size and gradation coefficient. As shown, the representative coarse fraction size, D_{cfm}, can reliably identify mixtures and therefore can be used in relationships to quantify the associated scour depths. In general, for the same dimensionless velocity factor, smaller D_{cfm} values are associated with larger scour depths. However, a more reliable factor in differentiating sediment properties of mixtures is the D_{cfm}/D_{50} ratio used in figure 9. This dimensionless parameter can be used to normalize different sediment sizes for their expected scour potential. In figure 9, D_{cfm}/D_{50} values of 1.23 and 1.46 represent two uniform mixtures with median sizes of 1.80 mm and 0.75 mm, respectively. For a given dimensionless velocity factor, the mixture with the larger sediment size but with smaller D_{cfm}/D_{50} ratio produces larger scour holes. This experimental observation can be used to formulate an expression by relating scour to flow intensity (as represented by dimensionless flow velocity factor, ψ) and the relative coarse fraction size, D_{cfm}/D_{50}.

To achieve this goal, scour taking place in uniform material must first be evaluated. Then, ratios of scour values observed in mixtures with varying amounts of coarse material to scour in uniform material must be evaluated. This ratio, which is termed as the "Coarse Fraction Reduction Factor," and denoted by K_4, must then be related to flow intensity and D_{cfm}/D_{50}. Figure 10 shows the results of this procedure for set 1 through 3 experiments. Several conclusions can be drawn from figure 10:

(1) Scour reduction due to presence of coarse material cannot be expressed with a single value.

(2) Scour reduction is a function of the coarse sediment fraction ratio D_{cfm}/D_{50}. The higher the ratio, the lower the minimum value of K_4.

(3) For low flow intensities, and therefore ψ values near zero, the K_4 value must be unity since at low flow intensities there could be no effects due to coarse fractions or gradation.

(4) For high flow intensities, and therefore ψ values near or greater than unity, the K_4 value must also approach unity. At high flow intensities with fully mobilized bed, effects due to the presence of coarse fractions must be minimal.

(5) There exists a certain flow intensity ψ at which the scour reduction is minimum for a given sediment mixture. The location and magnitude of the minimum depend on the distribution and modality of sediment mixtures.

DERIVATION OF K_4 RELATIONSHIP

Two steps are needed in order to derive a functional relationship for K_4: 1) develop an expression for pier scour in uniform mixtures; and 2) separate the effects due to coarse fractions and develop an appropriate function.

Set 8 experiments given in table 6 were used to define the variation of local scour with pier diameter. Figures 11 and 12 show the variation of dimensionless scour depth with approach velocity for the six pier diameters used in the study. Since the flow depth was kept relatively constant for these experiments, and since the investigation of these effects was beyond the scope of the experimental study, the commonly accepted depth dependency of $Y^{1/6}$ was assumed for this study in normalizing the results. The best-fit line for describing the variation of scour with pier width in the pier width effect experiments utilizing 0.55-mm graded sand and the corresponding correlation coefficient are given by:

$$\frac{D_s}{b^{0.66}Y^{0.17}} = 0.97\psi^{0.72}; \qquad R^2 = 0.90 \tag{11}$$

where D_s, b, and Y are in meters and R^2 is the correlation coefficient. This relationship demonstrates that scour is related to pier diameter according to $D_s \sim b^{0.66}$. The goodness of fit of this relationship is shown in figure 13.

Next, utilizing $D_s/(b^{0.66}Y^{0.17})$ and ψ as variables, an expression for pier scour in uniform mixtures was developed. For this purpose, the present experiments with median sediment sizes ranging from 0.75 mm to 1.80 mm and to 17 mm were utilized. The resulting expression in International System (SI) units is:

$$\frac{D_s}{b^{0.66}Y^{0.17}} = 0.99\ \psi^{0.55}; \qquad 0 \le \psi \le 1 \tag{12}$$

in which D_s, b, and Y are in meters. For preferred English units, the coefficient 0.99 becomes 1.21; D_s, b, and Y are in feet.

In using equation 12, a limiting value of 1 must be imposed on ψ to reflect maximum clear-water scour conditions. Figures 14 and 15 show the goodness of fit of the data to this equation. In figure 15 additional data (126 points) from Chabert and Engeldinger[16] and Shen, Schneider, Karaki[17, 18] that were used in the development of FHWA's CSU equation are included. This demonstrates the agreement of the new equation with other data sources. For comparison purposes, figure 16 presents the same uniform material data with the CSU equation. As expected, for coarse material and gravel, the CSU equation does not perform well.

The last stage in the development was the derivation of an expression to separate the effects due to coarse material fractions. This expression was derived through an extensive search for a function that could describe the physical phenomenon explained earlier in figure 10. These conditions are:

- At low flow intensities ($\psi \approx 0$), effects due to coarse fraction are negligible since at these flows only finer fractions are scoured;
- At high flow intensities ($\psi \geq 0.8$), effects due to coarse fraction are also negligible since at these flows the entire mixture is mobilized;
- At intermediate flow intensities scour reduction is a function of both ψ and D_{cfm}/D_{50}; and
- Maximum scour reduction takes place for ψ values varying from 0.1 to 0.3.

The resulting expression is:

$$\frac{D_s}{b^{0.66} Y^{0.17}} = K_U \; K_1 \; K_2 \, K_3 \, K_4 \; \psi^{0.55}; \qquad 0 \leq \psi \leq 1 \tag{13}$$

where K_U = 0.99 for SI units, in which D_s, b, and Y are in meters (=1.21 for preferred English units, in which D_s, b, and Y are in feet); K_1, K_2, and K_3 are as defined in HEC-18[13]; and K_4 is the Coarse Fraction Factor defined by:

$$K_4 = 1.25 + 3\sqrt{\frac{D_{cfm}}{D_{50}}} \; \psi^{0.60} \, ln(\psi + 0.5); \qquad 0 \leq K_4 \leq 1, \quad 0 \leq \psi \leq 1 \tag{14}$$

where ψ is the dimensionless excess velocity from equation 4.

Figure 17 shows the data from set 1 through 3 experiments along with predictions from FHWA's CSU equation[13] and the new K_4 relationship. The goodness of fit is demonstrated in figure 18. In these figures, at low flow intensities and in the presence of coarse material, the performance of the CSU equation was poor. However, at high flow intensities, the CSU predictions converged with the new method and the measurements.

Figures 19 and 20 show the new equations with all available data from this study and with the data from earlier studies that were used in the development of the earlier CSU equation (a total of 310 data values). The performance of the CSU equation with the same data set is illustrated in figure 21.

2.5 ADJUSTMENTS TO FHWA'S CSU EQUATION

Figure 22 compares the present HEC-18[13] correction for coarse material size with the new approach. As shown, the modifications proposed in HEC-18 cannot fully

accommodate size corrections since this factor does not involve any sizes and provides maximum correction at $\psi = 0$ (no scour condition).

From the analysis of all data, it is concluded that two adjustments are needed for FHWA's CSU equation: 1) implementation of initiation of scour for uniform mixtures with larger sediment diameters than those used in the derivation of the model; and 2) implementation of gradation and coarse fraction size correction for nonuniform sediment mixtures.

Since the equation was originally developed for fine sands, the initiation of motion took place at very low velocities, and therefore the need for such correction was not obvious. For coarser sediments at low flow intensities, the present analysis amplifies this deficiency. The initiation of scour may be implemented into the CSU equation by the inclusion of a scour initiation factor, K_i. This factor was found to be:

$$K_i = \left(1 - \frac{V_i}{V}\right)^{0.45} \quad ; \qquad V > V_i \tag{15}$$

For values of $V \le V_i$, the value of the initiation of scour factor, K_i, is 0.

Figure 23 compares the adjusted scour computations with the presently used K_4 adjustment. The results are almost identical. The reason for this is due to the fact that the current K_4 is merely a correction for the initiation of motion since the expression used for K_4 in HEC-18 is independent of relative sizes.

The second adjustment to the CSU equation to implement gradation and coarse fraction size correction for nonuniform sediment mixtures may be accomplished through the K_4 factor defined earlier:

$$K_4 = 1.25 + 3\sqrt{\frac{D_{cfm}}{D_{50}}}\ \psi^{0.60}\ ln(\psi + 0.5); \qquad 0 \le K_4 \le 1, \qquad 0 \le \psi \le 1 \tag{14}$$

The final form of the CSU equation is:

$$\frac{D_s}{Y} = 2\ K_1\ K_2\ \ K_3\ K_i\ K_4 \left(\frac{b}{Y}\right)^{0.65} \left(\frac{V}{\sqrt{gY}}\right)^{0.43} \tag{16}$$

where the definition of terms K_1, K_2, and K_3 are as defined in HEC-18. Figures 24 and 25 show the results of pier scour depth computations using both K_i and K_4 and compares the results with the results from this study. As seen, major improvement takes place in the predictions. The final results are comparable to those obtained from the study with slight overestimations.

2.6 SUMMARY AND CONCLUSIONS

A new pier scour equation describing effects of gradation and coarse material fraction on pier scour was developed. This equation is given as:

$$\frac{D_s}{b^{0.66}\,Y^{0.17}} = K_U\ K_1\ K_2\,K_3\,K_4\ \psi^{0.55}; \qquad 0 \le \psi \le 1 \tag{13}$$

where K_U = 0.99 for SI units, in which D_s, b, and Y are in meters (= 1.21 for preferred English units, in which D_s, b, and Y are in feet); K_1, K_2, and K_3 are as defined in HEC-18; and ψ = the dimensionless excess velocity factor given by

$$\psi = \frac{V - V_i}{V_c - V_i}; \qquad 0 \le \psi \le 1 \tag{4}$$

The definitions of the critical and scour initiating velocities, V_c and V_i , respectively are:

$$V_c = K_c\ D_{cfm}^{1/3}\ Y^{1/6} \tag{8}$$

$$V_i = K_i\ D_{35}^{1/3}\ Y^{1/6} \tag{10}$$

where K_c = 6.625 for SI units (= 12.0 for preferred English units); K_i = 2.65 for SI units (= 4.8 for preferred English units); and D_{cfm} is the median size of the coarse material fractions (in meters for SI units and in feet for English units) computed from

$$D_{cfm} = \frac{D_{85} + 2D_{90} + 2D_{95} + D_{99}}{6} \tag{9}$$

The coarse fraction reduction factor K_4 is given by:

$$K_4 = 1.25 + 3\sqrt{\frac{D_{cfm}}{D_{50}}}\ \psi^{0.60}\ ln(\psi + 0.5); \qquad 0 \le K_4 \le 1, \qquad 0 \le \psi \le 1 \tag{14}$$

By definition, both K_4 and ψ cannot be greater than 1. The new equation has the following characteristics:

(1) For uniform mixtures, it accommodates the initiation of motion at low flow intensities; for velocities smaller than the scour initiating velocities, no scour is computed.

(2) The computed results are bounded by the imposition of a limiting condition for ψ of 1 (live-bed conditions).

(3) It is physically based. No scour reduction at initiation of motion or at high flow intensities.
(4) Scour reduction is expressed as a function of relative coarse fraction size and the intensity of flow.
(5) It was verified with past experimental data (170 points), including data used in the development of FHWA's CSU equation. It also showed excellent agreement with Jain and Fisher's data for supercritical flows.
(6) It was shown to be applicable to size ranges from 0.24-mm fine sand to 17-mm gravel mixtures.
(7) It was tested successfully with 370 data sets with close agreement.

The work on the existing FHWA CSU equation also provided very promising results. The adjustments needed for the FHWA equation were: 1) implementation of initiation of scour for uniform mixtures with larger sediment diameters than those used in the derivation of the model; and 2) implementation of gradation and coarse fraction size correction for nonuniform sediment mixtures.

The initiation of scour is implemented into the CSU equation by the inclusion of K_i factor. This factor was found to be:

$$K_i = \left(1 - \frac{V_i}{V}\right)^{0.45} \quad ; \qquad V > V_i \tag{15}$$

For values of $V \le V_i$, the value of the initiation of scour factor, K_i, is 0.

Gradation and coarse fraction size correction for nonuniform sediment mixtures is implemented into the CSU equation through the K_4 factor defined earlier as:

$$K_4 = 1.25 + 3\sqrt{\frac{D_{cfm}}{D_{50}}}\ \psi^{0.60}\ ln(\psi + 0.5); \qquad 0 \le K_4 \le 1, \quad 0 \le \psi \le 1 \tag{14}$$

The final form of the CSU equation is:

$$\frac{D_s}{Y} = 2\ K_1\ K_2\ \ K_3\ K_i\ K_4 \left(\frac{b}{Y}\right)^{0.65} \left(\frac{V}{\sqrt{gY}}\right)^{0.43} \tag{16}$$

where the definition of terms K_1, K_2, and K_3 are as defined in HEC-18.

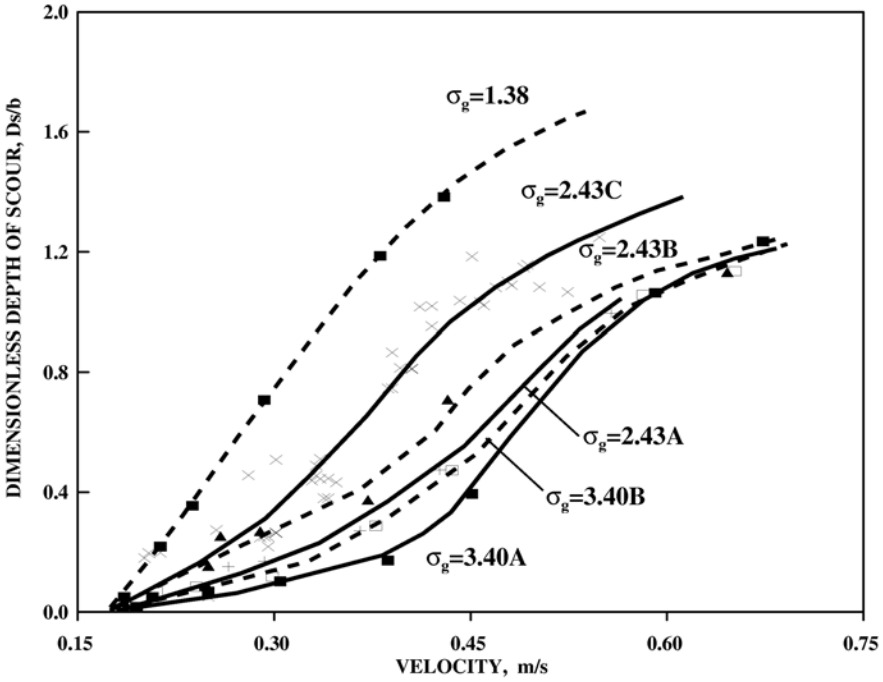

Figure 1. Variation of scour depth with velocity for sand mixtures used in sets 1 through 3.

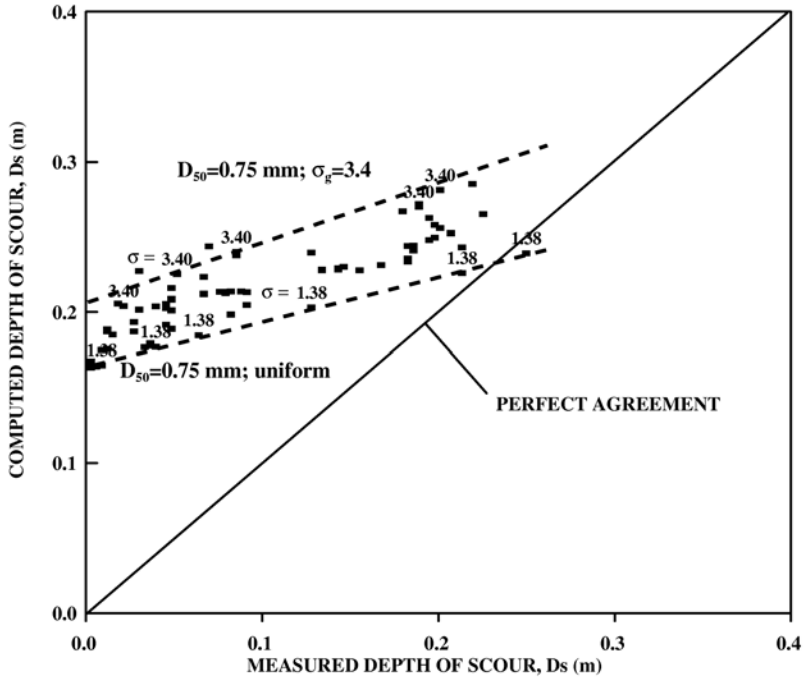

Figure 2. Comparison of FHWA's CSU equation with measured scour from sets 1 through 3.

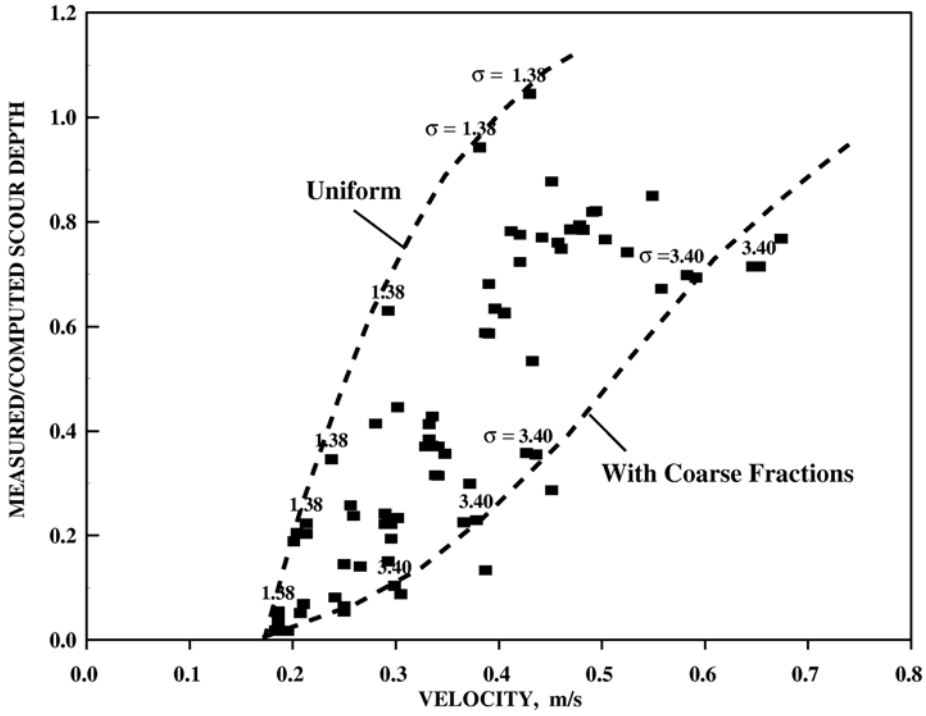

Figure 3. Velocity versus discrepancy ratio for sets 1 through 3 experiments.

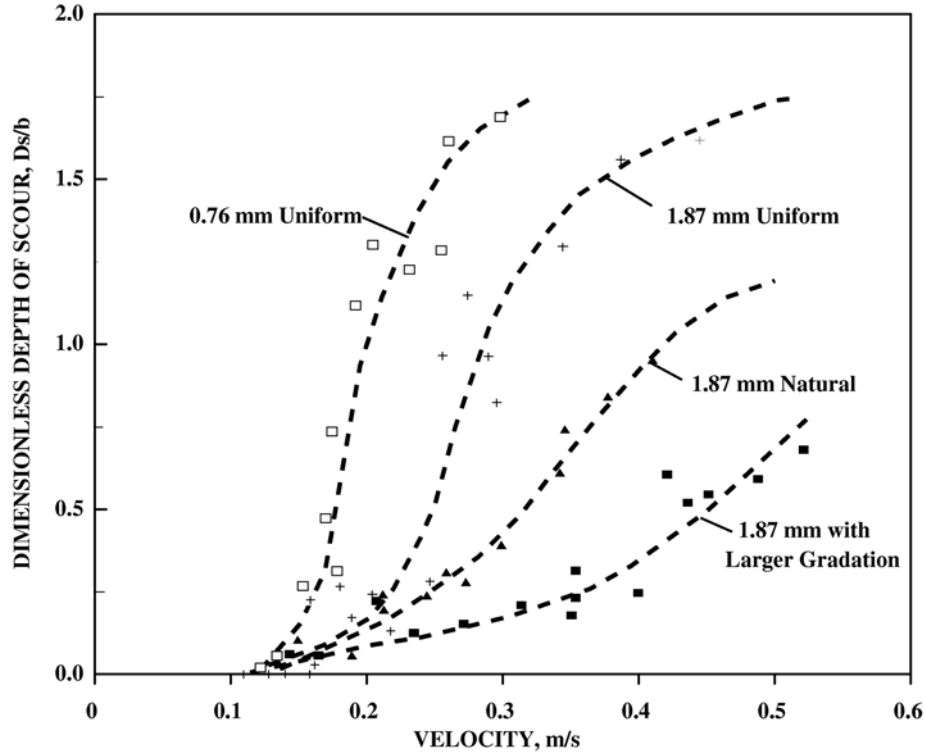

Figure 4. Flow velocity versus dimensionless scour for sets 4 through 7 experiments.

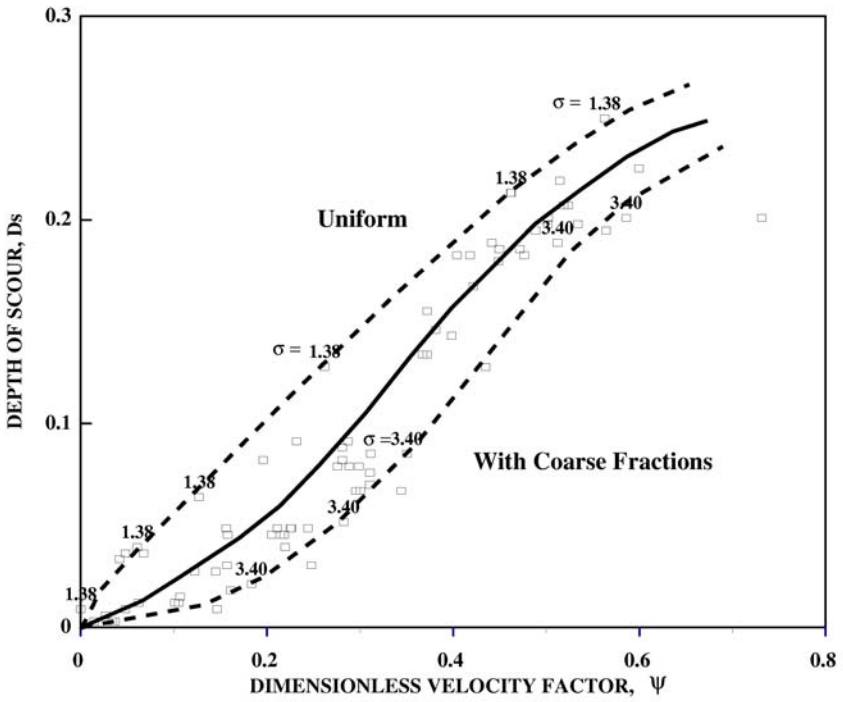

Figure 5. Dimensionless excess velocity factor, ψ, versus depth of scour for sets 1 through 3.

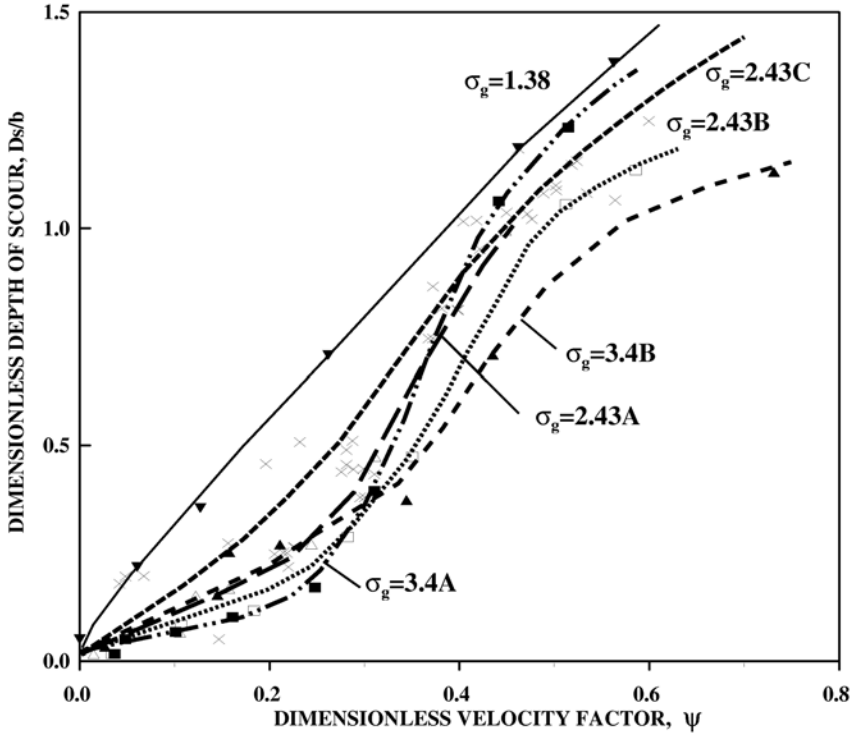

Figure 6. Variation of dimensionless scour with excess velocity factor for various mixtures.

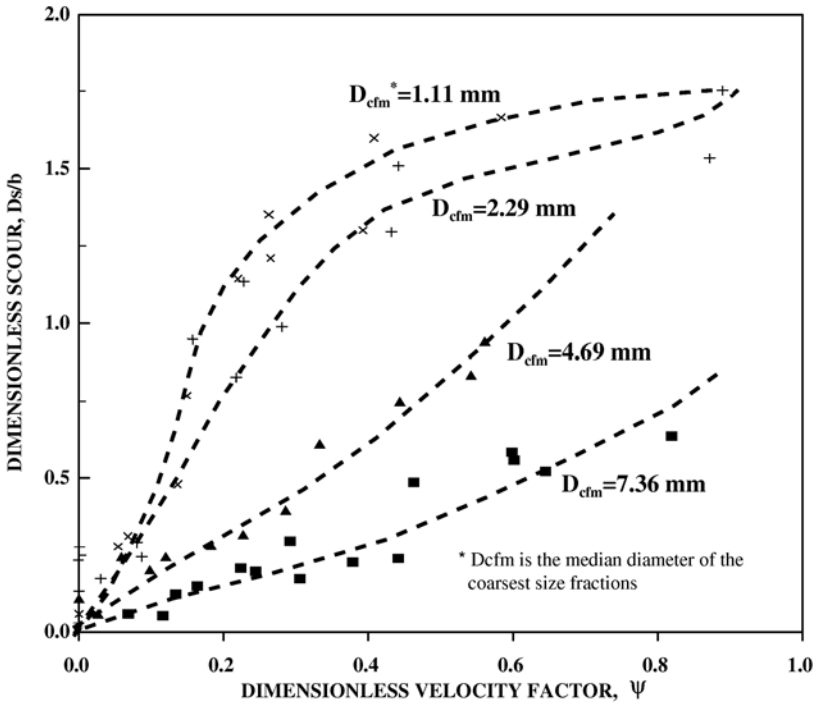

Figure 7. Variation of dimensionless scour with excess velocity factor, ψ, for different coarse fraction sizes used in sets 4 through 7 experiments.

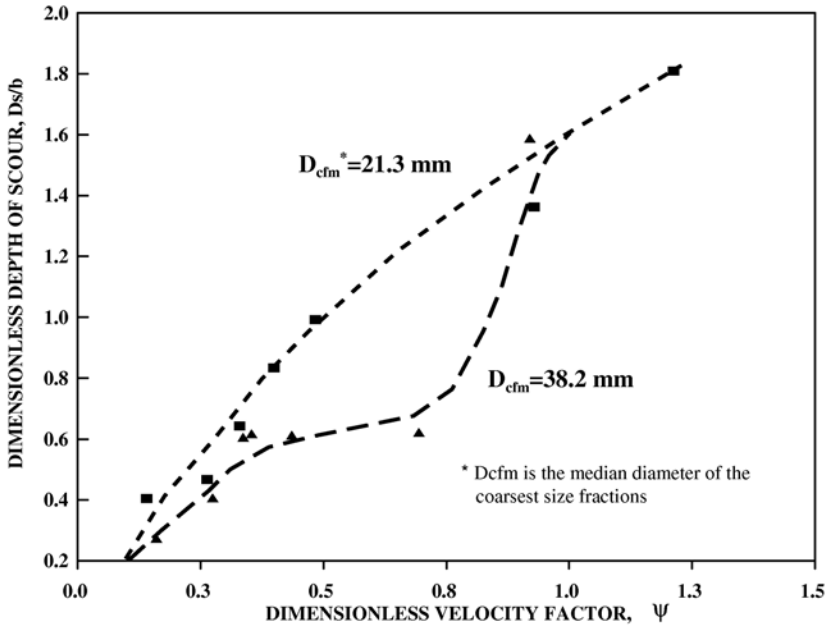

Figure 8. Variation of dimensionless scour with excess velocity factor, ψ, for different coarse fraction sizes used in sets 8 and 9.

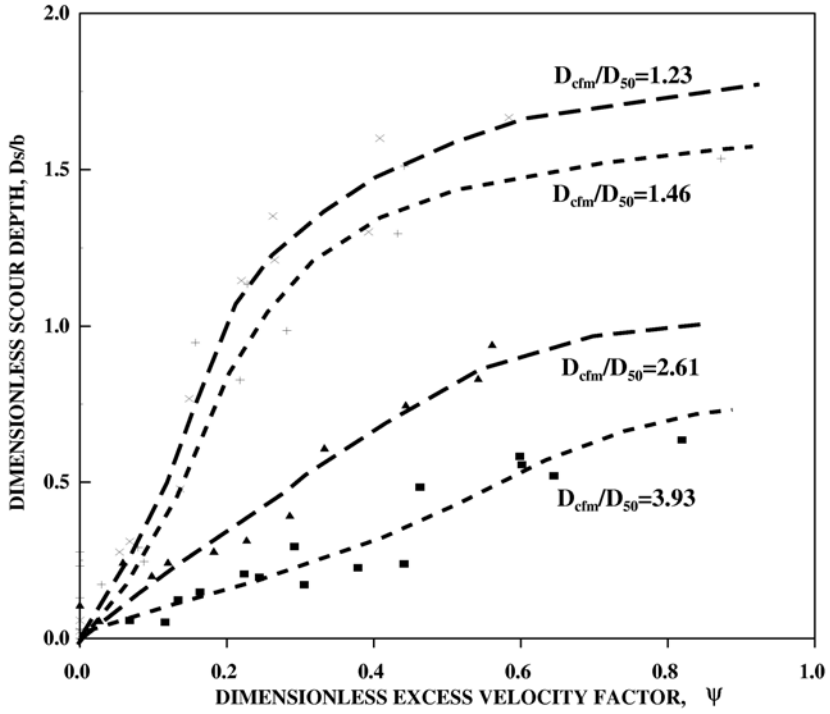

Figure 9. Variation of scour depth with excess velocity factor, ψ, for different coarse fraction size ratios used in sets 4 through 7 experiments.

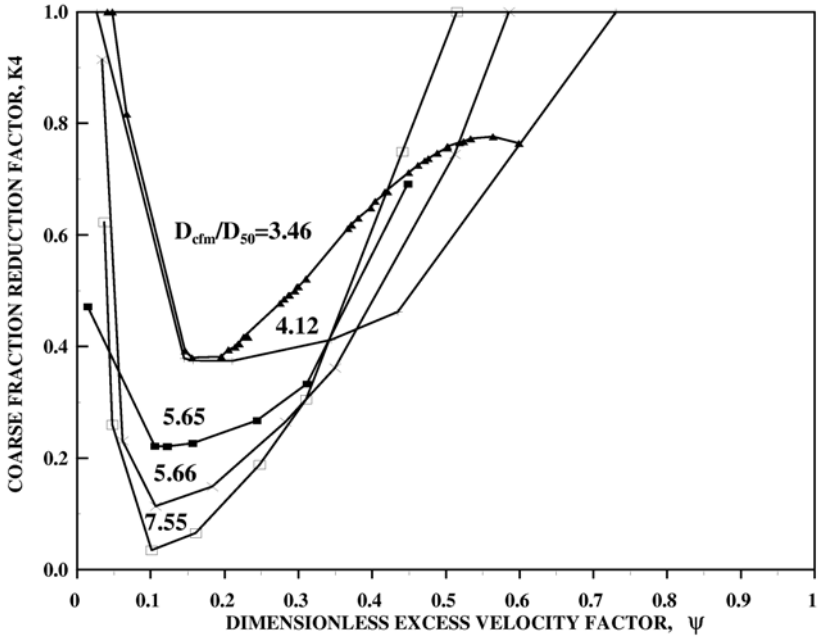

Figure 10. Variation of measured coarse fraction reduction factor, K_4, with excess velocity factor, ψ, for sets 1 through 3 experiments.

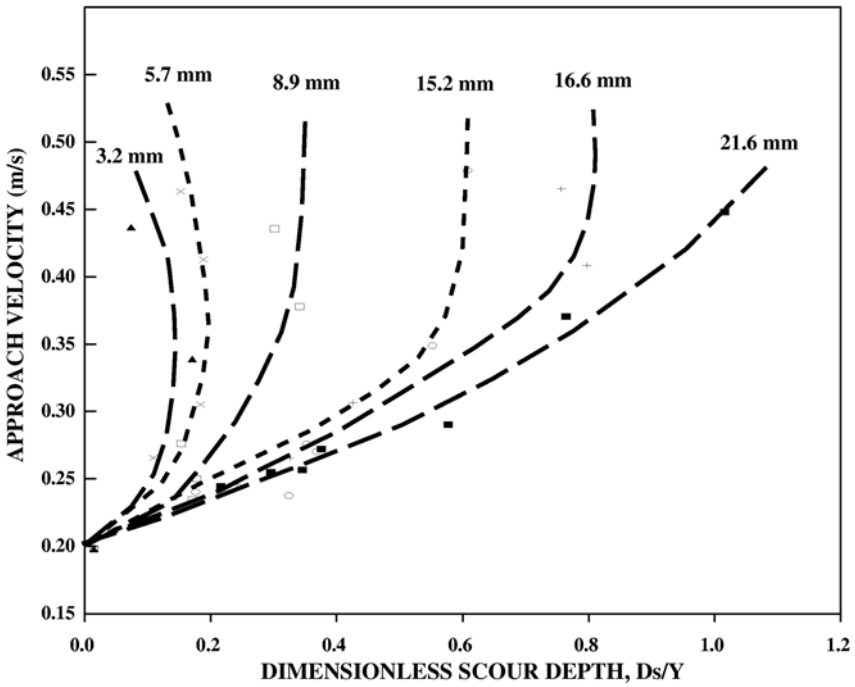

Figure 11. Variation of scour depth with pier size for the set 8 experiments.

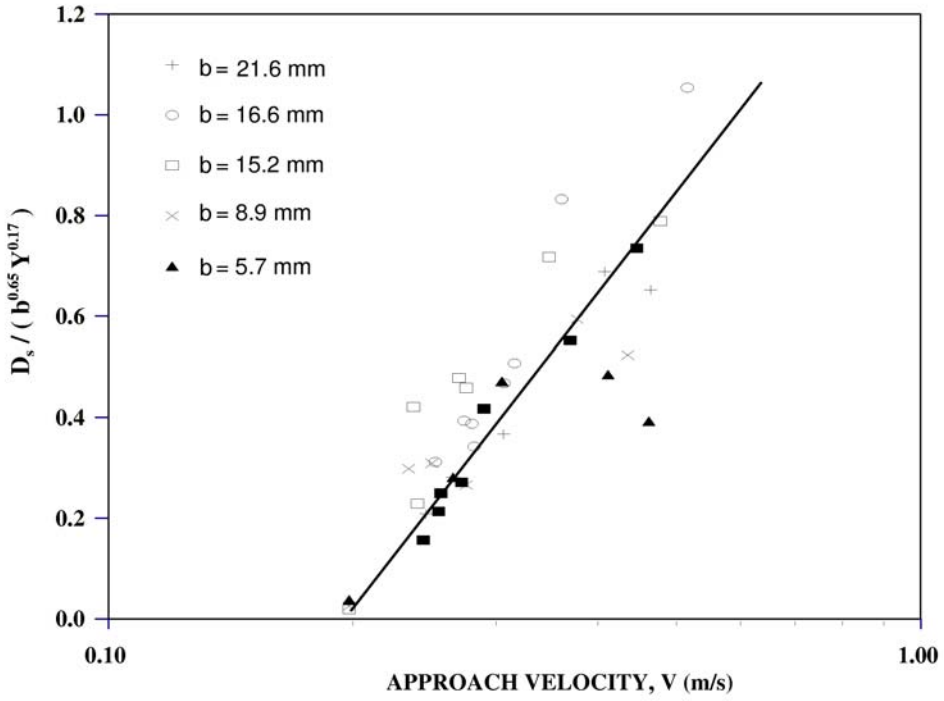

Figure 12. Relationship describing variation of pier scour with diameter.

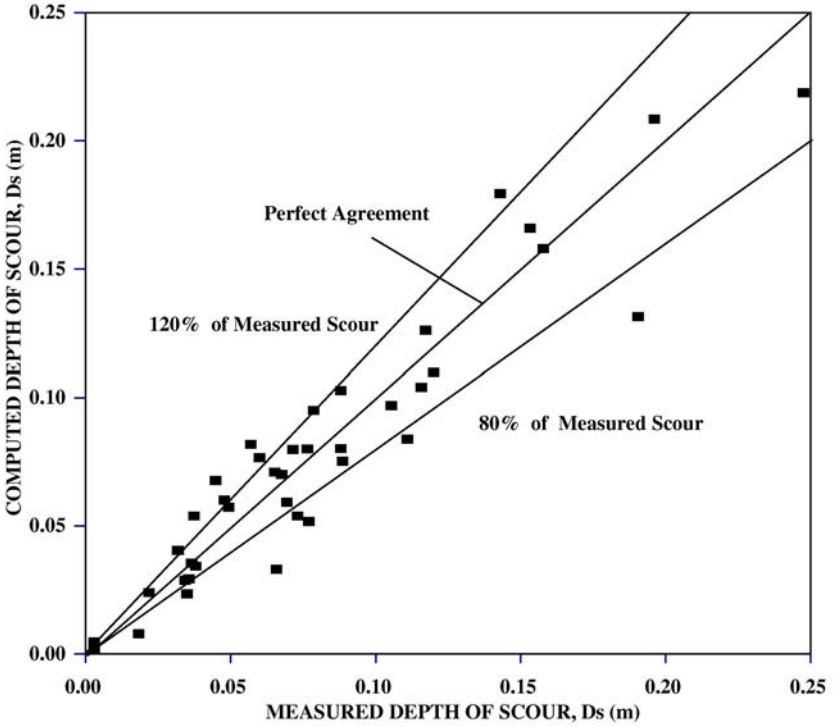

Figure 13. Computed and measured scour depths for the set 8 experiments.

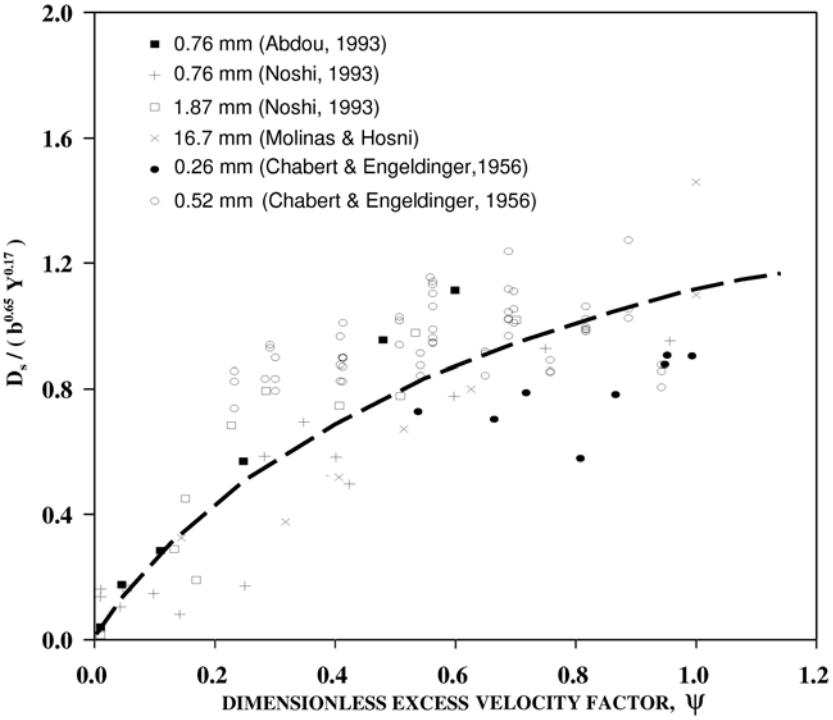

Figure 14. Variation of scour depth with excess velocity factor, ψ, for uniform sand and gravel.

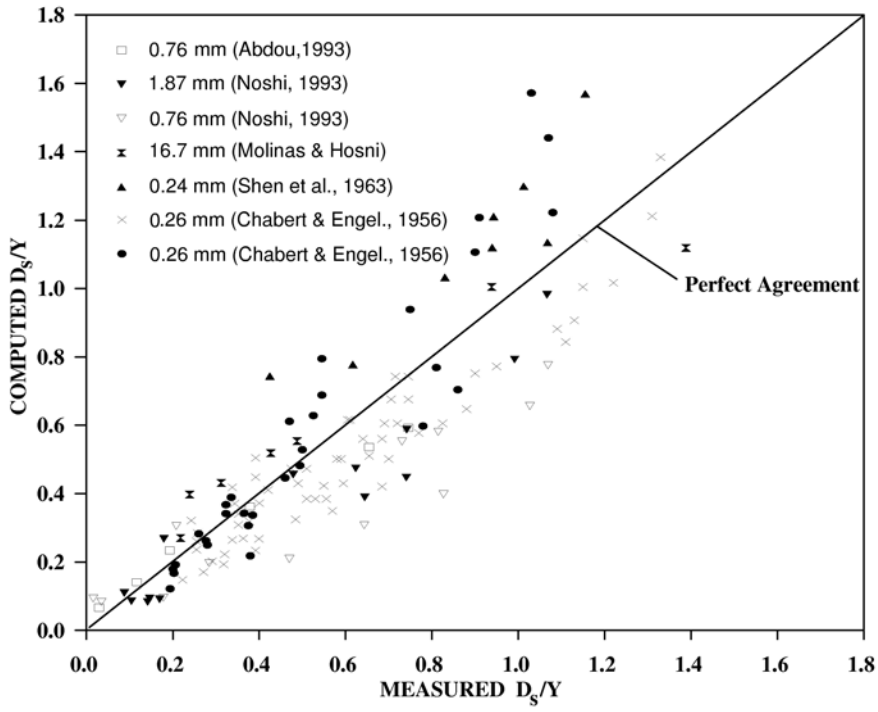

Figure 15. Measured and computed depth of scour for uniform sands and gravel using equation 12.

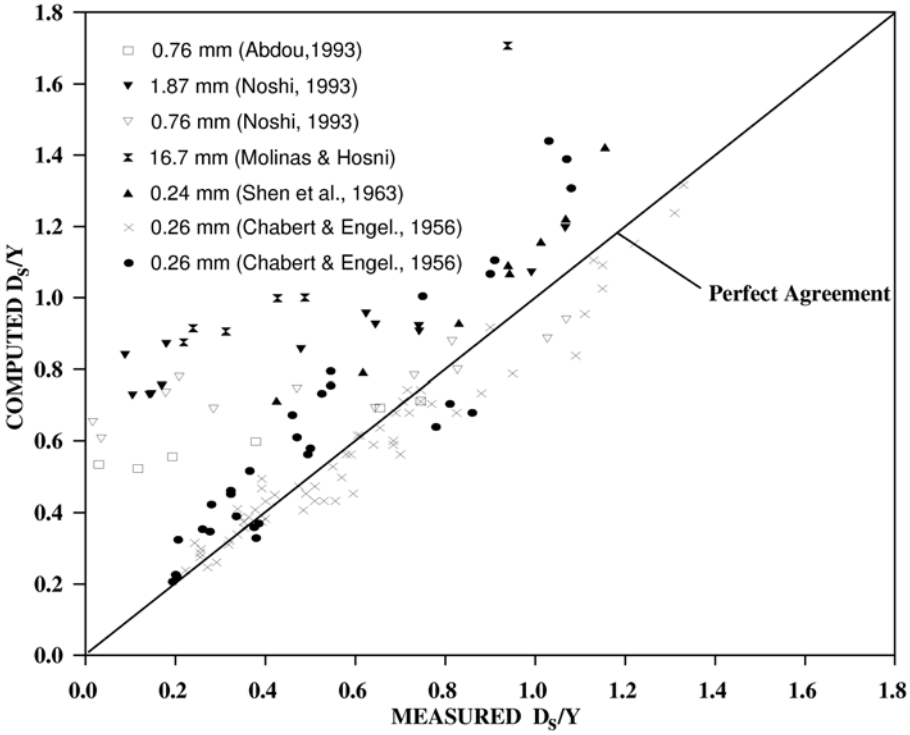

Figure 16. Measured and computed scour for uniform sediment using FHWA's CSU equation.

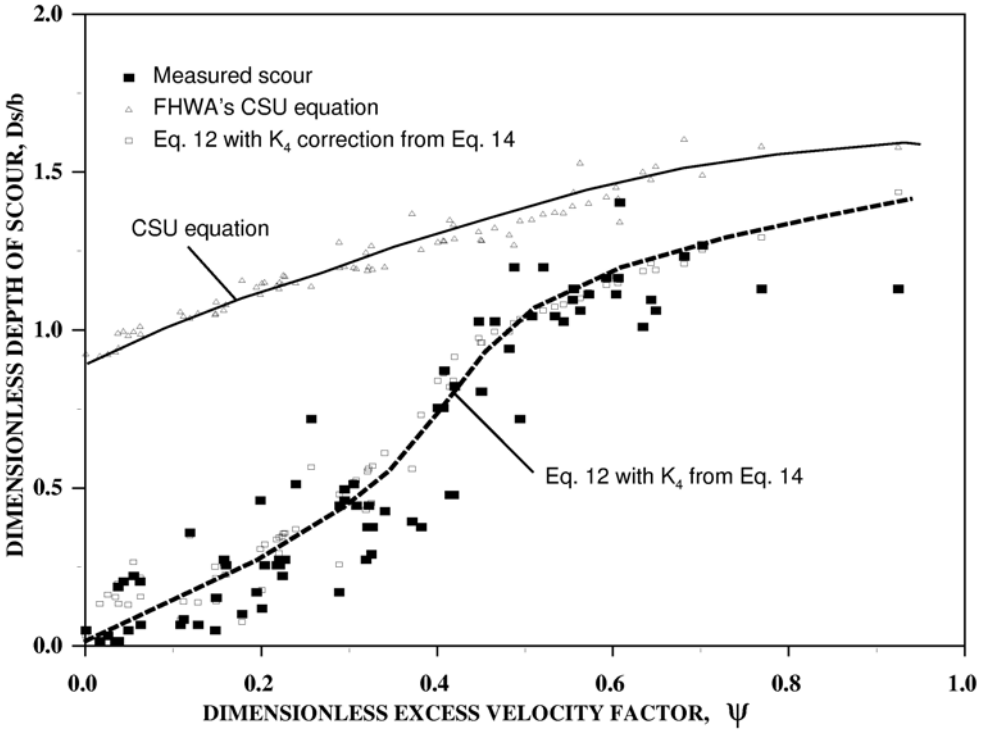

Figure 17. Computed scour for sets 1 through 3 experiments using equation 12 with K_4 from equation 14.

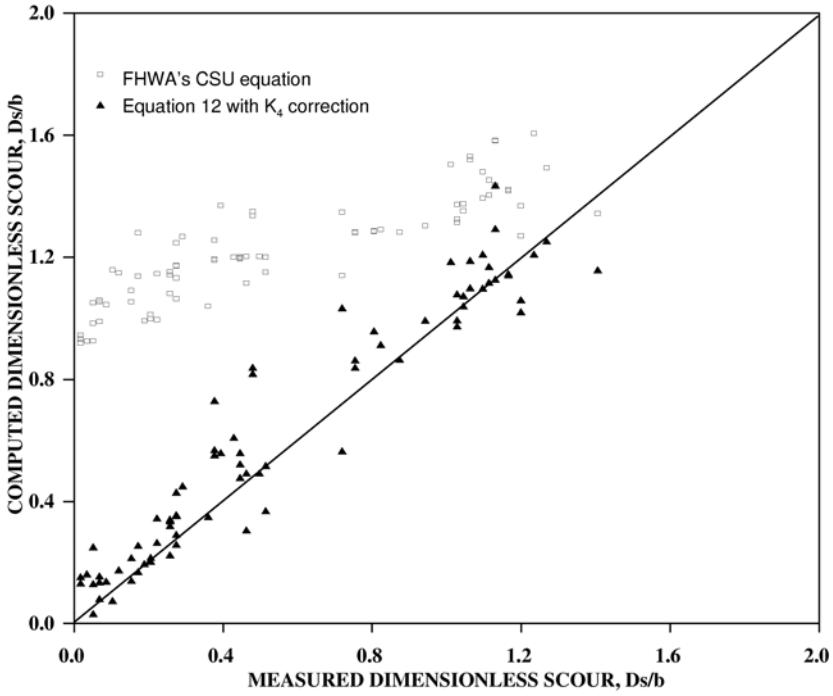

Figure 18. Measured and computed scour for nonuniform-sand experiments in sets 1 through 3.

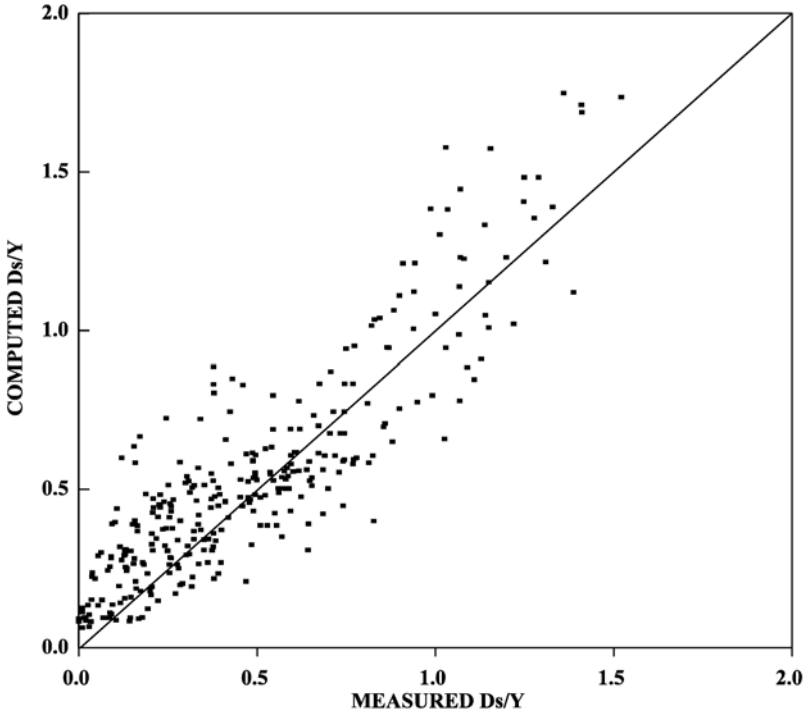

Figure 19. Computed and measured scour for all data using equation 12 (uniform-mixture equation).

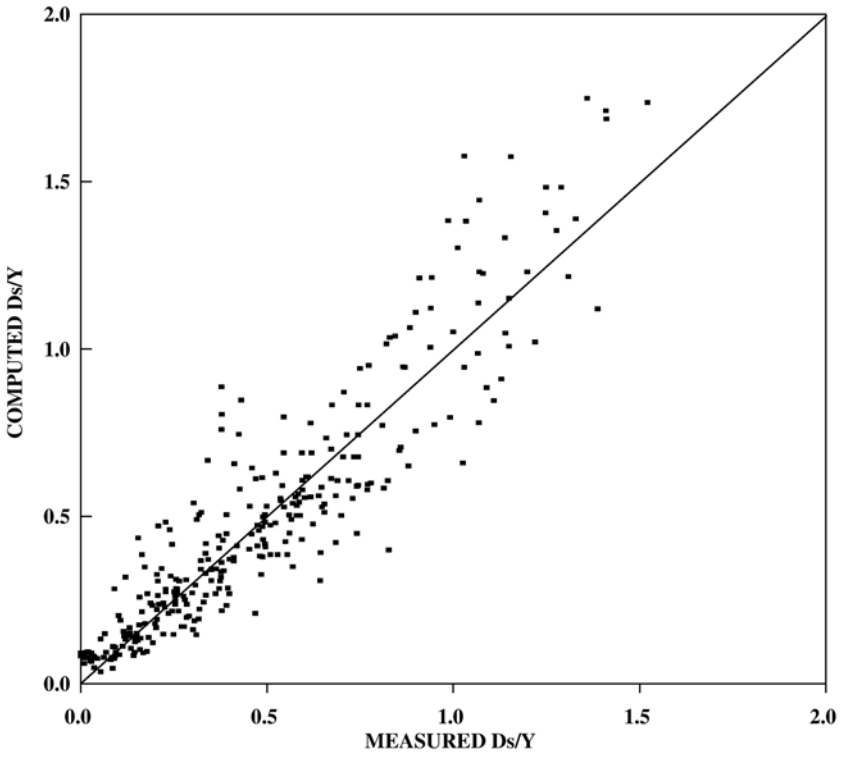

Figure 20. Computed and measured scour for all data using equation 12 with K_4 correction from equation 14.

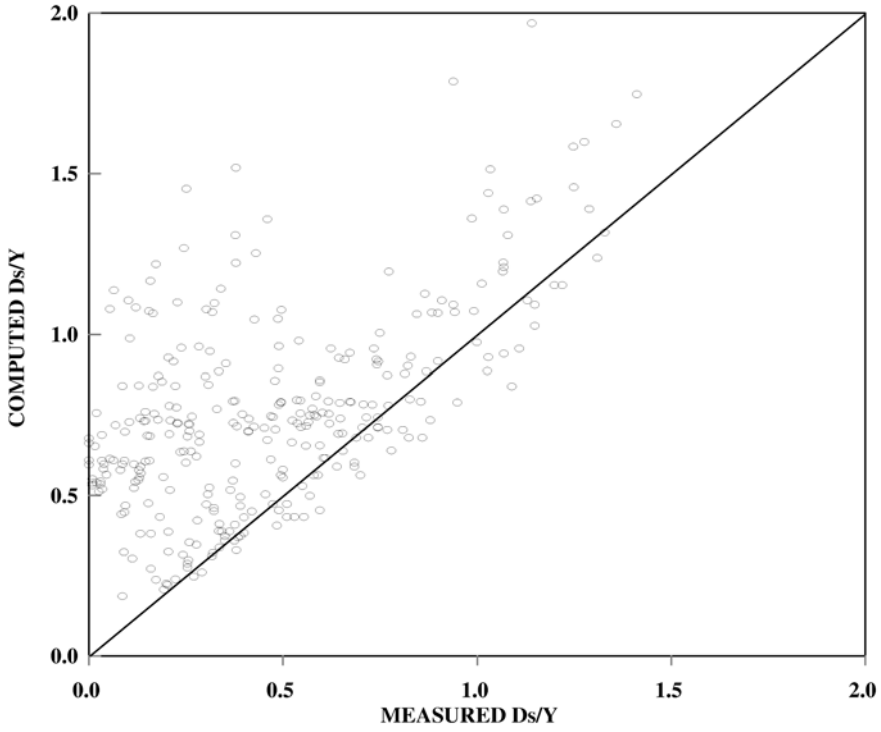

Figure 21. Computed scour using FHWA's CSU equation for uniform and nonuniform mixtures.

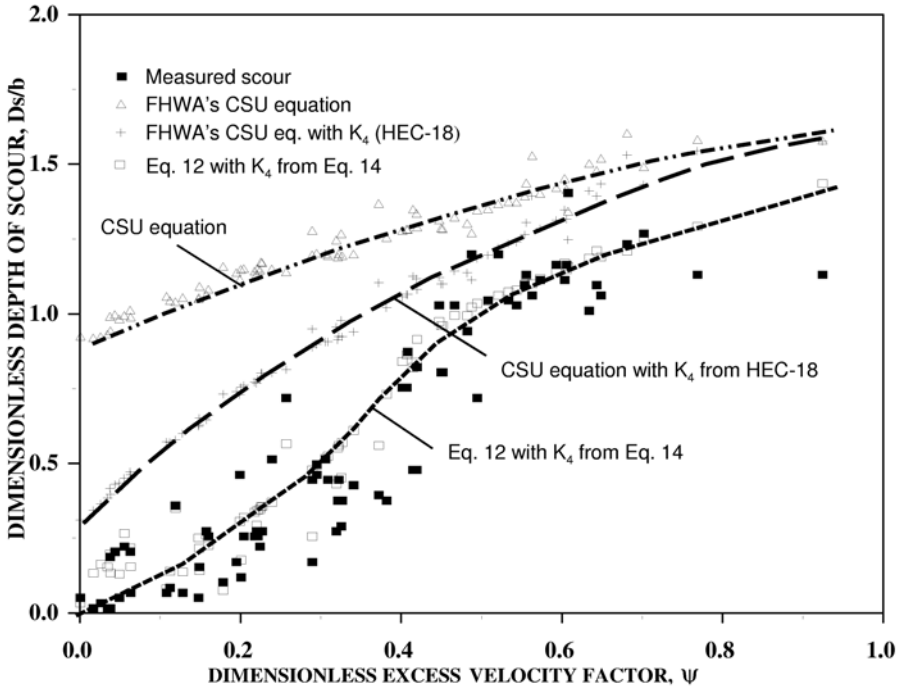

Figure 22. Computed scour by using FHWA's CSU equation with and without K_4 correction from HEC 18, and by using the newly developed equation 12 with K_4 correction from equation 14.

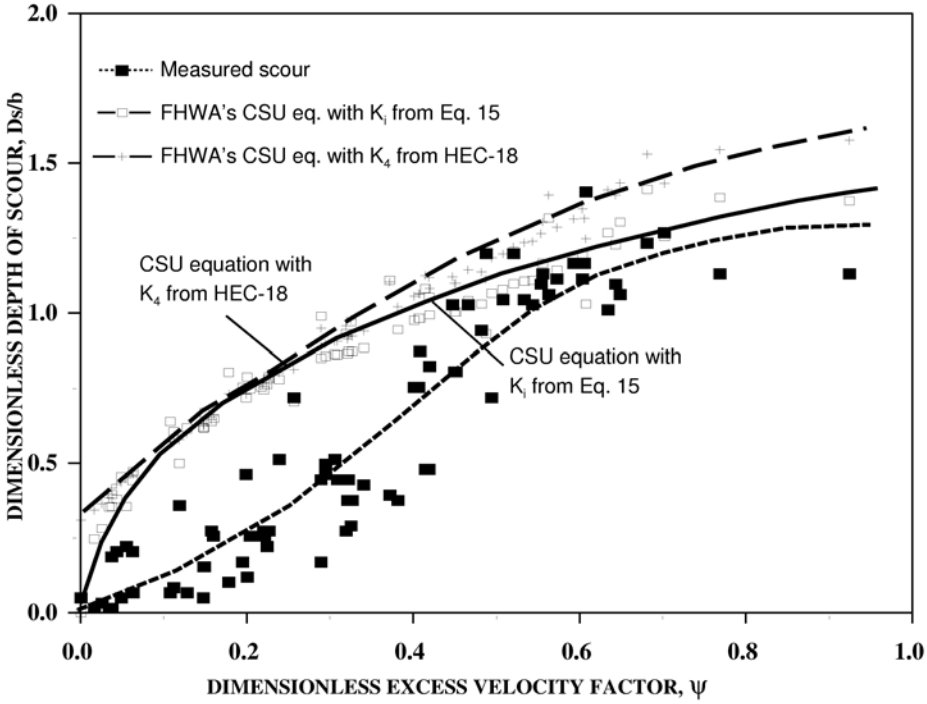

Figure 23. Comparison of FHWA's CSU equation with K_4 correction (according to HEC 18) and the initiation of motion correction, K_i (according to equation 15).

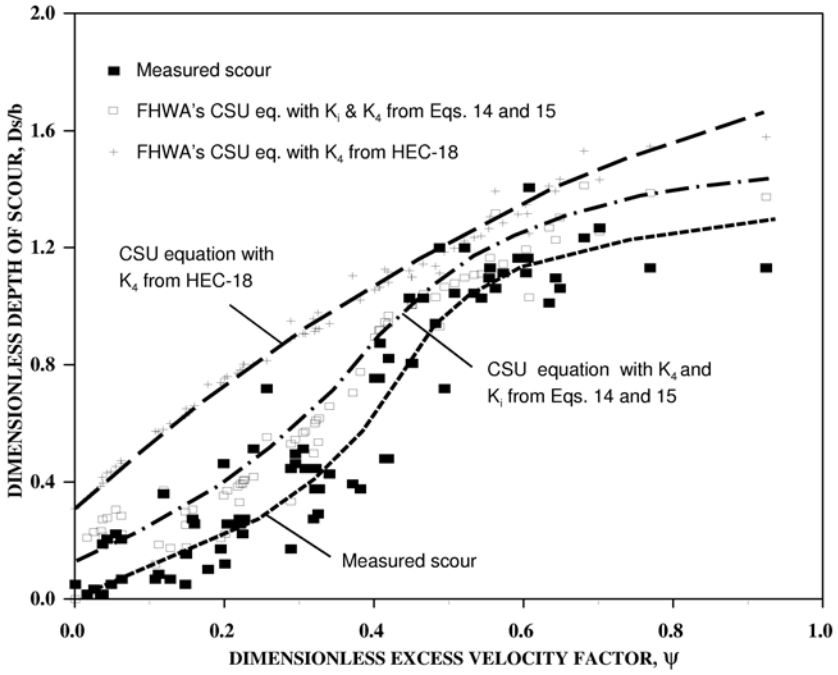

Figure 24. FHWA's CSU equation adjusted with K_i and K_4 and with the HEC 18 correction for K_4.

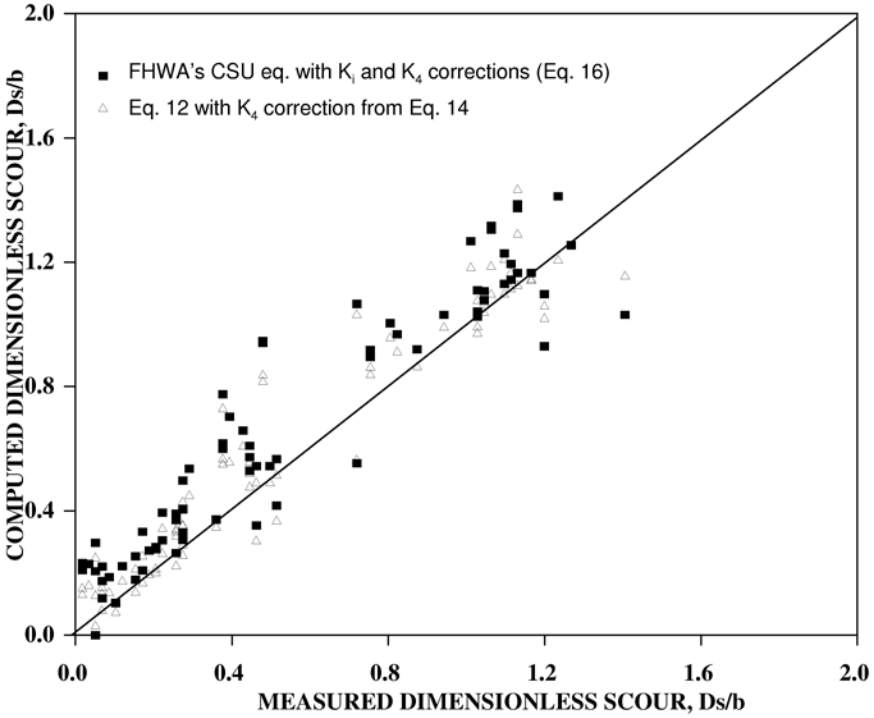

Figure 25. Comparison between computed and measured scour using K_i and K_4 corrections to the FHWA's CSU equation (equation 16) and by using equation 12 with K_4 correction from equation 14.

3. EFFECTS OF GRADATION AND COARSE MATERIAL FRACTION ON ABUTMENT SCOUR

3.1 GENERAL

The majority of currently available abutment scour predictors, including some of the methodologies recommended by FHWA, relate abutment scour to a characteristic length (such as flow depth, Y, abutment protrusion length, a, etc.) and the approach flow Froude number. Some of these regression equations include sediment size and gradation as independent variables. However, since these relationships were developed from limited laboratory and field data, they cannot reflect effects due to sediment size properties; therefore they often result in unrealistic scour estimations. As shown in figures 26(a) and 26(b), they provide no guidance when applied to graded sediment mixtures such as those used in the present experimental study.

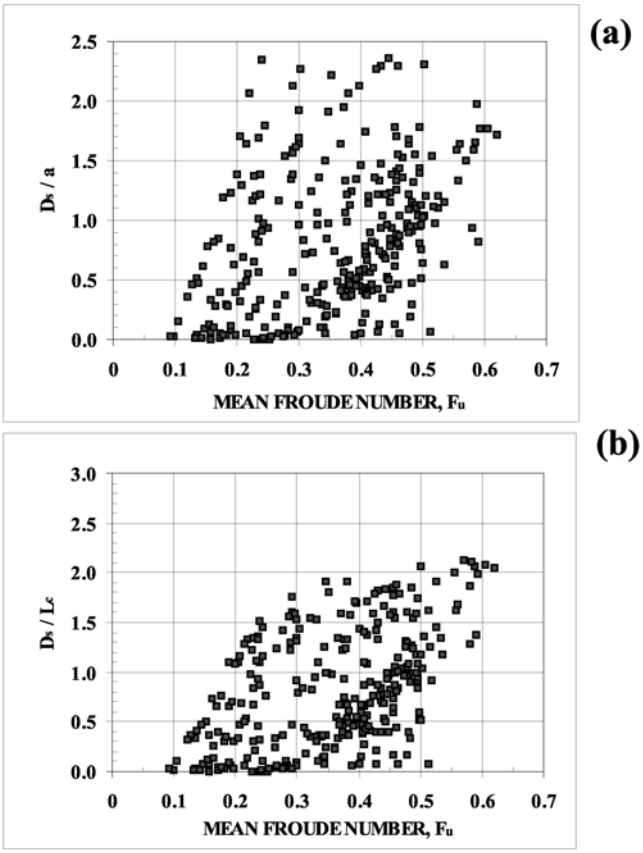

Figure 26. Variation of dimensionless abutment scour with Froude number: (a) abutment protrusion length, a, as characteristic length; (b) $L_c = \sqrt{aY}$ as characteristic length.

This chapter presents results of the experiments to analyze effects of gradation and coarse material fraction on abutment scour. As a result of this study, 384 new abutment scour data points covering a range of selected sediment mixtures have been contributed to the literature. Parameters controlling abutment scour in mixtures have been identified, and two new relationships for estimating abutment scour have been developed. The close agreement of these new relationships with laboratory experiments is encouraging.

3.2 EXPERIMENTAL SETUP AND MEASUREMENTS

This section presents details of the experimental setup, testing procedure, laboratory facilities, and measuring equipment that were utilized in the abutment scour experiments. First, the three laboratory test flumes used to study the effects of gradation on abutment scour are described. Next, individual measurements along with associated instrumentation and their accuracy are discussed. These measurements include initial and final bed topographies and slopes, hydraulic grade line, flow discharge, flow velocity, scour hole topography and its evolution with time, flow visualization, grain size distribution, and sampling of the armor layer. Finally, the experimental procedure followed for the various runs is discussed along with measures taken to ensure the accuracy and reliability of results.

LABORATORY FLUMES

Three laboratory flumes, designated as the hydrodynamics flume, sedimentation flume, and the river mechanics flume, were simultaneously utilized for conducting the abutment scour experiments in noncohesive sediment mixtures. The former two flumes are sediment recirculating facilities, while the latter does not recirculate sediment. All flumes are housed at the Hydraulics Laboratory of the Engineering Research Center at CSU. The water supply to these flumes is from the nearby Horsetooth Reservoir. The temperature of the water in the laboratory is controlled through a heating pipe system.

Hydrodynamics Flume

The hydrodynamics flume is a tilting, water and sediment recirculating laboratory facility. The flume is 0.6 m wide, 0.75 m deep, and 18 m long and is made of a steel bottom and Plexiglas side walls to facilitate visual observations. The facility is rigidly supported on U-shaped steel frames located every 1.2 m and is equipped with angled upper and lower flange stiffeners. The bottom flanges are supported on two I-beams spanning the full length of the flume and ground supported at the far upstream, middle, and far downstream. Two carefully leveled guide rails are mounted on the top flanges to provide an escorting track for the measuring carriage. The flume can be tilted around its middle lateral axis through the synchronized operation of two mechanical jacks located at the upstream and downstream ends. Flow is supplied to the flume from a ground sump via a 0.3-m diameter steel pipe line, equipped with a 0.15-m diameter bypass for fine

tuning of the flow, and a 20-HP centrifugal pump. The flow is first introduced to an upstream head box equipped with a multilayer screen containing gravel at its outlet to serve as a flow guide to provide uniform velocities and turbulence characteristics at the entrance of the flume. A wave suppressor is then introduced to ensure the accomplishment of the previous concerns. The flow depth is controlled by a downstream rotating gate hinged across the bottom of the flume, spanning the full width, and operated by a system of pulleys. Due to the tail gate control and the nature of the flume, a back water effect is sometimes noticed, causing the water depth to increase as the gate is approached. A 23-cm thick uniform sediment layer prepared from the tested mixture is spread along the full length of the flume, with provisions made for a downstream 1.8-m long sediment trap and an upstream 1.8-m long transition zone. The upstream transition zone is composed of coarser sediments, with a sloping profile carefully designed to provide excess friction to ensure the existence of fully developed turbulent flow and with a boundary layer hitting the free surface far upstream of the study reaches for all flow conditions.

Sedimentation Flume

The sedimentation flume is an elevated sediment transport testing facility that provides for both longitudinal tilting and sediment recirculation. The flume is 60 m long, 2.4 m wide, and 1.2 m deep and allows for slope adjustments up to 3 percent through a system of hydraulic jacks. The flume is constructed from steel plates at the bottom and sides with provisions for Plexiglas windows along specific locations at its side. The structure's skeleton is composed of U-shaped lateral steel frames with cantilevers for sidewalks and supported on box-sectioned longitudinal girders. The upper flanges house guide rails for an electrically motorized measuring carriage that can virtually move to any point in the flume. Three different pumps (125, 150, and 250 HP), with a maximum combined capacity of 3 m^3/s, can be simultaneously operated to supply water to the flume from a reservoir sump via three separate steel pipe lines. The flow is first introduced to the upstream head box, which contains several guide vanes and flow straighteners followed by a honeycomb mesh. The flow then passes through a gravel-filled screen succeeded by a wave suppressor. Rapid development of the fully turbulent boundary layer is achieved through an upstream concrete ramp and/or artificial roughening of the entrance zone. The flow depth is regulated through a manually operated downstream adjustable tail gate. The sediment bed is built to a thickness of about 0.4 m, with provisions made for a downstream sediment trap that extends for 6 m. To facilitate drainage of the flume after the experiments, a perforated 10-cm diameter PVC pipe was embedded in the bed material and spanned the full length of the study reach.

River Mechanics Flume

The river mechanics flume is a fixed-slope facility. The flume is 6 m wide, 0.9 m deep, and around 30 m long. The test section, however, was 24 m long, 5.1 m wide, and 0.9 m deep, providing for two Plexiglas viewing sections along one side of the flume and

a large upstream reservoir to create uniform entrance conditions. I-beam rails are mounted on the side walls to provide a track for the huge measuring carriage. A 75-HP axial pump of maximum capacity around 0.6 m^3/s supplies water to the flume through a 0.6-m diameter pipeline. The upstream main ends in a similar size diffuser located orthogonal to the main flow direction to distribute the flow uniformly across the flume width. The flow then passes through a gravel-filled screen followed by an artificially coarsened concrete ramp that joins the main sediment bed. The setup also provides for a downstream sediment trap and a downstream sill for depth regulation.

MEASUREMENTS

A series of measurements are needed in order to define the relationship between local scour at abutments and the various hydraulic, geometric, and sediment parameters, both quantitatively and qualitatively. These measurements are described below.

Flow Discharge

The water discharge in all three test flumes was measured through a system of orifice-meter and a differential manometer. For the hydrodynamics flume, two orifice plates were available: one mounted on the 0.3-m diameter main and the other attached to the 0.15-m diameter bypass line. Both orifice-plates are connected to a dual water-mercury manometer for detecting the pressure drop across the ends of the plate. The flow discharge was then computed from the calibration curves for the orifices. The pressure tapping across the orifice plate is connected to the manometer through hard vinyl tubing provided with bleeding valves for drainage and for ensuring an air-free environment. The sedimentation flume is equipped with three similar setups for measuring the discharge, each attached to a different pump. Extreme care was taken to ensure the release of air bubbles entrapped in all manometer lines. The error in measuring the discharge in the hydrodynamics flume is around 3 percent, in the sedimentation flume around 4 percent, and in the river mechanics flume around 5 percent. These error estimates are due to the calibration errors of orifice plates, unsteadiness in the pump discharge, and fluctuations in manometer readings.

Flow Velocity

In the hydrodynamics flume, velocities were measured utilizing two different size pitot tubes and a two-dimensional magnetic flow meter depending on the desired accuracy. A 3-mm diameter minute pitot tube, tapered to a 1.5-mm diameter total head sensor that is connected to a membrane-type transducer, was first used to detect the flow velocity with an accuracy of ±1.5 percent. However, the problems encountered with air entrainment and blockage of the sensing and conveying tubing led to the replacement of this pitot tube with a larger one. The second pitot tube had a 3-mm diameter sensing stem with a pressure take-off diameter of 3 mm and a probe length of 0.3 m. The pressure transducer that was connected to the pitot tubes contained a 0.7 kilo pascal (kPa) steel membrane and is commercially available as P7D±5 PSID SER. 11534. The output

signals from the transducer are amplified, filtered, and analyzed by a data acquisition board and a personal computer. The velocities sensed by this device are in the order of ±2.5 percent of accuracy. The second method for velocity measurements in the hydrodynamics flume utilized the 2-D electromagnetic Marsh McBirney, Model 523 flowmeter. The flowmeter consists of a spherical electromagnetic probe with cable and signal processor powered by 6-V DC externally charged with 110-V AC. The probe has a diameter of 12 mm and is mounted on a 6-mm diameter vertical standing rod. The analog signals corresponding to the two orthogonal velocities sensed by the probe are intercepted by a multichannel data acquisition board connected to a personal computer. The sampling frequency was 50 Hz. Overall accuracy of the latter setup is around 3.5 percent.

In the river mechanics and sedimentation flumes, velocities were measured with a one-dimensional Marsh McBirney, Model 2000 electromagnetic flowmeter with a 2.54-cm elliptic probe and a digital display conversion voltmeter. The accuracy of the flowmeter is reported to be ±2 percent by the manufacturer, and its operating range is from -0.015 m/s to +6.1 m/s within temperature extremes of 0 ^{o}C to 71 ^{o}C. Overall accuracy of the velocity measuring setup is estimated to be 5 percent.

Flow Visualization

Examination of flow field in the vicinity of the abutment was achieved through flow visualization techniques, including:

- Surface and subsurface floats made of hollow glass spheres partially filled with a fluid to maintain neutral buoyancy. These floats were 1 cm in diameter and were used in determining separation, reattachment, and reversed flow zones.
- Lightweight plastic pellets sprayed on the water surface gave a good picture of the surface stream lines, especially at low flows.
- Dye injection of potassium permanganate solution with the same density as water was very indicative of the nature of the horse vortex and other subsurface features. Other chemicals were tried but did not provide further improvement.
- Potassium permanganate crystals sprayed on the sediment bed surface, inside the scour hole or around it, provided visualization of boundary currents.
- Video and still picture cameras for documenting various phenomena.

Free Stream Bed and Scour Hole Topographies

The bed topographies for the scour holes and the free stream approaches are measured using point gauges. In all flumes, the standard topography measurement procedure started with the leveling of instrumentation carriages at each measurement location along and across the flume to account for the potential unevenness of tracks. Choosing an arbitrary fixed level, every location in the flume, as identified by its Cartesian coordinates, was assigned a correction factor reflecting its elevation relative to the fixed level.

In the hydrodynamics flume, three different point gauges were utilized for measuring purposes depending on the location and accuracy desired. The bed topographies at four different approach sections were measured for each abutment model to define the upstream bed elevation. At each cross section, the bed level was considered to be the average of 10 measurements evenly distributed across the flume's width. To define bed topography in the vicinity of local scour requires more intensive measurements. A measuring grid of an average of 17 cross sections, with a minimum of 21 points per section, was adopted to describe the scour hole region for each abutment.

A similar procedure was followed for the other two flumes, with provisions made for measuring the initial as well as the final levels. The raw measurements are adjusted with the leveling correction factors for each location and then regressed together to yield the value of the bed slope. Approximately 400 topography measurements were performed for each abutment model per experiment. Due to the large sampling size, the error in bed measurements is considered to be equal to 0.25 of the D_{90} grain size.

Hydraulic Grade Line

The water surface elevations were measured using point gauges with a resolution of ±0.3 mm. Water surface elevation measurements were conducted at a minimum of three approach cross sections per abutment and at a minimum of five locations across the flume width at each cross section. At every location in the cross section, the water level was considered to be the average of two minimum and maximum detected values, to account for any residual fluctuations in the supply discharge and any surface waves induced by the setup. This tedious procedure assumes an accuracy of 2 percent in the computed water depth. Again the hydraulic grade line is identified through regressing the measured water surface values after being adjusted with the level correction factors. The regression results in high correlation coefficients ($R^2 = 0.95$). The velocity head was then added to the hydraulic grade line to define the total energy line.

Sampling of the Armor Layer

Surface samples representing the armor coat formed at the approach to the abutment and inside the scour hole were carefully collected after the experiments were over and the bed was dried. Various techniques, including molten paraffin wax, sticky polymers, modeling clay, scraping the surface, and pebble counting from still photographs, were tried. Among these, the modeling clay method proved to be the most practical and the most accurate.

Soft modeling clay, sometimes treated with castor oil to make it softer, was used to prepare a thin paste around 5 mm thick. The paste was placed at the desired sampling location and gently stamped down under a uniformly distributed applied pressure. The paste was then carefully lifted up, thus collecting a patch of adhered sediments representing the armor coat. After waiting for a short time to allow the paste to become drier, the collected sediments were removed by scraping the surface. If the clay is left on for a long time (one day or more) it becomes very stiff and the removal process has to be

done under warm water. The following step was to wash the sediments to make sure that no residual clays are present, then oven dry them and finally prepare them for sieve analysis.

Grain Size Distribution

The relative size distributions for the various sediment mixtures and samples was determined using the sieve analysis method. The sieve sizes used were those defined by the U.S. Bureau of Standards, which represents the sieve number by the number of openings it has per square inch. An average shaking time of 10 minutes was applied for all tested samples.

EXPERIMENTAL PROCEDURE

The experimental procedure for the abutment scour experiments is summarized as follows:

(1) The sediment mixture forming the bed of the flume is naturally compacted in layers. A low flow is then introduced to the flume while raising the downstream gate (for the Hydrodynamics and river mechanics flumes), or lowering the downstream gate (for the sedimentation flume), and is allowed to prevail for long enough to saturate the bed and drive away any entrapped air.

(2) The flow is stopped and the bed is leveled to the desired elevation. Initial bed levels are then recorded at the desired sections. The bed around the abutments where local scour is expected to occur is protected with specially prepared shields.

(3) The flow is introduced to flumes at a very slow rate in order to avoid disturbing the bed topography, especially around the abutments. A depth of flow greater than the desired depth for the experiment is maintained within the flume. The shields around the abutments are then removed.

(4) The required flow depth and discharge are then achieved through simultaneous adjustment of the discharge valve and the downstream gate (or sill) position. Recording of scour development with time is immediately started.

(5) Water surface elevations and flow velocities are recorded following the procedure given above.

(6) Flow visualization and video recording, if any, are then performed.

(7) The shut down process includes raising the depth inside the flume through downstream gate adjustment while decreasing the flow rate in steps. At complete shut down, the flume has to be holding a sizable depth of water that is then allowed to drain very slowly. The current step is crucial for preserving the local scour features produced through the run.

(8) After allowing the bed to be completely drained, the final bed topographies are recorded, still camera photography is performed, and sampling of the armor layer is conducted.

(9) The local scour areas are then replenished with new sediments and the previous procedure is repeated for the next experiment.

3.3 EXPERIMENTAL RESULTS

A comprehensive experimental program was designed to investigate the different aspects of gradation and coarse material fraction effects on local abutment scour. These experiments are categorized into 14 different sets of runs labeled set A through set N. The experimental program was carried out concurrently in three different laboratory facilities. Sets A, B, C, G, H, I, J, K, L, M, and N were performed in the hydrodynamics flume, while sets D and E were conducted in the sedimentation flume. The river mechanics flume was assigned to set F experiments. Sixteen different sediment mixtures and 10 different abutment models were subjected to a range of flow conditions, resulting in a total of 384 different abutment case studies. Tables 8 through 21 present these cases. A summary table of the sediment characteristics associated with the different mixtures utilized in the study is given in table 22.

In the abutment scour experiments presented in this section, the effects of the following parameters on local abutment scour were investigated:

- Effect of mean sediment size, D_{50} (in sets I, G, and L).
- Effect of sediment gradation, σ_g (in sets A, B, and C, D-M1, E-M1, and E-M3).
- Effect of the coarsest tenth percentile of the sediment size gradation (sets I, K, and L, M, N, D-M1, D-M2, D-M3, E-M1, E-M2).
- Effect of flow depth, Y (sets H, I, and J).
- Effect of abutment protrusion length, a (all sets).

The following sections present details of each set of experiments and references to related summary tables whenever applicable.

HYDRODYNAMICS FLUME EXPERIMENTS

The majority of the experiments (304 different abutment case studies) were carried out in the hydrodynamics flume. The details of each set of experiments are given below.

Set A Experiments

Set A consisted of 18 different runs (A-1 through A-18). Four abutment models were tested in each of the runs A-1, A-2, and A-3. All the four abutment models had the same length of 11.4 cm in the direction of flow; however, their protrusion lengths (length orthogonal to flow) varied. The abutment with a protrusion length of 2.54 cm was identified as M1, that with a protrusion length of 5.08 cm was identified as M2, that with a protrusion length of 7.62 cm was identified as M3, and that with a protrusion length of 10.16 cm was identified as M4. In runs A-4 through A-18, the 2.54-cm model (M1) was dismantled, since its small size could introduce undesirable scale effects with the selected sediment sizes and therefore could influence the validity of the results. The bed material tested (sediment Type IV) was coarse graded sand with a D_{50} of 1.8 mm and a σ_g of 2.1, with an approximate log-normal size fraction distribution. The flow depth to abutment

protrusion length (*Y/a*) varied between 0.5 and 2.0, the average velocity was between 18 cm/s and 40 cm/s, and the mean Froude number ranged from 0.2 to 0.5. Table 8 shows a summary of the experimental conditions for set A runs. It should be noted that flow depth (*Y*) and flow velocities were all measured at an approach section located at a distance of (*10a*) upstream from each abutment, where a is the abutment protrusion length.

Set B Experiments

Set B included 16 different runs (B-1 through B-16). Three abutment models (M2, M3, and M4) were tested in each of the runs except for runs B-12 and B-13 where only M2 and M4 were examined. Sediment of Type III, which is a coarse uniform sand with a D_{50} of 1.8 mm and a σ_g of 1.17, was used throughout this set. The flow depth to abutment protrusion length (*Y/a*) varied between 0.3 and 2.3, the average velocity ranged between 0.21 m/s and 0.45 m/s, and the mean Froude number was between 0.25 and 0.6. Table 9 presents a summary of the experimental conditions for set B runs.

Set C Experiments

As shown in table 10, 21 case studies were included in set C (C-2 through C-8). Throughout this series and in the remaining sets that were conducted in the 0.61-m-wide flume, only abutment models M2, M3, and M4 were used. The bed material selected for this set was a coarse graded sand with a D_{50} of 1.8 mm, a σ_g of 3.9, and an approximate log-normal size fraction distribution (Type V sediment). The flow depth to abutment protrusion length (*Y/a*) varied between 0.38 and 1.7, the average velocity (V_u) was between 0.21 m/s and 0.44 m/s, and the mean Froude number ranged from 0.3 to 0.5. A summary of the experimental conditions for set C runs is presented in table 10.

Set G Experiments

This set was designed to test a second uniform medium sand mixture with a D_{50} of 0.78 mm, and a σ_g of 1.3 identified as Type II sediment. The set consisted of seven runs, which provided 21 data points as indicated in table 11. The experiments were conducted using a constant flow depth of 0.075 m for M2, 0.08 m for M3, and 0.09 m for M4. Mean velocity in set G experiments varied between 0.13 m/s and 0.3 m/s, and mean Froude number varied between 0.14 and 0.35.

Sets H, I, and J Experiments

Sets H, I, and J were all conducted with fine silica sand with a D_{50} of 0.1 mm and σ_g of 1.4 (Type I sediment). Set H consisted of 24 cases, all of which were run for a constant depth of 0.10 m. Set I included 18 study cases, all being tested at a constant depth of 0.075 m, and similarly, set J consisted of 18 tests conducted at a constant depth of 0.05 m. Tables 12 through 14 demonstrate the experimental conditions associated with each set. In each of these sets the most severe flow condition resulted in live bed scour, whereas the rest of the experiments were all conducted under clear-water

conditions. For set H, velocities and Froude numbers ranged between 0.01 m/s and 0.33 m/s and between 0.09 and 0.3, respectively; for set I, velocities and Froude numbers ranged between 0.075 m/s and 0.40 m/s and between 0.13 and 0.46, respectively; and for set J velocities and Froude numbers ranged between 0.11 m/s and 0.31 m/s and between 0.15 and 0.44, respectively.

Set K Experiments

Table 15 lists test conditions for the seven runs in the set K experiments using Type VII sediment. The Type VII sediment resembles the Type I sediment in all of its features except that the coarsest 15 percent fraction matches that of sediment Type III. All experiments were conducted at an almost constant flow depth of 0.075 m, while the flow velocity varied from conditions which initiated local scour at the abutments to conditions that resulted in the initiation of live-bed scour (clear-water scour limit).

Set L Experiments

This set of experiments is similar to set B in which Type III sediment with a D_{50} of 1.8 mm and a σ_g of 1.17 was used. However, in this set the flow depth was maintained at a constant value of about 0.08 m. Flow conditions for the 24 cases considered in set L are given in table 16.

Set M Experiments

As shown in table 17, 10 different experiments were performed in set M using a constant depth of 0.075 m. The bed material tested was Type VI sediment, which basically had the same D_{50} and σ_g as uniform coarse sand of Type III (1.8 mm and 1.17, respectively), while having the D_{90} (i.e. the same coarsest fraction) of the graded sediment mixture of Type IV. Flow conditions in this set of experiments varied from conditions that initiated scour to conditions that initiated bed forms.

Set N Experiments

This set of experiments is similar to set A, which used Type IV graded coarse sand. However, in these experiments the flow depth was kept at a constant value of 0.075 m. Flow conditions pertaining to set N experiments (27 cases) are given in table 18.

SEDIMENTATION FLUME EXPERIMENTS

Sixty-eight different abutment case studies were tested in the sedimentation flume; these studies constituted about 17 percent of the total number of abutment scour cases involved in this research. All the tests performed in the 2.44-m wide flume were conducted at a constant depth of 0.3 m. A total of eight different sediment mixtures were tested. Five different sand types, all having the same D_{50} of 0.78 mm but with varying gradation coefficients and ninety-percentile diameters, were selected to study

sensitivity to various sediment size characteristics. The experiments are divided into two major sets: D and E.

Set D Experiments

Set D consisted of eight different runs. As shown in table 19, four abutment models were tested in each of these runs. All the abutment models were 0.46 m long (in direction of flow) and were identified as M1, M2, M3, and M4. Abutments M1, M2, and M3 had a protrusion length of 0.22 m, while the protrusion length of M4 was 0.18 m. Abutment models M1 and M4 were used for testing an approximate log-normally graded medium sand mixture of D_{50} equal to 0.78 mm and σ_g equal to 2.43 (Type VIII sediment). Abutment M2 was designated for testing a mixture similar to that at M1, but with a coarser upper ten-percentile fraction (Type XI sediment). Similarly, a third mixture (Type X sediment), that was basically Type VIII sediment but with a coarser upper five-percentile fraction, was introduced at abutment M3.

Set E Experiments

Table 20 summarizes the 36 test conditions for the set E experiments. Four abutment models, which were also identified as M1, M2, M3, and M4, with protrusion lengths of 0.22 m and 0.45 m, were used in these experiments. In runs E-1 through E-8, abutment M1 was used for testing a graded medium sand mixture of D_{50} equal to 0.78 mm and σ_g equal to 3.4 (sediment Type IX). Abutment M2 was for testing a mixture similar to that at M1, but with a coarser upper ten-percentile fraction (sediment Type XII). A uniform medium sand with a D_{50} of 0.78 mm and σ_g of 1.3 (Type II) was utilized at M3. For comparison purposes, a mixture of sand and clay (70 percent sand and 30 percent clay) was introduced at M4. Runs E-9 and E-10 were conducted using a gravel mixture to examine potential variations due to median sediment size.

RIVER MECHANICS FLUME EXPERIMENTS

In the set F experiments, which were conducted in the 5.2-m wide river mechanics flume, a sediment mixture with mean diameter of 0.55 mm, a gradation coefficient of 2.1, and a D_{90} of 1.3 mm (sediment Type XV) was used. Table 21 summarizes the experimental conditions for this series. Set F experiments were conducted for the qualitative description of the scour hole and related geometric features.

Table 8. Experimental conditions for set A runs for abutment scour.

RUN ID	MODEL SIZE (cm x cm)	FLOW DISCHARGE Q (l/s)	APPROACH DEPTH Y (m)	AVERAGE VELOCITY V_u (m/s)	ABUTMENT VELOCITY V_a (m/s)	DIVERTED VELOCITY V_j (m/s)	SCOUR DEPTH D_s (m)	SEDIMENT TYPE
A1 - M1	2.5x11.4	12.621	0.061	0.34	0.33	0.31	0.016	IV
A1 - M2	5.1x11.4	12.621	0.211	1.06	0.98	0.93	0.072	IV
A1 - M3	7.6x11.4	12.621	0.220	1.01	0.85	0.83	0.089	IV
A1 - M4	10.2x11.4	12.621	0.238	0.94	0.78	0.72	0.098	IV
A2 - M1	2.5x11.4	16.170	0.068	0.39	0.38	0.36	0.023	IV
A2 - M2	5.1x11.4	16.170	0.211	1.24	1.17	1.13	0.072	IV
A2 - M3	7.6x11.4	16.170	0.220	1.17	0.99	0.96	0.089	IV
A2 - M4	10.2x11.4	16.170	0.238	1.11	0.96	0.89	0.098	IV
A3 - M1	2.5x11.4	18.502	0.087	0.35	0.33	0.32	0.025	IV
A3 - M2	5.1x11.4	18.502	0.211	1.14	1.06	1.02	0.072	IV
A3 - M3	7.6x11.4	18.502	0.220	1.04	0.88	0.85	0.089	IV
A3 - M4	10.2x11.4	18.502	0.238	1.01	0.85	0.79	0.098	IV
A4 - M2	5.1x11.4	19.502	0.075	0.42	0.40	0.40	0.073	IV
A4 - M3	7.6x11.4	19.502	0.082	0.39	0.33	0.32	0.054	IV
A4 - M4	10.2x11.4	19.502	0.084	0.38	0.34	0.32	0.083	IV
A5 - M2	5.1x11.4	19.884	0.080	0.41	0.39	0.38	0.064	IV
A5 - M3	7.6x11.4	19.884	0.087	0.38	0.32	0.31	0.054	IV
A5 - M4	10.2x11.4	19.884	0.091	0.36	0.31	0.29	0.052	IV
A6 - M2	5.1x11.4	15.874	0.066	0.40	0.38	0.36	0.048	IV
A6 - M3	7.6x11.4	15.874	0.071	0.37	0.31	0.30	0.040	IV
A6 - M4	10.2x11.4	15.874	0.075	0.35	0.30	0.28	0.042	IV
A7 - M2	5.1x11.4	20.445	0.083	0.40	0.38	0.37	0.062	IV
A7 - M3	7.6x11.4	20.445	0.088	0.38	0.32	0.32	0.053	IV
A7 - M4	10.2x11.4	20.445	0.094	0.35	0.31	0.29	0.066	IV
A8 - M2	5.1x11.4	17.306	0.071	0.40	0.38	0.37	0.059	IV
A8 - M3	7.6x11.4	17.306	0.076	0.38	0.32	0.31	0.055	IV
A8 - M4	10.2x11.4	17.306	0.080	0.36	0.31	0.29	0.060	IV
A9 - M2	5.1x11.4	14.130	0.065	0.36	0.34	0.32	0.047	IV
A9 - M3	7.6x11.4	14.130	0.069	0.33	0.28	0.27	0.043	IV
A9 - M4	10.2x11.4	14.130	0.074	0.31	0.27	0.25	0.044	IV
A10 - M2	5.1x11.4	10.227	0.049	0.34	0.32	0.31	0.026	IV
A10 - M3	7.6x11.4	10.227	0.055	0.30	0.25	0.25	0.030	IV
A10 - M4	10.2x11.4	10.227	0.062	0.27	0.22	0.20	0.029	IV
A11a - M2	5.1x11.4	4.573	0.029	0.26	0.23	0.22	0.007	IV
A11a - M3	7.6x11.4	4.573	0.030	0.25	0.21	0.20	0.010	IV
A11a - M4	10.2x11.4	4.573	0.039	0.19	0.15	0.13	0.006	IV

Table 8. Experimental conditions for set A runs for abutment scour (continued).

RUN ID	MODEL SIZE (cm x cm)	FLOW DISCHARGE Q (l/s)	APPROACH DEPTH Y (m)	AVERAGE VELOCITY V_u (m/s)	ABUTMENT VELOCITY V_a (m/s)	DIVERTED VELOCITY V_j (m/s)	SCOUR DEPTH D_s (m)	SEDIMENT TYPE
A11b - M2	5.1x11.4	7.232	0.039	0.30	0.28	0.26	0.015	IV
A11b - M3	7.6x11.4	7.232	0.044	0.27	0.22	0.22	0.016	IV
A11b - M4	10.2x11.4	7.232	0.050	0.24	0.19	0.17	0.010	IV
A11c - M2	5.1x11.4	20.454	0.082	0.41	0.39	0.38	0.068	IV
A11c - M3	7.6x11.4	20.454	0.086	0.39	0.33	0.32	0.062	IV
A11c - M4	10.2x11.4	20.454	0.093	0.36	0.32	0.30	0.067	IV
A15a - M2	5.1x11.4	13.790	0.102	0.22	0.20	0.18	0.010	IV
A15a - M3	7.6x11.4	13.790	0.113	0.20	0.17	0.16	0.005	IV
A15a - M4	10.2x11.4	13.790	0.121	0.19	0.14	0.13	0.005	IV
A15b - M2	5.1x11.4	13.790	0.077	0.29	0.27	0.25	0.023	IV
A15b - M3	7.6x11.4	13.790	0.087	0.26	0.22	0.21	0.008	IV
A15b - M4	10.2x11.4	13.790	0.096	0.24	0.19	0.17	0.010	IV
A16 - M2	5.1x11.4	13.529	0.057	0.39	0.37	0.36	0.049	IV
A16 - M3	7.6x11.4	13.529	0.059	0.38	0.32	0.31	0.061	IV
A16 - M4	10.2x11.4	13.529	0.062	0.36	0.32	0.30	0.080	IV
A18a - M2	5.1x11.4	15.263	0.065	0.39	0.36	0.35	0.057	IV
A18a - M3	7.6x11.4	15.263	0.067	0.37	0.31	0.31	0.047	IV
A18a - M4	10.2x11.4	15.263	0.073	0.34	0.30	0.28	0.075	IV
A18b - M2	5.1x11.4	15.574	0.068	0.37	0.35	0.34	0.043	IV
A18b - M3	7.6x11.4	15.574	0.073	0.35	0.30	0.29	0.043	IV
A18b - M4	10.2x11.4	15.574	0.080	0.32	0.27	0.26	0.049	IV

Notes:

1. Average Velocity: Mean velocity prevailing at the approach cross section.
2. Abutment Velocity: Velocity measured along the longitudinal passing through the abutment nose at the approach section.
3. Diverted Velocity: Integrated mean velocity prevailing across the deflected flow portion
4. All experiments are performed in a 0.61-m wide flume measured at the approach section.
5. Bed slope is set to a value of 0.0037.

Table 9. Experimental conditions for set B runs for abutment scour.

RUN ID	MODEL SIZE (cm x cm)	FLOW DISCHARGE Q (l/s)	APPROACH DEPTH Y (m)	AVERAGE VELOCITY V_u (m/s)	ABUTMENT VELOCITY V_a (m/s)	DIVERTED VELOCITY V_j (m/s)	SCOUR DEPTH D_s (m)	SEDIMENT TYPE
B1 - M2	5.1x11.4	14.130	0.064	0.365	0.341	0.329	0.1173	III
B1 - M3	7.6x11.4	14.130	0.064	0.362	0.296	0.293	0.1295	III
B1 - M4	10.2x11.4	14.130	0.066	0.349	0.304	0.285	0.1494	III
B2 - M2	5.1x11.4	11.118	0.048	0.384	0.361	0.349	0.0832	III
B2 - M3	7.6x11.4	11.118	0.046	0.395	0.322	0.321	0.1256	III
B2 - M4	10.2x11.4	11.118	0.052	0.348	0.303	0.284	0.1347	III
B3 - M2	5.1x11.4	8.011	0.037	0.352	0.328	0.315	0.0811	III
B3 - M3	7.6x11.4	8.011	0.038	0.348	0.283	0.281	0.1140	III
B3 - M4	10.2x11.4	8.011	0.040	0.329	0.283	0.264	0.1222	III
B4 - M2	5.1x11.4	4.876	0.027	0.298	0.274	0.258	0.0472	III
B4 - M3	7.6x11.4	4.876	0.026	0.303	0.247	0.243	0.0622	III
B4 - M4	10.2x11.4	4.876	0.028	0.282	0.234	0.215	0.0634	III
B5 - M2	5.1x11.4	6.895	0.035	0.326	0.301	0.287	0.0680	III
B5 - M3	7.6x11.4	6.895	0.039	0.292	0.238	0.234	0.0716	III
B5 - M4	10.2x11.4	6.895	0.045	0.252	0.204	0.187	0.0457	III
B6 - M2	5.1x11.4	8.011	0.036	0.369	0.345	0.333	0.0872	III
B6 - M3	7.6x11.4	8.011	0.042	0.312	0.254	0.251	0.0719	III
B6 - M4	10.2x11.4	8.011	0.048	0.272	0.223	0.205	0.0515	III
B7 - M2	5.1x11.4	11.117	0.046	0.395	0.373	0.362	0.1000	III
B7 - M3	7.6x11.4	11.117	0.048	0.382	0.311	0.310	0.1207	III
B7 - M4	10.2x11.4	11.117	0.052	0.350	0.305	0.286	0.1122	III
B8 - M2	5.1x11.4	9.121	0.040	0.372	0.349	0.336	0.0899	III
B8 - M3	7.6x11.4	9.121	0.044	0.343	0.280	0.277	0.0838	III
B8 - M4	10.2x11.4	9.121	0.052	0.290	0.242	0.224	0.0796	III
B9 - M2	5.1x11.4	9.121	0.048	0.311	0.286	0.271	0.0393	VI
B9 - M3	7.6x11.4	9.121	0.051	0.294	0.240	0.236	0.0402	VI
B9 - M4	10.2x11.4	9.121	0.055	0.274	0.226	0.208	0.0244	VI
B10 - M2	5.1x11.4	11.118	0.048	0.378	0.355	0.342	0.0241	VI
B10 - M3	7.6x11.4	11.118	0.050	0.366	0.298	0.296	0.0323	VI
B10 - M4	10.2x11.4	11.118	0.052	0.352	0.308	0.288	0.0372	VI
B12 - M2	5.1x11.4	8.011	0.036	0.362	0.338	0.325	0.0896	III
B12 - M4	10.2x11.4	8.011	0.050	0.264	0.215	0.197	0.0664	III
B13 - M2	5.1x11.4	33.980	0.120	0.463	0.445	0.440	0.1167	III
B13 - M4	10.2x11.4	33.980	0.152	0.366	0.323	0.304	0.1149	III

Table 9. Experimental conditions for set B runs for abutment scour (continued).

RUN ID	MODEL SIZE (cm x cm)	FLOW DISCHARGE Q (l/s)	APPROACH DEPTH Y (m)	AVERAGE VELOCITY V_u (m/s)	ABUTMENT VELOCITY V_a (m/s)	DIVERTED VELOCITY V_j (m/s)	SCOUR DEPTH D_s (m)	SEDIMENT TYPE
B14 - M2	5.1x11.4	9.504	0.042	0.368	0.345	0.332	0.078	III
B14 - M3	7.6x11.4	9.504	0.052	0.297	0.242	0.238	0.068	III
B14 - M4	10.2x11.4	9.504	0.058	0.269	0.221	0.203	0.076	III
B15 - M2	5.1x11.4	7.862	0.048	0.271	0.247	0.231	0.027	III
B15 - M3	7.6x11.4	7.862	0.055	0.235	0.192	0.187	0.023	III
B15 - M4	10.2x11.4	7.862	0.062	0.206	0.160	0.145	0.020	III
B16 - M2	5.1x11.4	11.742	0.054	0.359	0.335	0.322	0.091	III
B16 - M3	7.6x11.4	11.742	0.056	0.345	0.282	0.279	0.117	III
B16 - M4	10.2x11.4	11.742	0.063	0.304	0.256	0.237	0.126	III

Notes:

1. Average Velocity: Mean velocity prevailing at the approach cross section.
2. Abutment Velocity: Velocity measured along the longitudinal passing through the abutment nose at the approach section.
3. Diverted Velocity: Integrated mean velocity prevailing across the deflected flow portion.
4. All experiments are performed in a 0.61-m wide flume measured at the approach section.
5. Bed slope is set to a value of 0.0037.

Table 10. Experimental conditions for set C runs for abutment scour.

RUN ID	MODEL SIZE (cm x cm)	FLOW DISCHARGE Q (l/s)	APPROACH DEPTH Y (m)	AVERAGE VELOCITY V_u (m/s)	ABUTMENT VELOCITY V_a (m/s)	DIVERTED VELOCITY V_j (m/s)	SCOUR DEPTH D_s (m)	SEDIMENT TYPE
C2 - M2	5.1x11.4	7.553	0.039	0.318	0.293	0.278	0.003	V
C2 - M3	7.6x11.4	7.553	0.042	0.297	0.242	0.238	0.004	V
C2 - M4	10.2x11.4	7.553	0.046	0.270	0.221	0.204	0.005	V
C3 - M2	5.1x11.4	17.306	0.071	0.402	0.380	0.370	0.024	V
C3 - M3	7.6x11.4	17.306	0.075	0.381	0.311	0.309	0.038	V
C3 - M4	10.2x11.4	17.306	0.078	0.362	0.319	0.299	0.038	V
C4 - M2	5.1x11.4	4.876	0.033	0.243	0.220	0.204	0.003	V
C4 - M3	7.6x11.4	4.876	0.035	0.228	0.186	0.181	0.003	V
C4 - M4	10.2x11.4	4.876	0.038	0.210	0.164	0.148	0.005	V
C5 - M2	5.1x11.4	20.454	0.084	0.401	0.379	0.369	0.026	V
C5 - M3	7.6x11.4	20.454	0.086	0.392	0.321	0.319	0.033	V
C5 - M4	10.2x11.4	20.454	0.090	0.374	0.332	0.313	0.045	V
C6 - M2	5.1x11.4	14.298	0.062	0.375	0.352	0.340	0.010	V
C6 - M3	7.6x11.4	14.298	0.070	0.335	0.273	0.270	0.011	V
C6 - M4	10.2x11.4	14.298	0.076	0.310	0.263	0.244	0.022	V
C7 - M2	5.1x11.4	21.912	0.081	0.443	0.424	0.417	0.039	V
C7 - M3	7.6x11.4	21.912	0.087	0.414	0.339	0.338	0.032	V
C7 - M4	10.2x11.4	21.912	0.093	0.388	0.348	0.329	0.039	V
C8 - M2	5.1x11.4	19.502	0.075	0.428	0.408	0.400	0.032	V
C8 - M3	7.6x11.4	19.502	0.079	0.405	0.331	0.330	0.035	V
C8 - M4	10.2x11.4	19.502	0.082	0.390	0.351	0.332	0.036	V

Notes:

1. Average Velocity: Mean velocity prevailing at the approach cross section.
2. Abutment Velocity: Approach velocity measured along the longitudinal passing through the abutment nose.
3. Diverted Velocity: Integrated mean velocity prevailing across the deflected flow portion measured at the approach section.
4. All experiments are performed in a 0.61-m wide flume.

Table 11. Experimental conditions for set G runs for abutment scour.

RUN ID	MODEL SIZE (cm x cm)	FLOW DISCHARGE Q (l/s)	APPROACH DEPTH Y (m)	AVERAGE VELOCITY V_u (m/s)	ABUTMENT VELOCITY V_a (m/s)	DIVERTED VELOCITY V_j (m/s)	SCOUR DEPTH D_s (m)	SEDIMENT TYPE
G1 - M2	5.1x11.4	7.552	0.076	0.163	0.144	0.130	0.006	II
G1 - M3	7.6x11.4	7.553	0.086	0.144	0.118	0.113	0.005	II
G1 - M4	10.2x11.4	7.553	0.092	0.135	0.099	0.087	0.001	II
G2 - M2	5.1x11.4	8.990	0.083	0.178	0.158	0.143	0.020	II
G2 - M3	7.6x11.4	8.990	0.094	0.158	0.129	0.124	0.022	II
G2 - M4	10.2x11.4	8.990	0.098	0.151	0.112	0.099	0.012	II
G3 - M2	5.1x11.4	9.751	0.075	0.214	0.192	0.176	0.047	II
G3 - M3	7.6x11.4	9.751	0.082	0.195	0.160	0.154	0.042	II
G3 - M4	10.2x11.4	9.751	0.092	0.173	0.131	0.117	0.030	II
G4 - M2	5.1x11.4	11.010	0.073	0.246	0.222	0.207	0.079	II
G4 - M3	7.6x11.4	11.010	0.086	0.210	0.172	0.167	0.068	II
G4 - M4	10.2x11.4	11.010	0.092	0.197	0.152	0.137	0.046	II
G5 - M2	5.1x11.4	11.941	0.076	0.258	0.234	0.218	0.084	II
G5 - M3	7.6x11.4	11.943	0.089	0.220	0.180	0.175	0.077	II
G5 - M4	10.2x11.4	11.943	0.095	0.207	0.161	0.145	0.049	II
G6 - M2	5.1x11.4	12.884	0.080	0.265	0.241	0.225	0.098	II
G6 - M3	7.6x11.4	12.884	0.093	0.227	0.186	0.181	0.093	II
G6 - M4	10.2x11.4	12.884	0.096	0.221	0.174	0.158	0.066	II
G7 - M2	5.1x11.4	14.130	0.076	0.304	0.280	0.265	0.113	II
G7 - M3	7.6x11.4	14.130	0.089	0.260	0.213	0.207	0.117	II
G7 - M4	10.2x11.4	14.130	0.091	0.253	0.205	0.188	0.119	II

Notes:

1. Average Velocity: Mean velocity prevailing at the approach cross section.
2. Abutment Velocity: Approach velocity measured along the longitudinal passing through the abutment nose.
3. Diverted Velocity: Integrated mean velocity prevailing across the deflected flow portion measured at the approach section.
4. All experiments are performed in a 0.61-m wide flume.

Table 12. Experimental conditions for set H runs for abutment scour.

RUN #	MODEL SIZE (cm x cm)	FLOW DISCHARGE Q (l/s)	APPROACH DEPTH Y (m)	AVERAGE VELOCITY V_u (m/s)	ABUTMENT VELOCITY V_a (m/s)	DIVERTED VELOCITY V_j (m/s)	SCOUR DEPTH D_s (m)	SEDIMENT TYPE
H1 - M2	5.1x11.4	8.155	0.119	0.112	0.098	0.087	0.008	I
H1 - M3	7.6x11.4	8.155	0.123	0.108	0.089	0.085	0.002	I
H1 - M4	10.2x11.4	8.155	0.129	0.104	0.074	0.064	0.003	I
H2 - M2	5.1x11.4	10.228	0.116	0.144	0.127	0.114	0.026	I
H2 - M3	7.6x11.4	10.228	0.121	0.139	0.114	0.109	0.035	I
H2 - M4	10.2x11.4	10.228	0.125	0.134	0.098	0.086	0.036	I
H3 - M2	5.1x11.4	11.941	0.119	0.164	0.145	0.131	0.040	I
H3 - M3	7.6x11.4	11.941	0.123	0.159	0.130	0.125	0.047	I
H3 - M4	10.2x11.4	11.941	0.128	0.153	0.114	0.101	0.048	I
H4 - M2	5.1x11.4	14.464	0.122	0.195	0.173	0.158	0.060	I
H4 - M3	7.6x11.4	14.464	0.126	0.188	0.155	0.149	0.064	I
H4 - M4	10.2x11.4	14.464	0.129	0.184	0.140	0.125	0.084	I
H5 - M2	5.1x11.4	16.605	0.122	0.224	0.201	0.186	0.087	I
H5 - M3	7.6x11.4	16.605	0.124	0.220	0.181	0.175	0.105	I
H5 - M4	10.2x11.4	16.605	0.128	0.213	0.167	0.151	0.125	I
H6 - M2	5.1x11.4	17.913	0.122	0.241	0.218	0.202	0.105	I
H6 - M3	7.6x11.4	17.913	0.124	0.237	0.195	0.189	0.125	I
H6 - M4	10.2x11.4	17.913	0.127	0.232	0.184	0.167	0.132	I
H7 - M2	5.1x11.4	19.502	0.122	0.262	0.238	0.222	0.119	I
H7 - M3	7.6x11.4	19.502	0.123	0.259	0.213	0.208	0.129	I
H7 - M4	10.2x11.4	19.502	0.126	0.254	0.205	0.188	0.139	I
H8 - M2	5.1x11.4	25.683	0.125	0.336	0.312	0.298	0.115	I
H8 - M3	7.6x11.4	25.683	0.126	0.333	0.274	0.270	0.129	I
H8 - M4	10.2x11.4	25.683	0.129	0.326	0.279	0.260	0.140	I

Notes:

1. Average Velocity: Mean velocity prevailing at the approach cross section.
2. Abutment Velocity: Approach velocity measured along the longitudinal passing through the abutment nose.
3. Diverted Velocity: Integrated mean velocity prevailing across the deflected flow portion measured at the approach section.
4. All experiments are performed in a 0.61-m wide flume.

Table 13. Experimental conditions for set I runs for abutment scour.

RUN ID	MODEL SIZE (cm x cm)	FLOW DISCHARGE Q (l/s)	APPROACH DEPTH Y (m)	AVERAGE VELOCITY V_u (m/s)	ABUTMENT VELOCITY V_a (m/s)	DIVERTED VELOCITY V_j (m/s)	SCOUR DEPTH D_s (m)	SEDIMENT TYPE
I1 - M2	5.1 x 11.4	6.881	0.071	0.158	0.140	0.126	0.0393	I
I1 - M3	7.6 x 11.4	6.881	0.076	0.148	0.121	0.116	0.0299	I
I1 - M4	10.2 x 11.4	6.881	0.080	0.140	0.103	0.091	0.0335	I
I2 - M2	5.1 x 11.4	8.438	0.073	0.190	0.169	0.154	0.0594	I
I2 - M3	7.6 x 11.4	8.438	0.076	0.182	0.149	0.143	0.0524	I
I2 - M4	10.2 x 11.4	8.438	0.080	0.173	0.130	0.116	0.0640	I
I3 - M2	5.1 x 11.4	9.990	0.077	0.213	0.190	0.175	0.0914	I
I3 - M3	7.6 x 11.4	9.990	0.079	0.208	0.170	0.165	0.1052	I
I3 - M4	10.2 x 11.4	9.990	0.080	0.204	0.158	0.143	0.1219	I
I4 - M2	5.1 x 11.4	11.330	0.075	0.249	0.225	0.209	0.1082	I
I4 - M3	7.6 x 11.4	11.330	0.075	0.249	0.203	0.198	0.1210	I
I4 - M4	10.2 x 11.4	11.330	0.075	0.247	0.199	0.181	0.1362	I
I5 - M2	5.1 x 11.4	18.501	0.076	0.398	0.376	0.365	0.1167	I
I5 - M3	7.6 x 11.4	18.501	0.077	0.395	0.323	0.322	0.1356	I
I5 - M4	10.2 x 11.4	18.501	0.077	0.392	0.353	0.334	0.1402	I
I6 - M2	5.1 x 11.4	5.768	0.075	0.127	0.111	0.099	0.0046	I
I6 - M3	7.6 x 11.4	5.768	0.079	0.119	0.098	0.093	0.0027	I
I6 - M4	10.2 x 11.4	5.768	0.081	0.117	0.084	0.074	0.0009	I

Notes:

1. Average Velocity: Mean velocity prevailing at the approach cross section.
2. Abutment Velocity: Approach velocity measured along the longitudinal passing through the abutment nose.
3. Diverted Velocity: Integrated mean velocity across the deflected flow portion measured at the approach section.
4. All experiments are performed in a 0.61-m wide flume.
5. Bed slope is set to a value of 0.0017.

Table 14. Experimental conditions for set J runs for abutment scour.

RUN ID	MODEL SIZE (cm x cm)	FLOW DISCHARGE Q (l/s)	APPROACH DEPTH Y (m)	AVERAGE VELOCITY V_u (m/s)	ABUTMENT VELOCITY V_a (m/s)	DIVERTED VELOCITY V_j (m/s)	SCOUR DEPTH D_s (m)	SEDIMENT TYPE
J1 - M2	5.1 x 11.4	3.786	0.045	0.137	0.120	0.107	0.0162	I
J1 - M3	7.6 x 11.4	3.786	0.048	0.128	0.104	0.100	0.0216	I
J1 - M4	10.2 x 11.4	3.786	0.053	0.118	0.085	0.074	0.0104	I
J2 - M2	5.1 x 11.4	5.295	0.054	0.160	0.141	0.128	0.0460	I
J2 - M3	7.6 x 11.4	5.295	0.054	0.162	0.132	0.127	0.0747	I
J2 - M4	10.2 x 11.4	5.295	0.055	0.158	0.118	0.105	0.0829	I
J3 - M2	5.1 x 11.4	6.711	0.052	0.210	0.188	0.173	0.0823	I
J3 - M3	7.6 x 11.4	6.711	0.050	0.222	0.181	0.176	0.0948	I
J3 - M4	10.2 x 11.4	6.711	0.049	0.226	0.178	0.162	0.1076	I
J4 - M2	5.1 x 11.4	7.561	0.051	0.245	0.222	0.206	0.0969	I
J4 - M3	7.6 x 11.4	7.561	0.047	0.266	0.217	0.212	0.1024	I
J4 - M4	10.2 x 11.4	7.561	0.045	0.275	0.226	0.208	0.1158	I
J5 - M2	5.1 x 11.4	10.449	0.059	0.290	0.266	0.250	0.1052	I
J5 - M3	7.6 x 11.4	10.449	0.055	0.311	0.253	0.250	0.1036	I
J5 - M4	10.2 x 11.4	10.449	0.054	0.320	0.272	0.254	0.1234	I
J6 - M2	5.1 x 11.4	3.455	0.045	0.126	0.110	0.098	0.0021	I
J6 - M3	7.6 x 11.4	3.455	0.049	0.116	0.095	0.091	0.0009	I
J6 - M4	10.2 x 11.4	3.455	0.049	0.116	0.083	0.073	0.0003	I

Notes:

1. Average Velocity: Mean velocity prevailing at the approach cross section.
2. Abutment Velocity: Velocity measured along the longitudinal passing through the abutment nose at the approach section.
3. Diverted Velocity: Integrated mean velocity prevailing across the deflected flow portion.
4. All experiments are performed in a 0.61-m wide flume measured at the approach section.
5. Bed slope is set to a value of 0.0017.

Table 15. Experimental conditions for set K runs for abutment scour.

RUN ID	MODEL SIZE (cm x cm)	FLOW DISCHARGE Q (l/s)	APPROACH DEPTH Y (m)	AVERAGE VELOCITY V_u (m/s)	ABUTMENT VELOCITY V_a (m/s)	DIVERTED VELOCITY V_j (m/s)	SCOUR DEPTH D_s (m)	SEDIMENT TYPE
K1 - M2	5.1 x 11.4	6.895	0.073	0.155	0.136	0.123	0.0021	VII
K1 - M3	7.6 x 11.4	6.895	0.076	0.148	0.121	0.117	0.0009	VII
K1 - M4	10.2 x 11.4	6.895	0.081	0.140	0.102	0.090	0.0006	VII
K2 - M2	5.1 x 11.4	8.444	0.072	0.193	0.172	0.157	0.0128	VII
K2 - M3	7.6 x 11.4	8.444	0.075	0.185	0.151	0.146	0.0043	VII
K2 - M4	10.2 x 11.4	8.444	0.080	0.174	0.132	0.118	0.0034	VII
K3 - M2	5.1 x 11.4	9.992	0.079	0.208	0.186	0.170	0.0287	VII
K3 - M3	7.6 x 11.4	9.992	0.078	0.209	0.171	0.166	0.0250	VII
K3 - M4	10.2 x 11.4	9.992	0.080	0.204	0.158	0.143	0.0277	VII
K4 - M2	5.1 x 11.4	11.640	0.074	0.257	0.233	0.217	0.0491	VII
K4 - M3	7.6 x 11.4	11.640	0.073	0.261	0.213	0.208	0.0631	VII
K4 - M4	10.2 x 11.4	11.640	0.073	0.262	0.214	0.196	0.0728	VII
K5 - M2	5.1 x 11.4	12.898	0.073	0.290	0.266	0.251	0.0762	VII
K5 - M3	7.6 x 11.4	12.898	0.072	0.293	0.239	0.235	0.0741	VII
K5 - M4	10.2 x 11.4	12.898	0.073	0.292	0.243	0.225	0.0860	VII
K6 - M2	5.1 x 11.4	14.626	0.076	0.316	0.292	0.277	0.0835	VII
K6 - M3	7.6 x 11.4	14.626	0.074	0.323	0.264	0.260	0.0933	VII
K6 - M4	10.2 x 11.4	14.626	0.074	0.325	0.279	0.260	0.1149	VII
K7 - M2	5.1 x 11.4	16.889	0.078	0.356	0.333	0.319	0.0884	VII
K7 - M3	7.6 x 11.4	16.889	0.075	0.370	0.302	0.300	0.1012	VII
K7 - M4	10.2 x 11.4	16.889	0.075	0.368	0.326	0.306	0.1244	VII

Notes:

1. Average Velocity: Mean velocity prevailing at the approach cross section.
2. Abutment Velocity: Velocity measured along the longitudinal passing through the abutment nose at the approach section.
3. Diverted Velocity: Integrated mean velocity prevailing across the deflected flow portion.
4. All experiments are performed in a 0.61-m wide flume measured at the approach section.
5. Bed slope is set to a value of 0.0017.

Table 16. Experimental conditions for set L runs for abutment scour.

RUN ID	MODEL SIZE (cm x cm)	FLOW DISCHARGE Q (l/s)	APPROACH DEPTH Y (m)	AVERAGE VELOCITY V_u (m/s)	ABUTMENT VELOCITY V_a (m/s)	DIVERTED VELOCITY V_j (m/s)	SCOUR DEPTH D_s (m)	SEDIMENT TYPE
L1 - M2	5.1 x 11.4	11.327	0.075	0.249	0.225	0.209	0.0290	III
L1 - M3	7.6 x 11.4	11.327	0.077	0.241	0.197	0.192	0.0283	III
L1 - M4	10.2 x 11.4	11.327	0.080	0.234	0.186	0.169	0.0302	III
L2 - M2	5.1 x 11.4	15.106	0.077	0.323	0.298	0.284	0.0991	III
L2 - M3	7.6 x 11.4	15.106	0.076	0.325	0.266	0.262	0.1015	III
L2 - M4	10.2 x 11.4	15.106	0.077	0.324	0.277	0.258	0.1082	III
L3 - M2	5.1 x 11.4	16.888	0.079	0.350	0.326	0.312	0.1082	III
L3 - M3	7.6 x 11.4	16.888	0.079	0.352	0.288	0.285	0.1109	III
L3 - M4	10.2 x 11.4	16.888	0.077	0.359	0.316	0.297	0.1222	III
L4 - M2	5.1 x 11.4	18.882	0.081	0.381	0.358	0.346	0.1155	III
L4 - M3	7.6 x 11.4	18.883	0.077	0.400	0.327	0.326	0.1183	III
L4 - M4	10.2 x 11.4	18.882	0.078	0.399	0.361	0.342	0.1433	III
L5 - M2	5.1 x 11.4	20.453	0.084	0.402	0.380	0.369	0.1201	III
L5 - M3	7.6 x 11.4	20.453	0.080	0.422	0.345	0.345	0.1253	III
L5 - M4	10.2 x 11.4	20.453	0.078	0.432	0.400	0.382	0.1420	III
L6 - M2	5.1 x 11.4	9.992	0.073	0.226	0.203	0.188	0.0027	III
L6 - M3	7.6 x 11.4	9.992	0.075	0.219	0.179	0.174	0.0018	III
L6 - M4	10.2 x 11.4	9.992	0.078	0.211	0.165	0.149	0.0015	III
L7 - M2	5.1 x 11.4	9.251	0.073	0.207	0.186	0.170	0.0003	III
L7 - M3	7.6 x 11.4	9.251	0.076	0.201	0.164	0.159	0.0003	III
L7 - M4	10.2 x 11.4	9.251	0.078	0.194	0.149	0.134	0.0003	III
L8 - M2	5.1 x 11.4	13.790	0.078	0.291	0.267	0.251	0.0692	III
L8 - M3	7.6 x 11.4	13.790	0.078	0.289	0.236	0.232	0.0732	III
L8 - M4	10.2 x 11.4	13.790	0.079	0.285	0.237	0.219	0.0741	III

Notes:

1. Average Velocity: Mean velocity prevailing at the approach cross section.
2. Abutment Velocity: Velocity measured along the longitudinal passing through the abutment nose at the approach section.
3. Diverted Velocity: Integrated mean velocity prevailing across the deflected flow portion.
4. All experiments are performed in a 0.61-m wide flume measured at the approach section.
5. Bed slope is set to a value of 0.0017.

Table 17. Experimental conditions for set M runs for abutment scour.

RUN ID	MODEL SIZE (cm x cm)	FLOW DISCHARGE Q (l/s)	APPROACH DEPTH Y (m)	AVERAGE VELOCITY V_u (m/s)	ABUTMENT VELOCITY V_a (m/s)	DIVERTED VELOCITY V_j (m/s)	SCOUR DEPTH D_s (m)	SEDIMENT TYPE
M1 - M2	5.1 x 11.4	13.441	0.075	0.293	0.269	0.253	0.0232	VI
M1 - M3	7.6 x 11.4	13.441	0.077	0.287	0.235	0.230	0.0238	VI
M1 - M4	10.2 x 11.4	13.441	0.079	0.279	0.231	0.213	0.0344	VI
M2 - M2	5.1 x 11.4	14.627	0.075	0.320	0.296	0.281	0.0283	VI
M2 - M3	7.6 x 11.4	14.627	0.075	0.320	0.262	0.258	0.0280	VI
M2 - M4	10.2 x 11.4	14.627	0.076	0.317	0.270	0.251	0.0421	VI
M3 - M2	5.1 x 11.4	15.571	0.075	0.341	0.317	0.303	0.0293	VI
M3 - M3	7.6 x 11.4	15.571	0.076	0.338	0.276	0.273	0.0344	VI
M3 - M4	10.2 x 11.4	15.571	0.077	0.333	0.286	0.267	0.0546	VI
M4 - M2	5.1 x 11.4	17.169	0.076	0.373	0.349	0.337	0.0479	VI
M4 - M3	7.6 x 11.4	17.169	0.075	0.377	0.308	0.306	0.0515	VI
M4 - M4	10.2 x 11.4	17.169	0.076	0.371	0.329	0.310	0.0762	VI
M5 - M2	5.1 x 11.4	17.714	0.077	0.378	0.355	0.343	0.0527	VI
M5 - M3	7.6 x 11.4	17.714	0.076	0.384	0.314	0.312	0.0594	VI
M5 - M4	10.2 x 11.4	17.714	0.076	0.384	0.344	0.325	0.0866	VI
M6 - M2	5.1 x 11.4	18.372	0.077	0.389	0.367	0.355	0.0588	VI
M6 - M3	7.6 x 11.4	18.372	0.076	0.396	0.323	0.322	0.0671	VI
M6 - M4	10.2 x 11.4	18.372	0.076	0.399	0.361	0.342	0.0887	VI
M7 - M2	5.1 x 11.4	19.502	0.079	0.407	0.385	0.375	0.0728	VI
M7 - M3	7.6 x 11.4	19.502	0.077	0.413	0.338	0.337	0.0744	VI
M7 - M4	10.2 x 11.4	19.502	0.077	0.415	0.380	0.361	0.1113	VI
M8 - M2	5.1 x 11.4	20.685	0.079	0.430	0.410	0.401	0.0789	VI
M8 - M3	7.6 x 11.4	20.685	0.077	0.438	0.358	0.359	0.0796	VI
M8 - M4	10.2 x 11.4	20.685	0.074	0.456	0.431	0.412	0.1177	VI
M9 - M2	5.1 x 11.4	22.128	0.084	0.433	0.413	0.405	0.0853	VI
M9 - M3	7.6 x 11.4	22.128	0.082	0.444	0.364	0.364	0.0856	VI
M9 - M4	10.2 x 11.4	22.128	0.081	0.449	0.422	0.404	0.1228	VI
M10 - M2	5.1 x 11.4	11.327	0.076	0.245	0.221	0.206	0.0037	VI
M10 - M3	7.6 x 11.4	11.327	0.077	0.242	0.198	0.193	0.0030	VI
M10 - M4	10.2 x 11.4	11.327	0.079	0.235	0.188	0.171	0.0055	VI

Notes:

1. Average Velocity: Mean velocity prevailing at the approach cross section.
2. Abutment Velocity: Velocity measured along the longitudinal passing through the abutment nose at the approach section.
3. Diverted Velocity: Integrated mean velocity prevailing across the deflected flow portion.
4. All experiments are performed in a 0.61-m wide flume measured at the approach section.
5. Bed slope is set to a value of 0.0017.

Table 18. Experimental conditions for set N runs for abutment scour.

RUN ID	MODEL SIZE (cm x cm)	FLOW DISCHARGE Q (l/s)	APPROACH DEPTH Y (m)	AVERAGE VELOCITY V_u (m/s)	ABUTMENT VELOCITY V_a (m/s)	DIVERTED VELOCITY V_j (m/s)	SCOUR DEPTH D_s (m)	SEDIMENT TYPE
N1 - M2	5.1 x 11.4	13.441	0.075	0.294	0.270	0.254	0.0098	IV
N1 - M3	7.6 x 11.4	13.441	0.076	0.289	0.237	0.232	0.0079	IV
N1 - M4	10.2 x 11.4	13.441	0.080	0.277	0.229	0.210	0.0158	IV
N2 - M2	5.1 x 11.4	14.463	0.075	0.315	0.291	0.276	0.0207	IV
N2 - M3	7.6 x 11.4	14.463	0.076	0.311	0.255	0.250	0.0174	IV
N2 - M4	10.2 x 11.4	14.463	0.078	0.303	0.255	0.236	0.0213	IV
N3 - M2	5.1 x 11.4	15.416	0.077	0.331	0.306	0.292	0.0235	IV
N3 - M3	7.6 x 11.4	15.416	0.076	0.332	0.271	0.268	0.0283	IV
N3 - M4	10.2 x 11.4	15.416	0.077	0.327	0.280	0.261	0.0360	IV
N4 - M2	5.1 x 11.4	17.029	0.078	0.358	0.334	0.321	0.0338	IV
N4 - M3	7.6 x 11.4	17.029	0.077	0.362	0.296	0.294	0.0347	IV
N4 - M4	10.2 x 11.4	17.029	0.077	0.364	0.321	0.302	0.0610	IV
N5 - M2	5.1 x 11.4	18.372	0.078	0.386	0.364	0.352	0.0488	IV
N5 - M3	7.6 x 11.4	18.372	0.076	0.397	0.325	0.323	0.0619	IV
N5 - M4	10.2 x 11.4	18.372	0.074	0.407	0.371	0.352	0.0914	IV
N6 - M2	5.1 x 11.4	19.502	0.079	0.407	0.385	0.375	0.0527	IV
N6 - M3	7.6 x 11.4	19.502	0.077	0.418	0.342	0.342	0.0689	IV
N6 - M4	10.2 x 11.4	19.502	0.077	0.416	0.382	0.363	0.0963	IV
N7 - M2	5.1 x 11.4	20.685	0.080	0.423	0.403	0.394	0.0619	IV
N7 - M3	7.6 x 11.4	20.685	0.078	0.435	0.356	0.356	0.0728	IV
N7 - M4	10.2 x 11.4	20.685	0.078	0.437	0.406	0.388	0.1045	IV
N8 - M2	5.1 x 11.4	22.128	0.085	0.427	0.406	0.398	0.0689	IV
N8 - M3	7.6 x 11.4	22.128	0.082	0.443	0.362	0.363	0.0789	IV
N8 - M4	10.2 x 11.4	22.128	0.080	0.456	0.431	0.413	0.1128	IV
N9 - M2	5.1 x 11.4	11.740	0.075	0.257	0.233	0.217	0.0040	IV
N9 - M3	7.6 x 11.4	11.740	0.076	0.253	0.207	0.202	0.0027	IV
N9 - M4	10.2 x 11.4	11.740	0.079	0.243	0.195	0.178	0.0021	IV

Notes:

1. Average Velocity: Mean velocity prevailing at the approach cross section.
2. Abutment Velocity: Approach velocity measured along the longitudinal passing through the abutment nose.
3. Diverted Velocity: Integrated mean velocity prevailing across the deflected flow portion.
4. All experiments are performed in a 0.61-m wide flume measured at the approach section.
5. Bed slope is set to a value of 0.0017.

Table 19. Experimental conditions for set D runs for abutment scour.

RUN ID	MODEL SIZE (cm x cm)	FLOW DISCHARGE Q (l/s)	APPROACH DEPTH Y (m)	AVERAGE VELOCITY V_u (m/s)	ABUTMENT VELOCITY V_a (m/s)	DIVERTED VELOCITY V_j (m/s)	SCOUR DEPTH D_s (m)	SEDIMENT TYPE
D1 - M1	21.6 x 45.7	184.060	0.323	0.233	0.236	0.235	0.0579	VIII
D1 - M2	21.6 x 45.7	184.060	0.326	0.231	0.206	0.195	0.0320	XI
D1 - M3	21.6 x 45.7	184.060	0.326	0.231	0.195	0.192	0.0323	X
D1 - M4	17.8 x 45.7	184.060	0.326	0.231	0.175	0.161	0.0253	VIII
D2 - M1	21.6 x 45.7	176.980	0.324	0.224	0.222	0.216	0.0472	VIII
D2 - M2	21.6 x 45.7	176.980	0.326	0.223	0.191	0.189	0.0122	XI
D2 - M3	21.6 x 45.7	176.980	0.326	0.223	0.186	0.180	0.0137	X
D2 - M4	17.8 x 45.7	176.980	0.317	0.229	0.172	0.155	0.0198	VIII
D3 - M1	21.6 x 45.7	198.218	0.308	0.264	0.247	0.244	0.0625	VIII
D3 - M2	21.6 x 45.7	198.218	0.309	0.263	0.219	0.204	0.0140	XI
D3 - M3	21.6 x 45.7	198.218	0.314	0.259	0.201	0.189	0.1234	X
D3 - M4	17.8 x 45.7	198.218	0.316	0.257	0.183	0.172	0.0256	VIII
D4 - M1	21.6 x 45.7	229.366	0.317	0.296	0.267	0.265	0.0686	VIII
D4 - M2	21.6 x 45.7	229.366	0.321	0.293	0.234	0.219	0.0204	XI
D4 - M3	21.6 x 45.7	229.366	0.323	0.291	0.219	0.213	0.0344	X
D4 - M4	17.8 x 45.7	229.366	0.326	0.288	0.202	0.192	0.0445	VIII
D5 - M1	21.6 x 45.7	257.117	0.324	0.325	0.300	0.299	0.1103	VIII
D5 - M2	21.6 x 45.7	257.117	0.331	0.319	0.265	0.250	0.0299	XI
D5 - M3	21.6 x 45.7	257.117	0.334	0.316	0.255	0.244	0.0485	X
D5 - M4	17.8 x 45.7	257.117	0.325	0.325	0.249	0.216	0.0564	VIII
D6 - M1	21.6 x 45.7	295.628	0.327	0.371	0.331	0.329	0.1692	VIII
D6 - M2	21.6 x 45.7	295.628	0.331	0.367	0.299	0.277	0.0451	XI
D6 - M3	21.6 x 45.7	295.628	0.329	0.369	0.289	0.274	0.0671	X
D6 - M4	17.8 x 45.7	295.628	0.327	0.371	0.265	0.245	0.0817	VIII
D7 - M1	21.6 x 45.7	242.392	0.327	0.304	0.272	0.271	0.0866	VIII
D7 - M2	21.6 x 45.7	242.392	0.333	0.299	0.241	0.229	0.0320	XI
D7 - M3	21.6 x 45.7	242.392	0.336	0.296	0.231	0.223	0.0421	X
D7 - M4	17.8 x 45.7	242.392	0.336	0.296	0.219	0.202	0.0415	VIII
D8 - M1	21.6 x 45.7	144.416	0.311	0.191	0.189	0.183	0.0204	VIII
D8 - M2	21.6 x 45.7	144.416	0.311	0.190	0.165	0.152	0.0024	XI
D8 - M3	21.6 x 45.7	144.416	0.312	0.190	0.158	0.149	0.0076	X
D8 - M4	17.8 x 45.7	144.416	0.312	0.190	0.146	0.131	0.0058	VIII

Notes:

1. Average Velocity: Mean velocity prevailing at the approach cross section.
2. Abutment Velocity: Velocity measured along the longitudinal passing through the abutment nose at the approach section.
3. Diverted Velocity: Integrated mean velocity prevailing across the deflected flow portion.
4. All experiments are performed in a 2.44-m wide flume measured at the approach section.
5. Bed slope is set to a value of 0.0007.

Table 20. Experimental conditions for set E runs for abutment scour.

RUN ID	MODEL SIZE (cm x cm)	FLOW DISCHARGE Q (l/s)	APPROACH DEPTH Y (m)	AVERAGE VELOCITY V_u (m)	ABUTMENT VELOCITY V_a (m)	DIVERTED VELOCITY V_j (m/s)	SCOUR DEPTH D_s (m)	SEDIMENT TYPE
E1 - M1	21.6 x 45.7	147.25	0.279	0.216	0.206	0.204	0.0189	IX
E1 - M2	21.6 x 45.7	147.25	0.284	0.213	0.182	0.173	0.0168	XII
E1 - M3	21.6 x 45.7	147.25	0.292	0.207	0.166	0.155	0.0320	II
E1 - M4	21.6 x 45.7	147.25	0.283	0.213	0.152	0.136	0.0213	XIII
E2 - M1	21.6 x 45.7	172.73	0.305	0.232	0.236	0.234	0.0317	IX
E2 - M2	21.6 x 45.7	172.73	0.297	0.238	0.202	0.188	0.0213	XII
E2 - M3	21.6 x 45.7	172.73	0.293	0.242	0.183	0.178	0.0774	II
E2 - M4	21.6 x 45.7	172.73	0.299	0.237	0.155	0.155	0.0579	XIII
E3 - M1	21.6 x 45.7	202.47	0.293	0.283	0.268	0.265	0.0152	IX
E3 - M2	21.6 x 45.7	202.47	0.299	0.278	0.230	0.223	0.0229	XII
E3 - M3	21.6 x 45.7	202.47	0.305	0.272	0.212	0.204	0.0844	II
E3 - M4	21.6 x 45.7	202.47	0.301	0.276	0.193	0.168	0.0457	XIII
E4 - M1	21.6 x 45.7	232.20	0.294	0.324	0.300	0.297	0.0360	IX
E4 - M2	21.6 x 45.7	232.20	0.300	0.317	0.260	0.248	0.0256	XII
E4 - M3	21.6 x 45.7	232.20	0.305	0.312	0.243	0.233	0.0957	II
E4 - M4	21.6 x 45.7	232.20	0.299	0.319	0.213	0.173	0.0579	XIII
E5 - M1	21.6 x 45.7	263.35	0.299	0.362	0.332	0.329	0.0500	IX
E5 - M2	21.6 x 45.7	263.35	0.303	0.357	0.298	0.286	0.0399	XII
E5 - M3	21.6 x 45.7	263.35	0.313	0.345	0.272	0.267	0.1481	II
E5 - M4	21.6 x 45.7	263.35	0.301	0.359	0.251	0.223	0.0671	XIII
E6 - M1	21.6 x 45.7	311.49	0.293	0.437	0.416	0.417	0.1094	IX
E6 - M2	21.6 x 45.7	311.49	0.298	0.429	0.356	0.337	0.0884	XII
E6 - M3	21.6 x 45.7	311.49	0.307	0.417	0.320	0.292	0.2060	II
E6 - M4	21.6 x 45.7	311.49	0.287	0.446	0.337	0.320	0.1301	XIII
E7 - M1	21.6 x 45.7	368.12	0.306	0.493	0.477	0.475	0.1576	IX
E7 - M2	21.6 x 45.7	368.12	0.310	0.488	0.412	0.395	0.1027	XII
E7 - M3	21.6 x 45.7	368.12	0.315	0.479	0.383	0.360	0.2652	II
E7 - M4	21.6 x 45.7	368.12	0.288	0.524	0.405	0.386	0.2103	XIII
E8 - M1	21.6 x 45.7	450.24	0.307	0.601	0.593	0.583	0.3216	IX
E8 - M2	21.6 x 45.7	450.24	0.308	0.600	0.511	0.501	0.2188	XII
E8 - M3	21.6 x 45.7	450.24	0.297	0.621	0.506	0.486	0.0884	XIV
E8 - M4	21.6 x 45.7	450.24	0.296	0.625	0.390	0.309	0.2149	XIII
E9 - M3	21.6 x 45.7	478.55	0.299	0.657	0.649	0.612	0.1890	XIV
E9 - M4	21.6 x 45.7	478.55	0.274	0.715	0.519	0.496	0.1728	XVI
E10 - M3	21.6 x 45.7	518.20	0.283	0.750	0.713	0.685	0.3158	XIV
E10 - M4	21.6 x 45.7	518.20	0.274	0.775	0.669	0.601	0.3136	XVI

Notes:

1. Average Velocity: Mean velocity prevailing at the approach cross section.
2. Abutment Velocity: Velocity measured along the longitudinal passing through the abutment nose at the approach section.
3. Diverted Velocity: Integrated mean velocity prevailing across the deflected flow portion.
4. All experiments are performed in a 2.44-m wide flume measured at the approach section.
5. Bed slope is set to a value of 0.0007.

Table 21. Experimental conditions for set F runs for abutment scour.

RUN ID	MODEL SIZE (cm x cm)	FLOW DISCHARGE Q (l/s)	APPROACH DEPTH Y (m)	AVERAGE VELOCITY V_u (m/s)	DIVERTED VELOCITY V_j (m/s)	SEDIMENT TYPE
F1 - MA	20.3 x 96.5	277.505	0.226	0.226	0.241	XV
F1 - MB	21.6 x 96.5	277.505	0.216	0.216	0.253	XV
F1 - MC	64.8 x 96.5	277.505	0.223	0.223	0.241	XV
F1 - MD	43.2 x 96.5	277.505	0.213	0.213	0.253	XV
F2 - MA	20.3 x 96.5	351.129	0.226	0.226	0.308	XV
F2 - MB	21.6 x 96.5	351.129	0.213	0.213	0.323	XV
F2 - MC	64.8 x 96.5	351.129	0.219	0.219	0.308	XV
F2 - MD	43.2 x 96.5	351.129	0.210	0.210	0.323	XV
F3 - MA	20.3 x 96.5	390.772	0.198	0.198	0.393	XV
F3 - MB	21.6 x 96.5	390.772	0.185	0.185	0.411	XV
F3 - MC	64.8 x 96.5	390.772	0.192	0.192	0.393	XV
F4 - MD	43.2 x 96.5	390.772	0.183	0.183	0.411	XV

Notes:

1. Average Velocity: Mean velocity prevailing at the approach cross section.
2. Abutment Velocity: Velocity measured along the longitudinal passing through the abutment nose at the approach section.
3. Diverted Velocity: Integrated mean velocity prevailing across the deflected flow portion.
4. All experiments are performed in a 5.2-m wide flume measured at the approach section.
5. Bed slope is set to a value of 0.0007.

Table 22. Properties of sediment mixture types used in abutment scour experiments.

SEDIMENT TYPE	D_{16} (mm)	D_{50} (mm)	D_{84} (mm)	D_{90} (mm)	D_{95} (mm)	D_{100} (mm)	σ_g
I	0.07	0.10	0.14	0.15	0.17	0.25	1.40
II	0.59	0.78	1.00	1.10	1.15	1.19	1.30
II	1.60	1.80	2.20	2.30	2.35	2.38	1.17
IV	0.86	1.80	3.70	4.10	5.00	5.60	2.07
V	0.36	1.80	5.50	6.70	8.00	10.00	3.91
VI	1.60	1.80	2.20	3.90	4.80	5.60	1.17
VII	0.07	0.10	0.14	2.20	2.35	2.83	1.40
VIII	0.31	0.78	1.83	2.10	2.35	4.00	2.43
IX	0.23	0.78	2.65	3.20	4.20	9.00	3.40
X	0.31	0.78	1.83	2.10	2.35	10.00	2.43
XI	0.31	0.78	1.83	2.80	5.00	10.00	2.43
XII	0.23	0.78	2.65	4.76	6.40	9.00	3.40
XIII	0.02	0.65	0.95	1.05	1.10	1.20	6.60
XIV	2.00	3.10	4.20	4.50	5.00	7.00	1.45
XV	0.25	0.55	1.10	1.30	1.50	2.38	2.10
XVI	1.30	2.70	3.70	3.90	4.20	7.00	1.68

Notes:

D_{16}, D_{50}, D_{84}, D_{90}, D_{95}, D_{100} = Sediment size for which 26, 50, 84, 90, 95, and 100 percent of sediment is finer by weight, respectively.

σ_g = Gradation Coefficient, $(D_{84}/D_{16})^{0.5}$.

3.4 ANALYSIS

In the following analysis, the governing parameters that were found to be affecting abutment scour are presented first. Second, the results of scour experiments utilizing fine uniform sand with 0.1-mm median diameter are given. Third, adjustments to nonuniform mixtures are discussed as a function of gradation coefficients. Finally, the newly developed equation for nonuniform sediment mixtures is presented, including adjustments for coarse fractions.

Governing Parameters

In designing the experimental program given in section 3.3, series of geometry, flow, and sediment properties were considered for relating the local scour to physical parameters. Among the geometric properties, abutment protrusion length is the most commonly used scaling parameter. In a physical sense, the larger the vertically projected length of the protrusion into the flow, the larger the expected local scour. However, as commonly observed in the field, beyond a certain protrusion length, the stagnation zone that forms in front of the abutment alters the behavior. Along with the protrusion length, the second commonly used parameter in relating scour to a physical length dimension is the flow depth. For this purpose, various depth values at various locations along and across the channel have been proposed in the past. Since the present experiments were conducted in a rectangular channel with no overbank regions, and since the main focus of the study was quantifying effects of sediment properties, the effects of return flows could not be accounted. However, to account for the governing geometric length parameter, after examining various scaling parameters, the square root of the blocked flow area was adopted for the length scaling.

$$L_c = \sqrt{aY_j} \tag{17}$$

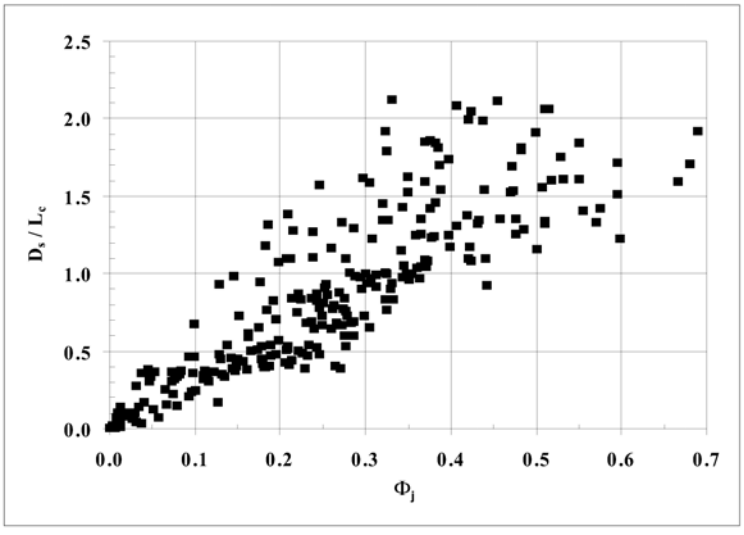

Figure 27. Variation of dimensionless abutment scour with deflected flow excess velocity.

where Y_j is the average depth in the approach to the abutment. Flow parameters considered in the analysis included: average free stream velocity, V_u, abutment in-line velocity, V_a, depth- and width-averaged deflected flow zone velocity, V_j, and the Froude number, momentum, and energy of the deflected flow . Among these flow variables, V_a and V_j were found to be the most significant parameters. Since V_j reflects the approach region upstream from the abutment, and since it is related to the abutment nose velocities, it was chosen as the dominant velocity parameter. Using an approach similar to the approach for pier scour, a dimensionless velocity termed as deflected flow excess velocity was derived. This velocity is given by:

$$\Phi_j = \frac{V_j - V_i}{V_c} \tag{18}$$

where V_c and V_i are the critical velocity at the approach mobilizing the bed, and scour initiating velocity at the abutment nose, respectively. These two quantities were measured in the experiments. However, they can be obtained through Neill's equation[19]:

$$V_c = 1.58\ [(S_s - 1)\, g\, D_{50}]^{1/2}\ (\frac{Y}{D_{50}})^{1/6} \tag{19}$$

and V_i . *0.4* V_c for abutment scour initiation. According to Abdou[7], in computing V_c for nonuniform mixtures using equation 19, the term D_{50} should be replaced by D_{90}. Utilizing D_s / L_c and Φ_j as the dependent and independent parameters, the data in figure 26 are replotted in figure 27. As can be seen, the improvement is remarkable.

SCOUR IN UNIFORM MIXTURES

To eliminate the effects of coarse size fraction on the resulting abutment scour, a series of experiments was conducted using a uniform fine sand mixture with median diameter of 0.1 mm. The scour corresponding to these conditions represents an envelop condition where adjustments for size gradation and coarse fraction can be applied. Using D_s / L_c and Φ_j, and accommodating a residual correction factor due to (Y/a), the following relationship was derived [20]:

$$\frac{D_s}{L_c} = K_\Phi\, \Phi_j \tag{20}$$

where

$$K_\Phi = 3.75 - 0.41\,(\frac{a}{Y}) \tag{21}$$

Figure 28(a) presents the measured and computed abutment scour for the uniform fine sand. The uniform scour relationship given above can be adjusted for gradation and coarse fraction effects by introducing additional parameters. For this purpose two different approaches are followed. The first approach makes gradation corrections to the predicted scour values, whereas the second approach introduces a coarse fraction correction. These approaches are given below.

Scour in Graded Mixtures

The scour in mixtures with different gradations can be adjusted by introducing a gradation adjustment factor, K_s. This adjustment factor was determined from experimental data by obtaining ratios of scour in graded material and uniform mixtures. A series of curves was developed for 0.78-mm and 1.8-mm sand. These curves, which exhibited very similar features, were then combined into a single set of curves given in figure 28(a). As shown in this figure, K_s is not a constant but varies with flow intensity. Similar to the pier scour corrections, the scour reductions are negligible for low flows and for flows with high intensities. However, the adjustments are significant for a wide range of intermediate flows. The values obtained from figure 28(a) can be directly applied to uniform scour estimates from equation 20 to obtain gradation adjusted estimates for given deflected flow excess velocities.

COARSE MATERIAL ADJUSTMENTS

Experimental results from the study have shown that abutment scour in nonuniform mixtures is greatly affected by the presence of coarse sizes. It was found that the sediment size corresponding to the coarsest 15 percent have a significant effect on the resulting scour. Using results of experiments, the following coarse fraction correction was developed.

$$\frac{D_s}{L_c} = K_n \, K_\theta \, K_{15} \, K_\Phi \, \Phi_j \tag{22}$$

where the adjustments K_Φ and K_2 (flow inclination factor in HEC-18[13]) are given by:

$$K_\Phi = 3.75 - 0.41 \left(\frac{a}{Y}\right) \tag{23}$$

$$K_\theta = \left(\frac{\theta}{90}\right)^{0.13} \tag{24}$$

and K_n is abutment shape factor (given in HEC-18 as 1.0 for vertical wall abutments; 0.82 for wing-wall abutments; and 0.55 for spillthrough abutments). The factor K_{15} is to account for the composition of the coarsest 15th percentile and is obtained from figure 28(b) graphically. It is expressed by Abdeldayem[20] in terms of a sediment weighing factor W_g:

$$K_{15} = f(W_g) \tag{25}$$

where

$$W_g = \sum_{j=85}^{j=100} p_j \, (d_j)^2 \tag{26}$$

p_j is the fraction falling into a size group j (percent finer by weight), and d_j is the sediment size for which j percent of sediment in the mixture are finer. The term W_g is a term similar to the coarse fraction size D_{cfm} used earlier in chapter 2. It represents the size of the coarse fraction by the ratio of areas occupied by them rather than the mean size represented by D_{cfm}. Figure 29 shows the agreement of this equation with the experimental data.

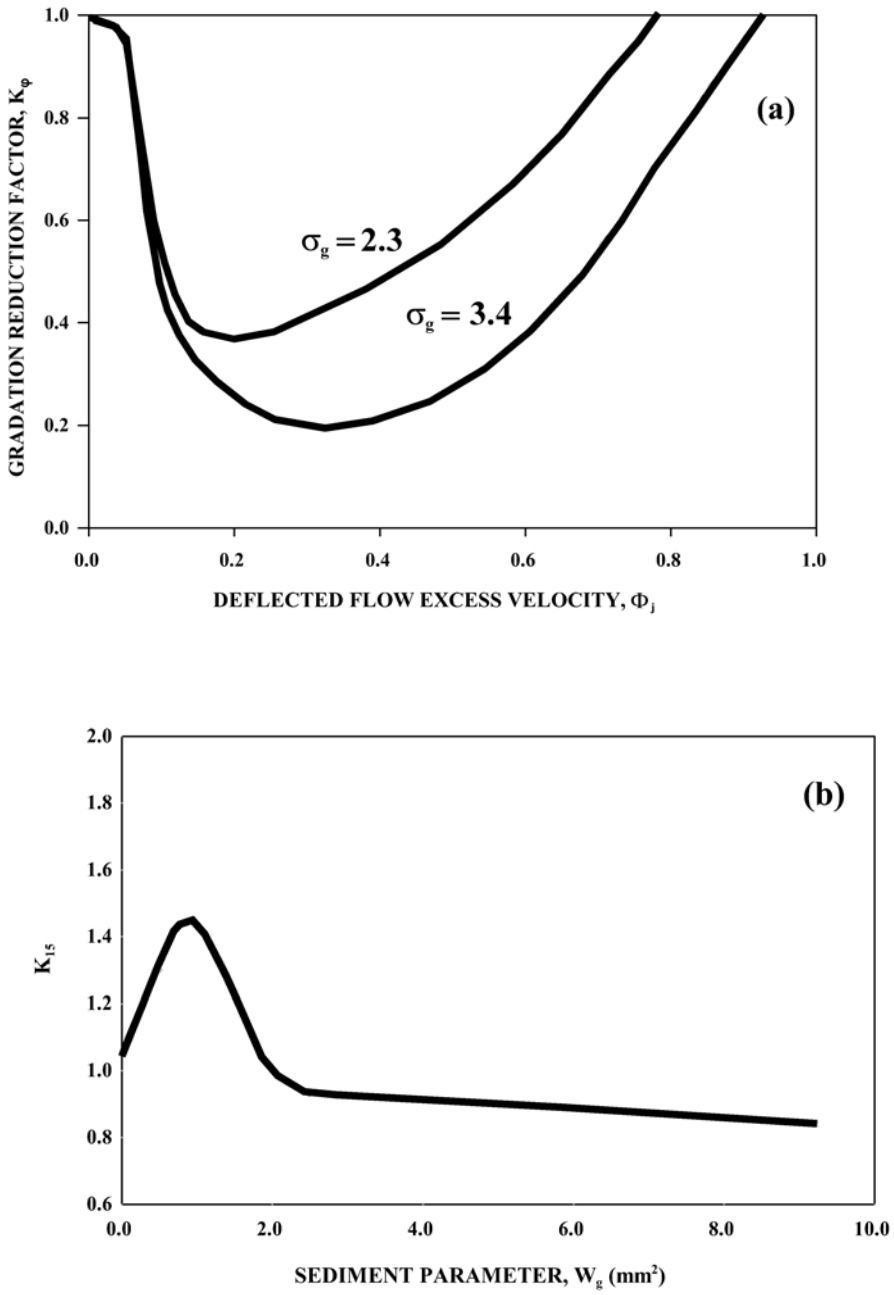

Figure 28. Adjustment factors for gradation and coarse material fraction: (a) gradation reduction factor; (b) coarse fraction adjustment, K_{15}.

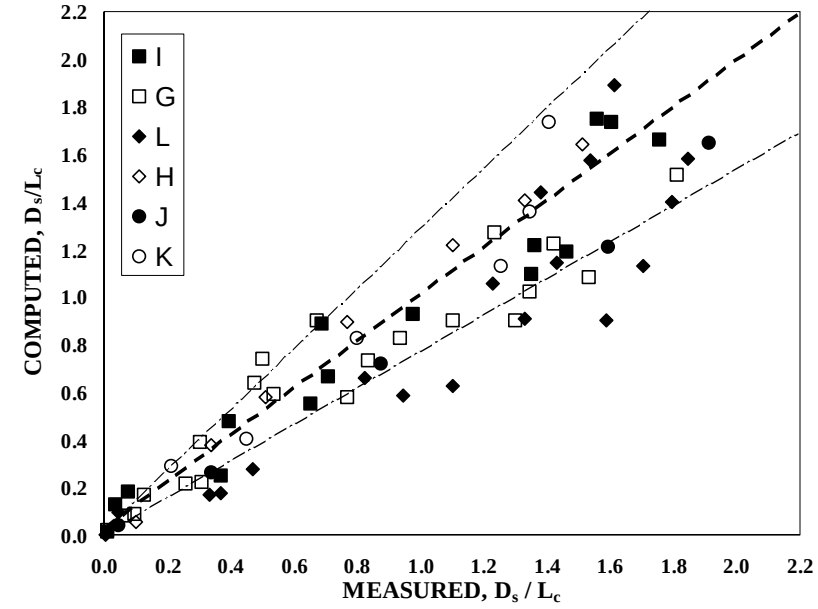

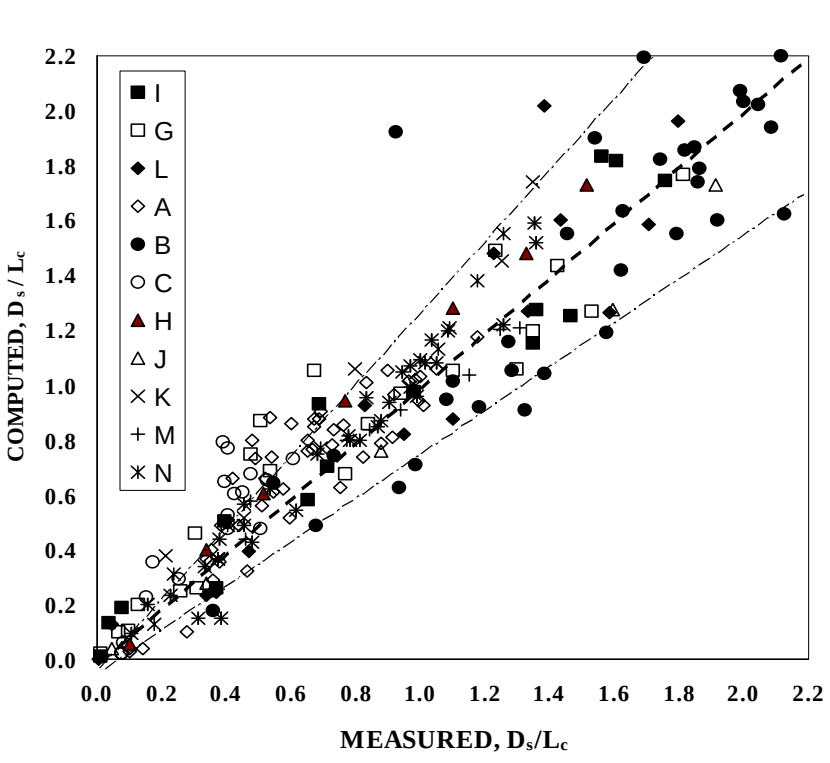

Figure 29. Measured and computed abutment scour for the hydrodynamics flume experiments: (a) for uniform mixtures; (b) all mixtures.

3.5 CONCLUSIONS

The following summarizes conclusions from this study:

(1) It is experimentally proven that clear-water scour at abutments is controlled primarily by the coarse fractions available in the sediment mixture. Sediment mixtures with the same coarse fraction distributions produce the same scour regardless of their mean diameter and gradation coefficients if they are subjected to the same flow intensities.

(2) A new clear-water scour predictor that relates the normalized scour depth (D_s / L_c) to the deflected flow excess velocity (Φ_j) was developed. This equation, which provides adjustments for the presence of coarse material in nonuniform mixtures, is given as:

$$\frac{D_s}{L_c} = K_n \, K_\theta \, K_{15} \, K_\Phi \, \Phi_j \tag{22}$$

(3) Gradation reduction factors for different flow conditions can be obtained from the K_s versus Φ_j chart given in figure 28(a). These factors can be used in conjunction with the clear-water scour predictor given by:

$$\frac{D_s}{L_c} = K_\Phi \, \Phi_j \tag{20}$$

(4) Local scour at abutments is related to flow parameters that represent the deflected mass of fluid that is diverted from its natural path due to the presence of the abutment.

(5) For graded sediment mixtures, clear-water scour at abutments is primarily dependent on the diverted velocity ($\sim V^{2.5}$), then on the abutment protrusion length ($\sim a^{1.1}$), and then to a lesser extent on the flow depth ($\sim Y^{0.27}$).

(6) The characteristic length, L_C, is a favorable length factor for normalizing the scour depth.

(7) The deflected flow excess velocity (Φ_j) can successfully describe the local scour phenomenon.

(8) For clear-water conditions, uniform sediments preserve the value of the gradient ($\partial D_s / \partial V_j$), and regardless of their mean size, result in the same ultimate scour.

(9) The available clear-water scour data are enriched with 384 case studies covering a wide range of hydraulic, geometric, and sediment conditions.

(10) Available data provide definite trends that support the dependence of local scour on the momentum and energy of the deflected flow to be explored in future studies.

The relationships derived in this study were aimed at quantifying the effects of sediment properties on abutment scour. Therefore, the experimental program was limited in its use of protrusion length-to-flow depth ratios ($0.3 \le Y / a \le 3.0$). For conditions involving ratios beyond the study, these effects must be adequately represented.

4. BRIDGE SCOUR IN CLAYEY SANDS

This chapter presents results of pier- and abutment-scour experiments to study effects of clay content on clear-water scour. Results show that the presence of even a small amount of cohesive material may reduce scour considerably. To quantify the impact of clay content, scour in clayey sands is expressed as a fraction of scour measured in noncohesive materials through a clay content reduction factor, K_{cc}. It is shown that K_{cc} is a function of clay content. It is also shown that different clay minerals have varying impacts on reducing bridge scour.

4.1 GENERAL

Scour at bridges has been studied extensively in the past for noncohesive sediments. The currently adopted scour estimation methodologies were basically developed from laboratory experiments conducted in sand or gravel beds. No method for scour depth estimation is available to account for the presence of cohesive materials in cases where bridges are founded in clayey sands. Figure 30 illustrates the effect of varying cohesive material content on abutment scour. As shown in this figure, as the cohesive material content is increased, the depth of scour is reduced. However, beyond a certain threshold this behavior is reversed. The ultimate scour depth computations for the sandy clay material described above is further complicated by the presence of different clay minerals. This chapter presents the results of the experimental study conducted at the CSU to account for the presence of clay on the resulting ultimate scour.

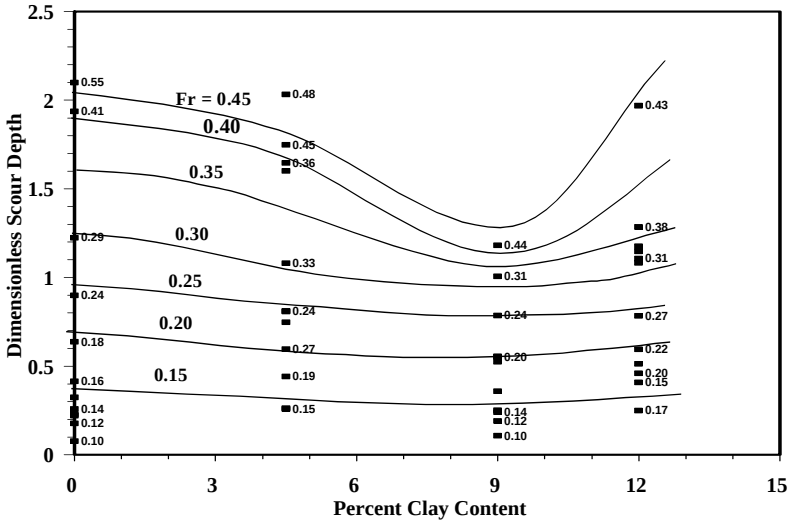

Figure 30. Effect of clay content on abutment scour.

4.2 EXPERIMENTAL SETUP AND MEASUREMENTS

Bridge scour experiments presented in this section are classified as pier scour and abutment scour experiments. In each category of experiments, series of runs utilizing different flumes were conducted by varying the clay content under different flow conditions. Additionally, in the abutment scour experiments, the effects of clay mineralogy were studied. Details of the experiments are presented in various publications [21, 22, 4, and 5].

FLUMES

Experiments were conducted in three different test flumes housed at the Engineering Research Center Hydraulics Laboratory at CSU. These flumes were identified as the river mechanics flume, sediment transport flume, and the steep flume. The river mechanics flume is 5 m wide by 30 m long, the sediment transport flume is 2.4 m wide by 60 m long, and the steep flume is 1.2 m wide by 12 m long. The flow depths in the experiments varied between 0.12 m and 0.3 m, and the corresponding approach Froude numbers ranged from 0.1 to 0.8.

MEASUREMENTS

Results of experiments were quantified through velocity, depth of flow, and depth of scour measurements. For velocity measurements, one- and two-dimensional magnetic flow-meters were utilized. In each experiment, approach velocity to each pier/abutment was determined by depth- and width-integrated average of seven vertical profiles, each with a minimum of 10 measurements. Similarly, the approach depth was a width- and length-averaged value of seven water surface elevation measurements. The bed elevations were measured along the test flumes before and after each experiment. The depth of scour was measured during and at the end of each experiment; it was determined by the difference between the measured minimum bottom elevation at the nose of a pier/abutment and the maximum elevation away from the structure. The accuracy of velocity measurements were within 5 percent, and scour depth measurements were within 3 percent.

SEDIMENTS

The sand used in mixing with clayey soils had a median diameter of 0.55 mm and a gradation coefficient σ_g of 2.43. In the pier scour experiments, Montmorillonite mineral clay was used in preparing the clayey sand mixtures. In the abutment scour experiments, both Montmorillonite and Kaolinite clays were utilized to study the effects due to the type of clay mineral present in mixtures.

PIERS AND ABUTMENTS

To isolate the effects due to the clay content, all variables other than flow velocity and clay content were kept constant. In all of the pier scour experiments, circular piers of 0.15 m diameter were used with a relatively constant approach depth of 0.24 m. In

abutment scour experiments, rectangular vertical-wall abutments with protrusion lengths of 0.20 m were used with an approach depth of 0.24 m. In the Kaolinite-clay experiments, geometrically similar 0.10-m abutments were used with 0.12-m flow depths.

4.3 EXPERIMENTAL RESULTS

Tables 23 and 24 present the experimental conditions as well as the resulting scour depths for the pier and abutment experiments, respectively. Pier scour experiments identified as runs MH 13-1 through MH 22-3 in table 23 were conducted in the 5-m wide flume, and runs MH30-1 through MH 32-3 were conducted in the 2.4-m wide flume. In these experiments sand-clay mixtures were prepared utilizing Montmorillonite clay soil. In addition to the measured depth of scour values, table 23 also presents scour hole volumes for each experiment. The pier diameter used in these experiments was 0.15 m.

Table 23. Summary of pier scour experiments in clayey sands.

Run ID (1)	Clay Content CC (%) (2)	Approach Froude No. F_r (3)	Depth of Scour D_{sc} (m) (4)	Dimensionless Scour D_{sc}/b (5)
MH13-1	0.0	0.184	0.088	0.58
MH13-2	1.6	0.198	0.076	0.50
MH13-3	3.2	0.204	0.092	0.61
MH14-1	0.0	0.176	0.069	0.46
MH14-2	1.6	0.196	0.077	0.50
MH14-3	3.2	0.189	0.066	0.43
MH15-1	0.0	0.185	0.089	0.58
MH15-2	1.6	0.207	0.105	0.69
MH15-3	3.2	0.211	0.091	0.60
MH16-1	0.0	0.205	0.116	0.76
MH16-2	1.6	0.230	0.127	0.83
MH16-3	3.2	0.244	0.144	0.94
MH17-1	6.4	0.176	0.045	0.30
MH17-2	9.6	0.196	0.052	0.34
MH17-3	12.8	0.189	0.051	0.34
MH18-1	6.4	0.185	0.058	0.38
MH18-2	9.6	0.207	0.057	0.37
MH18-3	12.8	0.211	0.060	0.39
MH19-1	6.4	0.212	0.066	0.44
MH19-2	9.6	0.232	0.096	0.63
MH19-3	12.8	0.235	0.084	0.55
MH20-1	6.4	0.212	0.079	0.52
MH20-2	9.6	0.231	0.105	0.69
MH20-3	12.8	0.232	0.096	0.63
MH21-1	6.4	0.185	0.058	0.38
MH21-2	1.6	0.207	0.105	0.69
MH21-3	3.2	0.211	0.092	0.60
MH22-1	6.4	0.180	0.054	0.35
MH22-2	1.6	0.195	0.077	0.50
MH22-3	3.2	0.188	0.068	0.44
MH30-1	0.0	0.307	0.248	1.63
MH30-2	6.4	0.317	0.158	1.04
MH30-3	12.8	0.329	0.094	0.62
MH31-1	3.2	0.307	0.210	1.38
MH31-2	9.6	0.310	0.166	1.09
MH31-3	12.8	0.329	0.135	0.88
MH32-1	0.0	0.232	0.191	1.25
MH32-2	6.4	0.227	0.122	0.80
MH32-3	12.8	0.228	0.089	0.58

Table 24. Summary of abutment scour experiments in clayey sands.

Run ID (1)	Clay Content CC (%) (2)	Scour Depth D_{sc} (m) (3)	Normalized Scour Depth D_{sc}/D_s (4)	Scour Hole Width W (m) (5)	Side Slope of Scour Hole 2 (degrees) (6)	Type of Clay Mineral (7)
NY81-A	0.0	0.253	1.00	0.399	32	Montmorillonite
NY82-A	0.0	0.158	1.00	0.293	28	Montmorillonite
NY83-A	0.0	0.113	1.00	0.241	25	Montmorillonite
NY84-B	0.0	0.274	1.00	0.402	34	Montmorillonite
NY81-B	4.5	0.210	0.88	0.439	26	Montmorillonite
NY82-B	4.5	0.104	0.81	0.259	22	Montmorillonite
NY83-B	4.5	0.094	1.21	0.189	27	Montmorillonite
NY84-B	4.5	0.262	1.01	0.418	32	Montmorillonite
NY81-C	9.0	0.131	0.74	0.247	28	Montmorillonite
NY82-C	9.0	0.073	0.68	0.128	30	Montmorillonite
NY83-C	9.0	0.067	1.08	0.128	28	Montmorillonite
NY84-C	9.0	0.152	0.60	0.326	25	Montmorillonite
NY81-D	12.0	0.140	0.84	0.265	28	Montmorillonite
NY82-D	12.0	0.067	0.75	0.107	32	Montmorillonite
NY83-D	12.0	0.052	1.15	0.107	26	Montmorillonite
NY84-D	12.0	0.165	0.74	0.369	24	Montmorillonite
NY81-A	0.0	0.253	1.00	0.399	32	Kaolinite
NY84-A	0.0	0.274	1.00	0.402	34	Kaolinite
NY78-A	10.0	0.229	0.83	0.384	31	Kaolinite
NY79-A	10.0	0.256	0.92	0.399	33	Kaolinite
NY79-B	20.0	0.052	0.19	0.040	52	Kaolinite
NY80-B	20.0	0.152	0.53	0.207	36	Kaolinite
NY77-B	20.0	0.012	0.21	0.015	39	Kaolinite
NY72-A	30.0	0.030	0.10	0.226	8	Kaolinite
NY71-B	30.0	0.000	0.00	0.000	0	Kaolinite
NY80-C	50.0	0.226	0.77	0.369	31	Kaolinite
NY77-C	50.0	0.094	2.30	0.326	16	Kaolinite

4.4 ANALYSIS

PIER SCOUR

Results of pier scour experiments in clayey sands are presented in figure 31. In deriving this figure scour, depths observed in Montmorillonitic clayey sand were normalized with the sand scour observed under similar flow and geometry conditions. In figure 31, pier scour results are expressed in terms of a reduction factor K_{cc} whose value ranges between 0 and 1; K_{cc} equal to unity denotes the depth scour being equal to that observed in sand. Since the pier shape and width, flow depth, and sand properties were kept near constant, it was possible to identify the effects of clay content under various flow conditions. Figure 31 shows that for a given clay content, the clay content reduction factor (K_{cc}) is independent of approach flow conditions.
The expression that best fits the data is given by [23]:

$$K_{CC} = \frac{1}{1+\left(\frac{CC}{11}\right)^{0.9}} \quad ; \qquad 0 \le CC \le 11 \tag{27}$$

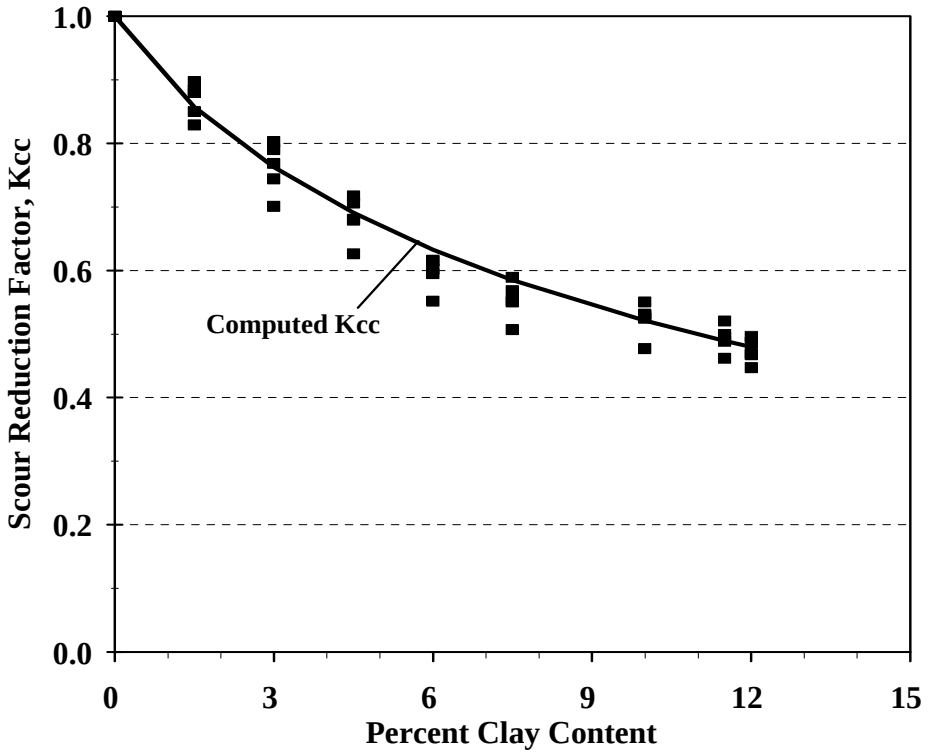

Figure 31. Pier scour reduction factor for Montmorillonite clay mixtures.

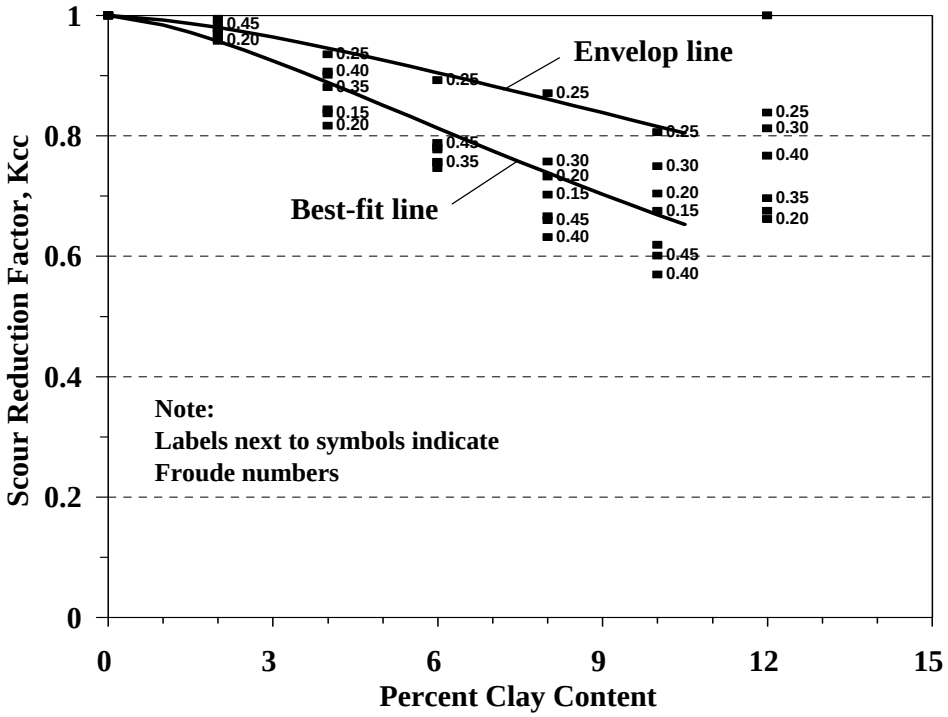

Figure 32. Abutment scour reduction factor for Montmorillonite clay mixtures.

ABUTMENT SCOUR

Results of abutment experiments in clayey sands are summarized in figures 32 and 33. Similar to pier scour experiments; in deriving these figures, scour depths observed in clayey sand were normalized with the scour observed in sand under similar flow and geometry conditions. In figures 32 and 33, abutment scour results are expressed in terms of a reduction factor, K_{cc}, whose value ranges between 0 and 1; K_{cc} equal to unity denotes the depth of scour being equal to that observed in sand. Since the abutment size and shape, flow depth, and sand properties were kept near constant, it was possible to identify the effects of clay content under various flow conditions. Figures 32 and 33 show that for a given clay content, the clay content reduction factor (K_{cc}) is independent of approach flow conditions. The expression that best fits the data for Montmorillonite clay mixtures is given by:

$$K_{CC} = \frac{1}{1+\left(\frac{CC}{\alpha}\right)^{\beta}} \; ; \qquad 0 \le CC \le 11 \tag{28}$$

α, β = 16 and 1.5 for the best-fit line; and 22 and 1.8 for the envelop line that can be used as a design equation, respectively.

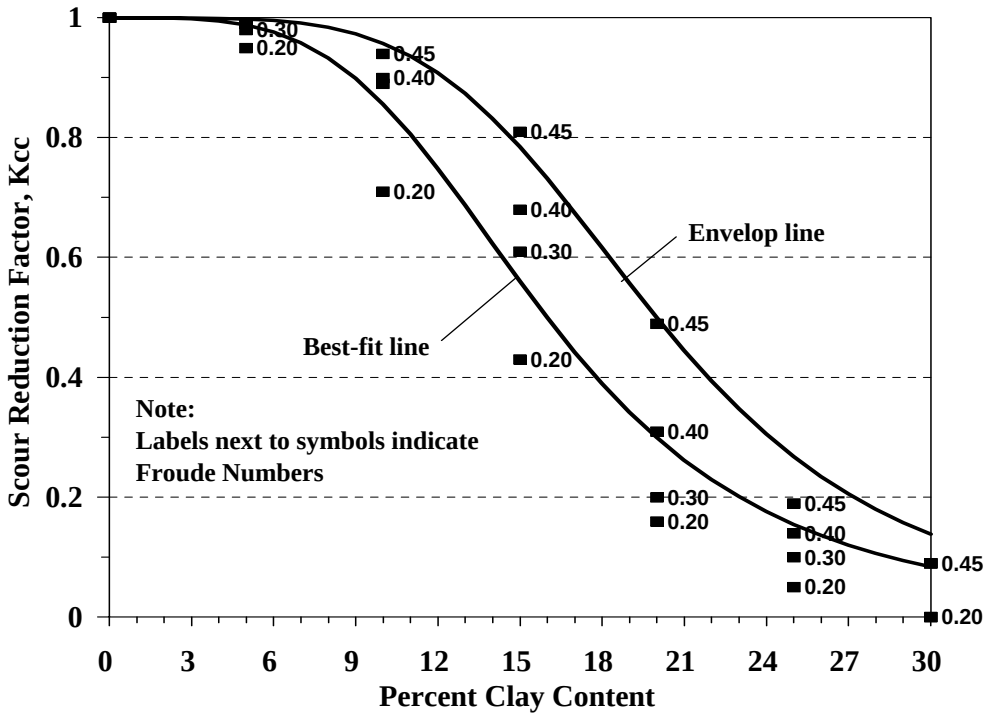

Figure 33. Abutment scour reduction factor for Kaolinite clay mixtures.

For the Kaolinite clay mixtures the expression that best fits the data is:

$$K_{CC} = \frac{1}{1+\left(\frac{CC}{\alpha}\right)^{\beta}} \quad ; \qquad 0 \le CC \le 11 \tag{29}$$

where α,β = 16 and 3.8 for the best-fit line and 20 and 4.5 for the envelop line, respectively.

4.5 CONCLUSIONS

Bed material mixtures that are predominately sand with low clay content can be analyzed using the traditional non cohesive soil parameters for scour with a reduction factor to account for the cohesive effects from the clay fraction. The reduction coefficients found in these experiments are given by equations 28 and 29 above for Montmorillonite and Kaolinite clays, respectively. Two sets of coefficients are given for equations 28 and 29 to represent the best-fit line through the data and the envelop-line that can be used as a design equation. Bed material mixtures with high clay contents are governed by clay properties that are the subject of the next chapter. There is no clear clay content percentage that determines where the shift occurs from noncohesive to clay properties. For the present study this limit was found to be around 12 percent and was affected by the clay mineralogy.

5. PIER SCOUR IN MONTMORILLONITE CLAY SOILS

Determination of local scour at bridge piers is one of the critical problems in the design of bridge foundations to resist the erosive action of oncoming flows. Even though local pier scour has been the topic of large numbers of research studies in noncohesive alluvial materials, very little effort has been devoted to the study of pier scour in cohesive materials. The focus of this experimental study is to identify the parameters affecting the scour mechanism at bridge piers located in unsaturated compacted cohesive soils and in saturated cohesive soils and to develop prediction equations to quantify the local scour depths. Based on the analysis of the experimental data, scour depth predictors are developed in terms of the approach flow conditions, initial water content, compaction, and soil shear strength using Montmorillonite clay soils.

5.1 GENERAL

In the past, numerous experimental and analytical investigations of local pier scour were conducted in alluvial channels, and series of prediction equations were developed by researchers to estimate the maximum scour depth at bridge piers under different approach flow conditions, for different sediment size and gradations, and for different pier type and sizes. Unfortunately, these studies have been all confined to noncohesive soils. This is undoubtedly due to not only the abundance of streams with these types of beds but also because sand and gravel are easier to both characterize and model physically.

The scour of cohesive materials is fundamentally different from that of noncohesive materials. It involves not only complex mechanical phenomena, including shear stress and shear strength of soils, but also the chemical and physical bonding of individual particles and properties of the eroding fluid. Cohesive materials, once eroded, remain in suspension such that clear-water scour conditions always prevail. Along with the eroding fluid properties, the scour process in this environment is strongly affected by the amount of cohesive material present in the soil mixture as well as the type of mineral clay, initial water content, soil shear strength, and compaction of the clay. The objectives of this paper are to apply the knowledge gained in the past in cohesive material scour to local pier scour, and specifically to: 1) study the effect of compaction, soil shear strength, and the approach flow conditions on pier scour in unsaturated cohesive soils; 2) specify the influence of initial water content of saturated clay on pier scour; and 3) develop scour prediction equations in unsaturated and saturated cohesive soils to quantify the scour that may occur around circular piers.

5.2 EXPERIMENTAL SETUP AND MEASUREMENTS

Pier scour experiments presented in this paper are broadly classified as unsaturated and saturated cohesive soil experiments. In each category of experiments, series of runs utilizing different flumes were conducted by varying the clay properties under different flow conditions. Details and scope of experiments are presented by Hosny[21] and by Molinas, Hosny, and Jones[24, 25].

FLUMES

Experiments were conducted in three different test flumes housed at the Engineering Research Center at CSU. These flumes were identified as the river mechanics flume, sediment transport flume, and the steep flume. The river mechanics flume is 5 m wide by 30 m long, the sediment transport flume is 2.4 m wide by 60 m long, and the steep flume is 1.2 m wide by 12 m long. The flow depths in the experiments varied between 0.12 m and 0.3 m, and the corresponding approach Froude numbers ranged from 0.1 to 1.4.

MEASUREMENTS

In pier scour experiments the measured flow and sediment parameters were velocity, depth of flow, depth of scour, initial water content of soil, Torvane shear strength, and degree of compaction. For velocity measurements, a one-dimensional magnetic flow-meter was utilized. In each experiment, approach velocity to each pier was determined by depth- and width-integrated average of vertical velocity profiles. Similarly, the approach depth was determined from a width- and length-averaged value of water surface elevation measurements. The bed elevations were measured along the test flumes before and after each experiment. The depth of scour was measured during and at the end of each experiment; it was determined by the difference between the measured minimum bottom elevation at the nose of a pier and the maximum elevation away from the structure.

COHESIVE SOILS

To achieve the objectives of this study, a homogeneous soil containing clay, silt, and fine sand particles, in which cohesion plays a predominant role, was used. Utilizing the X-Ray Diffraction Test, the dominant clay mineral was found to be Montmorillonite. According to the unified soil classification system, the cohesive soil was also classified as medium plasticity clay and the texture as clay loam.

In this study, three series of experiments were performed. In set 1, the effects of clay content were examined as the clay content was varied from 0 to 12 percent. In set 2 experiments, the effects of compaction on unsaturated cohesive soils were studied. The cohesive material placed around the piers was compacted at 58, 65, 73, 80, 87, and 93 percent degree of compaction. In set 3 experiments, the effects of initial water content on

saturated cohesive soil erosion were examined by saturating the soils at initial water contents of 32, 35, 40, and 45 percent.

PIERS

In the experiments, 1-m long cylindrical piers made of clear Plexiglas with 0.152-m and 0.102-m diameters were used. The scour depth development was measured against time utilizing three measuring tapes attached to the interior wall of each pier and a periscope manufactured by the use of a small inclined mirror.

5.3 EXPERIMENTAL RESULTS

Tables 25 through 28 present the experimental conditions as well as the resulting scour depths for pier experiments in Montmorillonite clay mixtures. Pier scour experiments, identified as runs MH 13-1 through MH 22-3 in table 25, were conducted in the 5-m wide flume, and runs MH30-1 through MH 32-3 were conducted in the 2.4-m wide flume. In these experiments sand-clay mixtures were prepared utilizing Montmorillonite clay soil. In addition to the measured depth of scour values, the summary tables also present scour hole volumes for each experiment. The pier diameter used in these experiments was 0.15 m.

Table 25. Results of set 1 experiments to study effects of clay content.

Run ID	Flow Discharge Q (l/s)	Clay Content CC (%)	Approach Depth Y (m)	Approach Velocity V (m/s)	Froude No. F_r	Scour Depth D_s (m)	Dimension-less Scour D_s / b	Volume of Scour V_s (l)	Dimension-less Volume V_s / b^3
MH 13-1	311.49	0.0	0.237	0.280	0.184	0.088	0.58	8.100	2.288
MH 13-B	311.49	1.5	0.237	0.301	0.198	0.076	0.50	6.701	1.893
MH 13-3	311.49	3.0	0.237	0.311	0.204	0.092	0.61	10.001	2.825
MH 14-1	283.17	0.0	0.210	0.253	0.176	0.069	0.46	2.701	0.763
MH 14-2	283.17	1.5	0.210	0.282	0.196	0.077	0.50	6.555	1.852
MH 14-3	283.17	3.0	0.210	0.271	0.189	0.066	0.43	3.449	0.975
MH 15-1	339.80	0.0	0.224	0.274	0.185	0.089	0.58	8.100	2.288
MH 15-2	339.80	1.5	0.224	0.307	0.207	0.105	0.69	13.999	3.955
MH 15-3	339.80	3.0	0.224	0.313	0.211	0.091	0.60	9.000	2.543
MH 16-1	413.43	0.0	0.244	0.316	0.205	0.116	0.76	16.600	4.690
MH 16-2	413.43	1.5	0.244	0.356	0.230	0.127	0.83	19.601	5.537
MH 16-3	413.43	3.0	0.244	0.377	0.244	0.144	0.94	19.992	5.648
MH 17-1	283.17	6.0	0.210	0.253	0.176	0.045	0.30	1.450	0.410
MH 17-2	283.17	9.0	0.210	0.282	0.196	0.052	0.34	2.730	0.771
MH 17-3	283.17	12.0	0.210	0.271	0.189	0.051	0.34	2.466	0.697
MH 18-1	339.80	6.0	0.224	0.274	0.185	0.058	0.38	3.089	0.873
MH 18-2	339.80	9.0	0.224	0.307	0.207	0.057	0.37	5.073	1.434
MH 18-3	339.80	12.0	0.224	0.313	0.211	0.060	0.39	4.105	1.160
MH 19-1	413.43	6.0	0.243	0.327	0.212	0.066	0.44	6.560	1.853
MH 19-2	413.43	9.0	0.243	0.358	0.232	0.096	0.63	14.584	4.120
MH 19-3	413.43	12.0	0.243	0.362	0.235	0.084	0.55	9.100	2.571
MH 20-1	382.28	6.0	0.230	0.319	0.212	0.079	0.52	6.350	1.794
MH 20-2	382.28	9.0	0.230	0.347	0.231	0.105	0.69	15.576	4.400
MH 20-3	382.28	12.0	0.230	0.349	0.232	0.096	0.63	11.317	3.197
MH 21-1	339.80	6.0	0.224	0.274	0.185	0.058	0.38	3.366	0.951
MH 21-2	339.80	1.5	0.224	0.307	0.207	0.105	0.69	13.999	3.955
MH 21-3	339.80	3.0	0.224	0.313	0.211	0.092	0.60	9.000	2.543
MH 22-1	283.17	6.0	0.214	0.261	0.180	0.054	0.35	1.450	0.410
MH 22-2	283.17	1.5	0.214	0.282	0.195	0.077	0.50	6.701	1.893
MH 22-3	283.17	3.0	0.214	0.272	0.188	0.068	0.44	5.088	1.438
MH 30-1	368.12	0.0	0.290	0.517	0.307	0.248	1.63	47.999	13.561
MH 30-2	368.12	6.0	0.290	0.534	0.317	0.158	1.04	38.000	10.736
MH 30-3	368.12	12.0	0.290	0.555	0.329	0.094	0.62	28.001	7.910
MH 31-1	368.12	3.0	0.290	0.517	0.307	0.210	1.38	46.400	13.109
MH 31-2	368.12	9.0	0.290	0.522	0.310	0.166	1.09	39.336	11.113
MH 31-3	368.12	12.0	0.290	0.555	0.329	0.135	0.88	31.140	8.798
MH 32-1	254.85	0.0	0.247	0.361	0.232	0.191	1.25	32.817	9.271
MH 32-2	254.85	6.0	0.247	0.353	0.227	0.122	0.80	16.387	4.630
MH 32-3	254.85	12.0	0.259	0.364	0.228	0.089	0.58	16.059	4.537

Notes:
1. Duration of experiments varied between 16 and 20 hours.
2. Runs 13 through 22 were conducted in the 5.2-m wide flume.
3. Runs 30 through 32 were conducted in the 2.44-m wide flume.

Table 26. Summary of experimental conditions and results for set 2 (effect of compaction on pier scour in cohesive soils).

RUN ID	Flow Discharge Q (l/s)	Shear Strength S (kPa)	Wet Density (γ_w (t/m^3)	Dry Density (γ_{dry} (t/m^3)	Compaction C (%)	Approach Depth Y (m)	Approach Velocity V (m/s)	Froude No. F_r	Scour Depth D_{sc} (m)	Dimension-less Scour D_{sc} / b	Scour Volume V_s (l)
MH 13-5	311.485	44.132	1.968	1.640	93	0.245	0.255	0.165	0.000	0.00	0.000
MH 13-6	311.485	37.267	1.841	1.534	87	0.245	0.260	0.168	0.000	0.00	0.000
MH 14-5	283.168	31.382	1.693	1.411	80	0.216	0.266	0.182	0.046	0.30	0.900
MH 14-6	283.168	25.498	1.545	1.287	73	0.216	0.264	0.181	0.057	0.37	1.050
MH 15-5	339.802	44.132	1.968	1.640	93	0.228	0.291	0.195	0.000	0.00	0.000
MH 15-6	339.802	37.267	1.841	1.534	87	0.228	0.302	0.202	0.000	0.00	0.000
MH 16-5	413.426	29.421	1.693	1.411	80	0.250	0.312	0.199	0.060	0.40	1.070
MH 16-6	413.426	24.518	1.545	1.287	73	0.250	0.344	0.220	0.073	0.48	2.794
MH 17-5	283.168	31.382	1.693	1.411	80	0.216	0.266	0.182	0.047	0.31	0.811
MH 17-6	283.168	25.498	1.545	1.287	73	0.216	0.264	0.181	0.053	0.35	1.231
MH 18-5	339.802	31.382	1.693	1.411	80	0.228	0.291	0.195	0.052	0.34	1.200
MH 18-6	339.802	19.614	1.545	1.287	73	0.228	0.302	0.202	0.065	0.42	1.513
MH 19-5	413.426	14.710	1.376	1.146	65	0.243	0.317	0.205	0.077	0.51	4.000
MH 19-6	413.426	6.865	1.227	1.023	58	0.243	0.330	0.214	0.099	0.65	7.350
MH 20-5	382.277	14.710	1.376	1.146	65	0.237	0.313	0.206	0.072	0.48	4.601
MH 20-6	382.277	9.807	1.227	1.023	58	0.237	0.325	0.213	0.095	0.63	6.534
MH 21-5	339.802	15.691	1.376	1.146	65	0.229	0.291	0.194	0.072	0.47	1.816
MH 21-6	339.802	8.826	1.227	1.023	58	0.229	0.302	0.202	0.101	0.66	3.436
MH 22-5	283.168	15.691	1.376	1.146	65	0.219	0.260	0.177	0.057	0.38	1.450
MH 22-6	283.168	8.826	1.227	1.023	58	0.219	0.261	0.178	0.070	0.46	2.350
MH 27-1	311.485	9.807	1.227	1.023	58	0.261	0.439	0.274	0.170	1.12	21.000
MH 27-2	311.485	24.518	1.545	1.287	73	0.261	0.437	0.273	0.125	0.82	12.500
MH 27-3	311.485	34.325	1.693	1.411	80	0.261	0.448	0.280	0.113	0.74	3.500
MH 35-1	424.753	9.807	1.227	1.023	58	0.271	0.549	0.336	0.229	1.50	36.101
MH 35-2	424.753	19.614	1.545	1.287	73	0.238	0.563	0.369	0.178	1.17	20.100
MH 35-3	424.753	44.132	1.841	1.534	87	0.256	0.585	0.369	0.134	0.88	13.500

Notes:
1. Duration of experiments varied between 16 and 20 hours.
2. Runs 13 through 22 were conducted in the river mechanics flume.
3. Runs 27 through 35 were conducted in the sediment transport flume.
4. The accuracy of compactions 58, 65, 73, 80, and 87% is (±1.5%).

Table 27. Summary of experimental conditions and results for set 3 (effect of initial water content on pier scour in cohesive soils).

Run ID	Flow Discharge Q (l/s)	Shear Strength S (kPa)	Wet Density γ_w (t/m^3)	Dry Density γ_{dry} (t/m^3)	Compac-tion C (%)	Depth Y (m)	Velocity V (m/s)	Froude No. F_r	Scour Depth D_{sc} (m)	Dimension-less Scour D_{sc} / b	Scour Volume V_s (l)	Dimension-less Volume V_s / b^3
MH 23-6	413.426	9.807	1.481	1.287	73	0.247	0.330	0.212	0.079	0.52	12.800	3.616
MH 24-5	382.277	6.865	1.176	1.023	58	0.237	0.313	0.206	0.117	0.77	14.290	4.037
MH 24-6	382.277	9.807	1.481	1.287	73	0.237	0.325	0.213	0.082	0.54	11.500	3.249
MH 25-4	339.802	14.710	1.623	1.411	80	0.229	0.284	0.189	0.085	0.39	3.150	0.890
MH 25-5	339.802	9.807	1.481	1.287	73	0.229	0.291	0.194	0.066	0.43	5.999	1.695
MH 25-6	339.802	6.865	1.176	1.023	58	0.229	0.302	0.201	0.113	0.74	7.700	2.175
MH 26-4	283.168	14.710	1.623	1.411	80	0.219	0.236	0.161	0.037	0.24	1.000	0.283
MH 26-5	283.168	9.807	1.481	1.287	73	0.219	0.260	0.177	0.047	0.31	1.450	0.410
MH 26-6	283.168	6.865	1.176	1.023	58	0.219	0.261	0.178	0.056	0.37	1.999	0.565
MH 33-1	311.485	6.865	1.176	1.023	58	0.259	0.439	0.275	0.187	1.23	30.000	8.476
MH 33-2	311.485	9.807	1.481	1.287	73	0.259	0.437	0.274	0.130	0.85	18.750	5.297
MH 33-3	311.485	17.653	1.764	1.534	87	0.261	0.448	0.280	0.094	0.62	9.999	2.285

Notes:
1. Duration of experiments varied between 16 and 20 hours.
2. Runs 23 through 26 were conducted in the river mechanics flume.
3. Run 33 was conducted in the sediment transport flume.
4. The accuracy of compactions 58, 65, 73, 80, and 87% is (±1.5%).

Table 28. Summary of experimental conditions and results for set 3 (effect of initial water content on pier scour for saturated clay).

Run ID	Flow Discharge Q (l/s)	Initial Water Content IWC (%)	Wet Density γ_w (t/m^3)	Dry Density γ_{dry} (t/m^3)	Compac-tion C (%)	Approach Depth Y (m)	Approach Velocity V (m/s)	Froude No. Fr	Scour Depth D_{sc} (m)	Dimension-less Scour D_{sc} / b	Scour Volume V_s (l)	Dimension-less Volume V_s / b^3
MH 13-4	311.5	32	2.002	1.517	86	0.245	0.224	0.145	0.000	0.00	0.000	0.000
MH 14-4	283.2	35	1.952	1.446	82	0.216	0.240	0.165	0.000	0.00	0.000	0.000
MH 15-4	339.8	35	1.952	1.446	82	0.228	0.264	0.177	0.000	0.00	0.000	0.000
MH 16-4	413.4	35	1.952	1.446	82	0.250	0.301	0.192	0.000	0.00	0.000	0.000
MH 17-4	283.2	40	1.852	1.323	75	0.216	0.240	0.165	0.000	0.00	0.000	0.000
MH 18-4	339.8	42	1.778	1.252	71	0.228	0.264	0.177	0.000	0.00	0.000	0.000
MH 19-4	413.4	45	1.688	1.164	66	0.243	0.304	0.197	0.000	0.00	0.000	0.000
MH 23-1	413.4	48	1.644	1.111	63	0.243	0.326	0.211	0.147	0.96	4.900	1.384
MH 24-1	382.3	40	1.852	1.323	75	0.230	0.319	0.212	0.057	0.37	1.000	0.283
MH 25-1	339.8	48	1.644	1.111	63	0.224	0.279	0.188	0.000	0.00	0.000	0.000
MH 28-1	518.2	32	2.002	1.517	86	0.299	0.628	0.367	0.000	0.00	0.000	0.000
MH 28-2	518.2	38	1.922	1.393	79	0.293	0.633	0.374	0.064	0.42	0.900	0.254
MH 28-3	518.2	43	1.791	1.252	71	0.293	0.675	0.398	0.104	0.68	2.701	0.763
MH 29-2	792.9	38	1.922	1.393	79	0.308	0.867	0.499	0.134	0.88	2.801	0.791
MH 29-3	792.9	43	1.791	1.252	71	0.308	0.877	0.504	0.165	1.08	9.808	2.771
MH 34-1	424.8	35	1.952	1.446	82	0.271	0.549	0.336	0.058	0.38	1.100	0.311
MH 34-2	424.8	40	1.852	1.323	75	0.265	0.563	0.349	0.076	0.50	1.650	0.466
MH 34-3	424.8	45	1.688	1.164	66	0.256	0.585	0.369	0.116	0.76	3.092	0.874
MH 36-1	501.2	35	1.952	1.446	82	0.290	0.619	0.367	0.049	0.32	1.139	0.322
MH 36-2	501.2	40	1.852	1.323	75	0.280	0.666	0.402	0.101	0.66	3.454	0.975
MH 36-3	501.2	45	1.688	1.164	66	0.262	0.713	0.445	0.165	1.08	5.578	1.576
MH 37-1	736.2	35	1.952	1.446	82	0.317	0.759	0.430	0.070	0.53	3.300	0.932
MH 37-2	736.2	40	1.852	1.323	75	0.314	0.828	0.472	0.145	0.95	8.000	2.260
MH 37-3	736.2	45	1.688	1.164	66	0.317	0.893	0.506	0.192	1.26	11.148	3.150
MH 38-1	948.6	35	1.952	1.446	82	0.427	0.867	0.424	0.081	0.46	1.811	0.512
MH 38-2	948.6	40	1.852	1.323	75	0.402	0.915	0.460	0.114	0.75	4.000	1.130
MH 38-3	948.6	45	1.688	1.164	66	0.378	0.967	0.502	0.192	1.26	13.000	3.673
MH 39-1	96.6	32	2.002	1.517	86	0.059	1.341	1.760	0.100	0.99	2.925	2.789
MH 40-1	78.6	32	2.002	1.517	86	0.057	1.088	1.450	0.096	0.95	2.550	2.431
MH 41-1	55.2	32	2.002	1.517	86	0.051	0.959	1.360	0.066	0.65	1.319	1.258
MH 42-1	64.6	32	2.002	1.517	86	0.055	0.991	1.349	0.069	0.68	1.291	1.231
MH 43-1	89.2	32	2.002	1.517	86	0.058	1.259	1.660	0.097	0.95	3.441	3.281
MH 44-1	78.4	32	2.002	1.517	86	0.112	0.686	0.660	0.037	0.36	0.750	0.715

Notes:
1. Duration of experiments varied between 16 and 20 hours.
2. Runs 13 through 25 were conducted in the 5.2-m wide flume with pier diameter of 0.127 m.
3. Runs 28 through 38 were conducted in the 2.44-m wide flume with pier diameter of 0.152 m.
4. Runs 39 through 44 were conducted in the 1.22-m wide flume with pier diameter of 0.102 m.

5.4 ANALYSIS

Dimensional analysis that has been used for correlating the variables affecting the local scour depth at bridge piers has been extended to include cohesive soil properties in order to account for the cohesive bed material. The variables used in the analysis are parameters defining the soil, the fluid, and the geometry of the modeled system. Depth of pier scour, D_s, which is the dependent variable in this analysis, can be expressed as a function of the following independent variables:

$$D_s = f(Y, b, V, D_{50}, \sigma_g, \varphi, \rho_s, t, g, \rho, \nu, S, CC, Mn, C, IWC) \tag{30}$$

in which D_s = depth of scour; Y = depth of approach flow; b = pier width; V = velocity of approach flow; D_{50} = mean sediment diameter; σ_g = standard deviation of sediment size; φ = pier shape factor; ρ_s=density of sediment particles; t = time; g = gravitational acceleration; ρ = fluid density; ν = fluid kinematic viscosity; S = soil shear strength; CC = clay content; Mn = origin of clay minerals (e.g. Kaolinite, Illite, Montmorillonite); C = degree of compaction; and IWC = initial water content.

Applying the dimensional analysis using b, V, and ρ as repeating variables, and using appropriate simplifications, the following set of dimensionless parameters can be obtained:

$$\frac{D_s}{b} = f\left(F_r, IWC, \frac{S}{\rho V^2}, C\right) \tag{31}$$

in which F_r is the approach Froude number ($=V/\sqrt{gY}$). In deriving equation 31, the clay content (CC) was eliminated as a variable since, as shown in chapter 4, the effects of this parameter was found to be an independent factor only up to 12 percent clay content. In the cohesive pier scour experiments in Montmorillonite clays, the clay content was kept constant at 32 percent. In the experiments, the variation of scour with time was measured. This relationship was shown to be an asymptotic function with a sharp initial scour development followed by a gradual increase[26]. The initial rate of scour hole development is generally controlled by the nature of the clay mineral and other cohesive material parameters such as compaction, initial water content, etc. Past experimental and theoretical studies have shown that the velocity at the nose region of a circular pier is amplified by a factor of 1.6 to 1.7 times the approach velocity, V. Accordingly, the bottom shear stresses that are related to V^2 are also amplified and cause local scour in the affected zone. If approach velocities are increased beyond a threshold value defined as critical velocity, the entire approach channel bottom becomes subject to general scour in addition to the local scour. Under these conditions, the scour hole development process continues until equilibrium slopes are attained for the entire reach and may last indefinitely. The experimental study presented in this report limited itself to conditions in which the oncoming flows do not scour the approach reach (clear water conditions). Under these conditions, as soon as the scour hole reaches a depth where the shear stress within the base becomes equal to the critical shear stress of the cohesive material, local

scouring ceases. The duration of experiments in the study were long enough to maintain the equilibrium condition for at least 4 hours. The final scour depth values obtained under these conditions are independent of time, and therefore in deriving equation 31 the time parameter, t, is eliminated.

Pier scour analysis in this study was conducted under two major categories: 1) unsaturated Montmorillonite clay scour and 2) saturated Montmorillonite clay scour. The distinction is made since for saturated cohesive materials, parameters such as Torvane shear strength and compaction have no physical significance; whereas these parameters are important in unsaturated cohesive material scour.

UNSATURATED CONDITIONS

The measured values of (D_s /b) were regressed against the remaining dimensionless groups in equation 31. The best-fit regression equation resulting from the statistical analysis of experimental data is:

$$\frac{D_s}{b} = 24{,}715\ (IWC)^{-0.36} F_r^{1.92}\ C^{-1.62} \tag{32}$$

where the initial water content (IWC) and compaction (C) are in percent. In deriving this expression, the initial water content ranged from 15 to 50 percent, and compaction ranged from 50 to 100 percent. The development of equation 32 is based on laboratory tests in which Froude numbers ranged from 0.18 to 0.37, and soil shear strength values ranged from 0.1 to 0.45 kg/cm^2. The higher value of the correlation coefficient, R^2 = 0.95, between the observed and predicted scour ratio indicates the strong correlation between measured scour depths and the parameters selected for defining flow and sediment properties. The plot of equation 32 with observed data is presented in figure 34. Pier scour corresponding to Froude numbers less than 0.2 and for compaction ratios higher than 85 percent is zero (scour threshold conditions).

SATURATED CONDITIONS

For saturated Montmorillonite clay soils, equation 31 can be simplified further by eliminating the dimensionless soil shear strength parameter, ($S/\rho V^2$), since this term has no physical meaning for saturated clays at high initial water contents (it approaches to 0). Also, for saturated conditions the compaction of cohesive soils, C, is mainly related to the water content and can therefore be removed from the list of independent variables. Introducing the pier scour initiating Froude number, F_i, to define threshold conditions for pier scour and replacing F_r by the excess Froude number, $(F_r\text{-}F_i)$, equation 31 becomes:

$$\frac{D_s}{b} = f(F_r - F_i, IWC) \tag{33}$$

Using the results of experimental study, F_i and D_s / b are determined as[25, 26]:

$$F_i = \frac{350}{(IWC)^2} \tag{34}$$

and

$$\frac{D_s}{b} = 0.0288\,(IWC)^{1.14}\left(F_r - F_i\right)^{0.6}; \qquad F_r \geq F_i \tag{35}$$

For approach Froude numbers less than the pier scour initiating Froude number (i.e., $F_r < F_i$), depth of scour is zero. For supercritical approach conditions, the value of experimental coefficient 0.0288 was found to be 0.0131. The plot of equation 35 with observed data is presented in figure 35.

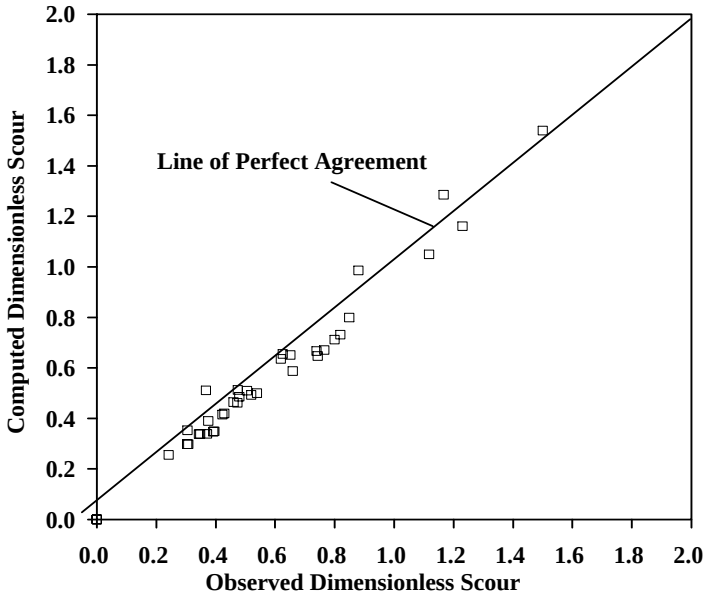

Figure 34. Computed and measured dimensionless pier scour depth for unsaturated Montmorillonite clay.

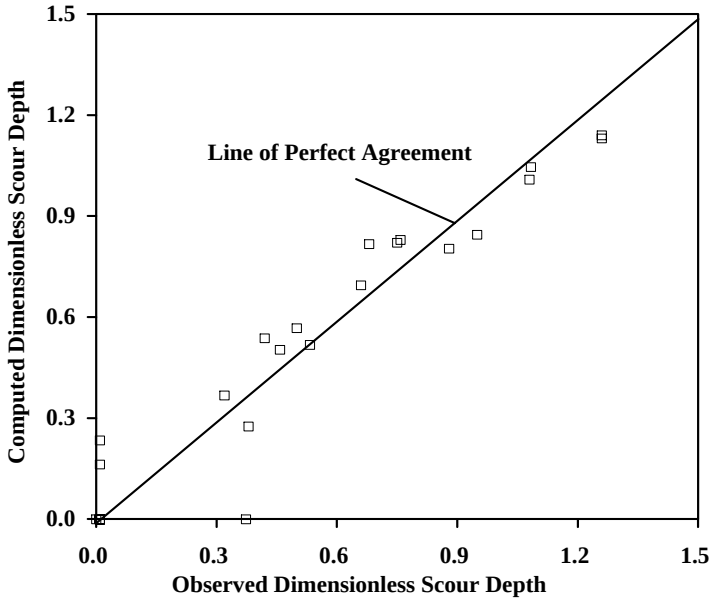

Figure 35. Computed and measured dimensionless pier scour depth for saturated Montmorillonite clay.

5.5 CONCLUSIONS

There is a distinction between pier scour taking place in unsaturated compacted clayey soils and saturated clayey soils. This differentiation affects parameters controlling local pier scour. For unsaturated compacted Montmorillonite clay soils, a new scour depth predictor is proposed in terms of initial water content, Froude number, soil shear strength, and degree of compaction. The pier scour depth and volume decrease as the compaction of cohesive soils increases. For saturated cohesive soils, the scour depth can be expressed as a function of initial water content and excess Froude number, (F_r-F_i). Under saturated conditions, the scour depth is directly proportional to excess Froude number and is inversely proportional to initial water content.

6. EFFECT OF COHESION ON ABUTMENT SCOUR

In this chapter, effects of cohesion on local abutment scour are investigated experimentally for Montmorillonitic and Kaolinitic clay mixtures using larger scale, 1.2-m and 2.4-m wide test flumes at the Engineering Research Center, CSU. For cohesive soils with significant clay content (30 percent for the present mixtures), soil parameters such as compaction, initial water content, degree of saturation, shear strength, and type of clay mineral dominate the abutment scour. In this study these effects are quantified for flow conditions with Froude numbers ranging from 0.2 to 0.9. Equations relating flow and selected cohesive soil parameters to abutment scour were developed to explain the variability of abutment scour with cohesion properties. These equations express abutment scour in cohesive soils relative to clear-water scour in noncohesive material for the same flow and geometry conditions. Under the same geometric and flow conditions, measured scour in cohesive materials varies from 7 percent to 140 percent of that measured in medium sand.

6.1 GENERAL

Flow structure around abutments and the resulting local scour were studied in the past in numerous experimental, numerical, and analytical investigations for noncohesive materials. As a result, series of empirical and semiempirical prediction equations were developed to relate the scour depth at bridge abutments to different approach flow conditions, to sediment size and gradations, and to different abutment types and sizes.

The mechanism of cohesive-material scour is significantly different from scouring of alluvial noncohesive materials. The process involves not only the balancing of flow-induced shear stresses and the shear strength of soils to withstand scour, but also the chemical and physical bonding of individual particles and the properties of the eroding fluid. Cohesive materials, once eroded, remain in suspension. As a result, the phenomenon identified as clear-water local scour in noncohesive materials always prevails. Along with the eroding fluid properties, the scour process in cohesive soils is strongly affected by the amount of cohesive material present in the soil mixture as well as the type of mineral clay, initial water content, soil shear strength, and compaction of the clay. The objectives of this paper are to apply the knowledge gained in the past in cohesive material scour to study local scour around abutments and to analyze effects of compaction, initial water content, soil shear strength, and the approach flow conditions on abutment scour. For this purpose two different types of clay mixtures were used. The first cohesive mixture was a naturally occurring soil that contained 32 percent Montmorillonite mineral clay with almost equal amounts of fine sand and silt. The second cohesive mixture was prepared by blending 30 percent pure Kaolinite clay with medium sand. Experiments using the first soil were conducted under unsaturated and saturated soil conditions. The Kaolinite clay scour experiments were limited to

unsaturated conditions where compaction and initial water content of the mixture were varied. As a result of this experimental study, empirical relationships were developed relating the scour in cohesive material to that observed in the noncohesive material that was used in preparing the mixtures under the same flow and geometric conditions.

6.2 EXPERIMENTAL SETUP AND MEASUREMENTS

The two categories of abutment scour experiments presented in this paper are classified as Montmorillonite and Kaolinite clay experiments. In each category of experiments, series of runs utilizing two experimental flumes were conducted by varying the clay properties under different flow conditions. A total of 126 experiments were conducted covering a wide range of flow and soil conditions. Details of the experiments are presented by Yakoub[22] and Molinas and Reiad [5].

FLUMES

Experiments were conducted in two different larger scale test flumes housed at the Engineering Research Center at CSU to achieve desired flow intensities. These flumes are identified as the sediment transport flume and the steep flume. The sediment transport flume is 2.4 m wide by 60 m long, and the steep flume is 1.2 m wide by 12 m long. The flow depths used in the experiments varied between 0.12 m and 0.3 m, and approach Froude numbers ranged from 0.1 to 0.9.

MEASUREMENTS

Flow and sediment parameters measured in experiments were velocity distribution (vertical, longitudinal, and lateral), depth of flow, depth of scour, initial water content of soil, Torvane shear strength, and degree of compaction. Velocity measurements were carried out by the use of a magnetic flow-meter. In the experiments, approach velocity to each abutment was determined by depth- and width-integrated average of vertical velocity profiles. Similarly, the approach depth was determined from a width- and length-averaged value of water surface and bed elevation measurements. The bed elevations were measured along the flumes across the flow channel before and after each experiment. The depth of abutment scour was measured during and at the end of each experiment; it was determined by the difference between the minimum bottom elevation at the nose region of abutment and the maximum elevation away from the structure.

COHESIVE SOILS

In this study, two cohesive soil mixtures were used. The first is a naturally occurring homogeneous soil containing 32 percent clay, 30 silt, and 38 percent fine sand particles. Utilizing the X-Ray Diffraction Test, the dominant clay mineral was found to be Montmorillonite. According to the unified soil classification system, the cohesive soil is classified as medium plasticity clay and the texture as clay loam. The second cohesive soil mixture was prepared by blending commercially obtained pure Kaolinite clay with

medium sand. This mixture was composed of 30 percent clay and 70 percent sand. Montmorillonite clay experiments studied the effects of compaction, initial water content, and shear strength for unsaturated and saturated soil conditions. This was achieved by compacting the cohesive material placed around the abutments at various degrees of compaction and by using soils of different initial water content, whereas Kaolinite clay experiments investigated the effects of initial water content on unsaturated clay erosion by preparing mixtures with varying initial water contents. In these experiments compaction was also varied over a narrow range of conditions.

ABUTMENTS

In the experiments, rectangular vertical-wall abutments constructed of clear Plexiglas with protrusion lengths of 0.22 m and 0.11 m were used. Lengths of these abutments in the direction of flow were 0.44 m and 0.22 m, respectively. The scour depth development was measured against time utilizing three measuring tapes attached to the interior wall of each abutment and by the use of a small inclined mirror.

6.3 EXPERIMENTAL RESULTS

Results of abutment scour experiments in cohesive materials are presented in tables 29 through 32. These tables present the flow conditions and volumetric scour measurements along with cohesive soil properties and measured maximum local scour values. The clay mineral present in the cohesive soil mixtures used in set 1 and set 2 experiments (given in tables 29 and 30) was Montmorillonite. Tables 31 and 32 present results of experiments utilizing Kaolinite clay mixtures. The analysis that is presented in this study is aimed at quantifying cohesive material effects in terms of easily obtainable soil parameters. For this purpose, the parameters selected to represent the scour resistance of cohesive materials were limited to those given in tables 29 through 32. They were: clay content, compaction, initial water content, shear strength, and clay mineral. The effects of clay content on bridge scour are treated in a separate chapter in this report. In the following analysis, effects due to cohesive material properties other than clay content are investigated. In the past, erodibility of cohesive soils was also related to surrounding fluid, disturbed versus undisturbed soils, sodium adsorption ratio, plasticity, etc. Due to the complexities involved in quantifying these effects (a much larger variety of clays), these parameters were excluded from the present analysis.

Table 29. Results of Montmorillonite clay experiments conducted in the 2.44-m wide sedimentation flume using a 0.22-m abutment protrusion length.

RUN ID	Flow Discharge Q (l/s)	Percent Clay Content CC (%)	Initial Water Content IWC (%)	Dry Density γ_{dry} (t/m^3)	Compaction C (%)	Torvane Shear Strength S (kPa)	Flow Depth Y (m)	Approach Velocity V (m/s)	Scour Depth D_{sc} (m)	Scour Volume V_{sc} (l)	Flow Temp. T (^oC)
8-12-MA	144.42	0	4.0	1.758	91.4	3.655	0.311	0.171	0.020	1.812	17.2
8-13-MA	184.06	0	4.0	1.758	91.4	3.655	0.312	0.223	0.058	4.106	17.2
8-14-MA	176.98	0	4.0	1.758	91.4	3.655	0.320	0.207	0.047	3.313	17.2
8-15-MA	198.22	0	4.0	1.758	91.4	3.655	0.309	0.235	0.060	4.191	17.2
8-16-MA	229.37	0	4.0	1.758	91.4	3.655	0.319	0.250	0.069	4.899	17.2
8-17-MA	257.12	0	4.0	1.758	91.4	3.655	0.322	0.287	0.110	9.090	17.2
8-18-MA	295.63	0	4.0	1.758	91.4	3.655	0.326	0.317	0.171	14.102	17.2
8-19-MA	242.39	0	4.0	1.758	91.4	3.655	0.327	0.253	0.087	3.398	17.2
8-20-MA	172.73	10	5.5	1.510	74.2	9.204	0.275	0.171	0.088	5.607	17.2
8-21-MA	147.25	10	5.5	1.510	74.2	9.204	0.282	0.162	0.027	2.039	17.2
8-22-MA	202.47	10	5.5	1.510	74.2	9.204	0.296	0.210	0.049	3.511	17.2
8-23-MA	232.20	10	5.5	1.510	74.2	9.204	0.289	0.229	0.061	4.304	17.2
8-24-MA	263.35	10	5.5	1.510	74.2	9.204	0.307	0.271	0.066	4.587	16.7
8-25-MA	311.49	10	5.5	1.510	74.2	9.204	0.298	0.341	0.142	10.987	16.7
8-26-MA	368.12	10	5.5	1.510	74.2	9.204	0.307	0.424	0.204	25.287	16.7
8-27-MA	311.49	32	29.7	1.483	85.8	9.786	0.245	0.448	0.000	0.000	13.3
8-27-MB	311.49	32	13.1	1.266	73.2	44.037	0.258	0.378	0.110	9.005	13.3
8-28-MA	518.20	32	27.5	1.483	85.8	14.679	0.248	0.704	0.000	0.000	12.2
8-28-MB	518.20	32	38.1	1.363	78.8	2.936	0.242	0.646	0.107	2.492	12.2
8-29-MA	792.87	32	27.5	1.091	63.1	14.679	0.244	0.869	0.000	0.000	12.2
8-29-MB	792.87	32	38.1	1.141	66.0	2.936	0.258	0.674	0.162	8.495	12.2
8-30-MA	368.12	32	16.7	1.271	73.5	46.973	0.252	0.549	0.249	15.489	12.8
8-30-MB	368.12	32	20.8	1.295	74.9	44.037	0.260	0.479	0.122	3.993	12.8
8-31-MA	368.12	32	17.7	1.000	57.9	17.615	0.257	0.451	0.354	54.000	12.2
8-31-MB	368.12	32	13.4	1.110	64.3	10.765	0.273	0.415	0.271	47.997	12.2
8-32-MA	254.85	13	8.7	1.581	80.0	11.743	0.252	0.351	0.140	10.506	13.3
8-32-MB	254.85	5	6.1	1.691	86.5	5.872	0.264	0.314	0.107	9.005	13.3
8-33-MA	311.49	13	6.4	1.352	68.4	11.743	0.253	0.436	0.277	28.005	12.8
8-33-MB	311.49	5	4.0	1.432	73.3	5.872	0.265	0.390	0.195	24.013	12.8
8-34-MA	424.75	13	2.4	1.420	71.9	9.786	0.233	0.646	0.445	95.003	13.3
8-34-MB	424.75	5	3.1	1.501	76.8	7.829	0.238	0.558	0.366	78.013	13.3
8-35-MA	424.75	32	17.1	1.306	75.5	48.930	0.245	0.631	0.198	25.995	13.3
8-35-MB	424.75	32	16.4	1.260	72.9	34.251	0.244	0.594	0.357	44.995	13.3
8-36-MA	501.21	32	34.4	1.380	79.8	2.936	0.246	0.838	0.155	16.509	15.0
8-36-MB	501.21	32	44.6	1.240	71.7	0.979	0.230	0.799	0.238	25.995	15.0
8-37-MA	736.24	32	35.7	1.363	78.8	2.936	0.306	0.911	0.082	2.407	15.0
8-37-MB	736.24	32	45.3	1.329	76.9	0.979	0.292	0.951	0.271	44.004	15.0
8-38-MA	948.61	32	36.8	1.340	77.5	2.936	0.351	0.997	0.091	4.502	15.6
8-38-MB	948.61	32	44.4	1.237	71.6	0.979	0.320	1.039	0.338	95.994	15.6

Note:
Duration of experiments varied between 12 to 16 hours.

Table 30. Results of Montmorillonite clay experiments conducted in the 1.22-m wide flume using a 0.11-m abutment protrusion length.

Run ID	Flow Discharge Q (l/s)	Percent Clay Content CC (%)	Initial Water Content IWC (%)	Dry Density γ_{dry} (t/m^3)	Compaction C (%)	Torvane Shear Strength S (kPa)	Flow Depth Y (m)	Approach Velocity V (m/s)	Scour Depth D_{sc} (m)	Scour Volume V_{sc} (l)	Flow Temp. T (^oC)
4-39	36.81	32	20.2	1.363	78.8	34.251	0.140	0.149	0.025	0.113	13.3
4-40	59.47	32	19.7	1.369	79.2	31.316	0.143	0.271	0.064	1.161	13.3
4-41	48.14	32	19.8	1.300	75.2	34.251	0.146	0.198	0.041	0.510	13.3
4-42	70.79	32	19.6	1.317	76.2	40.123	0.144	0.360	0.109	4.191	13.3
4-43	39.64	32	20.0	1.088	63.0	13.113	0.135	0.165	0.029	0.255	13.3
4-44	55.78	32	19.6	1.139	65.9	13.700	0.140	0.256	0.063	1.104	13.9
4-45	67.96	32	20.2	1.134	65.6	14.092	0.140	0.351	0.137	8.495	13.9
4-46	90.61	32	19.5	1.409	81.5	66.056	0.129	0.503	0.168	9.486	13.9
4-47	49.55	32	12.3	1.214	70.2	37.187	0.131	0.238	0.081	3.398	13.9
4-48	36.81	32	12.3	1.168	67.6	36.209	0.129	0.192	0.049	1.246	13.9
4-49	55.22	32	11.1	1.139	65.9	27.401	0.132	0.311	0.145	9.713	13.9
4-50	66.54	32	10.8	1.141	66.0	23.487	0.135	0.372	0.193	17.500	13.9
4-51	45.31	5	6.2	1.472	75.3	5.480	0.130	0.223	0.031	0.425	13.9
4-52	70.79	5	6.2	1.472	75.3	5.480	0.131	0.378	0.130	11.497	13.9
4-53	53.80	5	6.2	1.472	75.3	5.480	0.130	0.305	0.071	1.897	13.9
4-54	35.40	5	6.2	1.472	75.3	5.480	0.126	0.168	0.030	0.113	13.9
4-55	87.78	5	6.2	1.472	75.3	5.480	0.130	0.506	0.209	25.513	13.9
4-56	38.23	13	11.2	1.478	74.8	27.401	0.132	0.198	0.030	0.113	13.3
4-57	48.14	13	11.2	1.478	74.8	27.401	0.129	0.226	0.055	0.850	13.3
4-58	56.63	13	11.2	1.478	74.8	27.401	0.135	0.308	0.096	3.200	13.9
4-59	65.13	13	11.2	1.478	74.8	27.401	0.130	0.357	0.130	5.493	13.3
4-60	82.12	13	11.2	1.478	74.8	27.401	0.129	0.491	0.137	7.108	12.8
4-61	80.70	32	35.6	1.371	79.3	4.698	0.129	0.482	0.081	0.595	13.3
4-62	101.94	32	30.4	1.413	81.7	4.893	0.131	0.616	0.066	1.897	13.3
4-63	120.35	32	29.0	1.420	82.1	5.480	0.134	0.683	0.034	2.209	13.3
4-64	106.19	32	35.3	1.380	79.8	3.327	0.134	0.637	0.085	3.511	13.3
4-65	121.76	32	34.8	1.415	81.9	4.306	0.133	0.686	0.107	3.908	14.4
4-66	52.39	32	43.3	1.323	76.5	1.566	0.129	0.287	0.074	1.388	14.4
4-67	65.13	32	40.3	1.363	78.8	1.175	0.130	0.384	0.093	2.209	14.4
4-68	82.12	32	44.5	1.323	76.5	1.370	0.128	0.482	0.119	5.409	13.9
4-69	48.14	32	45.8	1.351	78.1	1.370	0.131	0.250	0.044	0.311	13.3
4-70	104.77	32	45.8	1.351	78.1	1.370	0.141	0.619	0.172	5.805	13.9

Note:
Duration of experiments varied between 12 to 16 hours.

Table 31. Results of Montmorillonite clay experiments conducted in the 2.44-m wide flume using a 0.1-m abutment protrusion length.

RUN ID	Flow Discharge Q (l/s)	Percent Clay Content CC (%)	Initial Water Content IWC (%)	Dry Density γ_{dry} (t/m^3)	Compaction C (%)	Torvane Shear Strength S (kPa)	Flow Depth Y (m)	Approach Velocity U (m/s)	Scour Depth D_{sc} (m)	Scour Volume V_{sc} (l)	Flow Temp. T (^oC)
8-80-MA	356.79	32	46.7	1.226	70.9	0.979	0.177	0.664	0.113	4.899	20.0
8-81-MA	240.69	0	4.0	1.758	91.4	3.655	0.155	0.503	0.253	21.011	18.3
8-81-MB	240.69	5	6.9	1.363	69.7	1.957	0.148	0.433	0.210	5.097	18.3
8-81-MC	240.69	10	11.4	1.463	71.9	7.829	0.155	0.384	0.131	0.963	18.3
8-81-MD	240.69	13	11.0	1.254	63.5	7.829	0.146	0.366	0.140	1.161	18.3
8-82-MA	172.73	0	4.0	1.758	91.4	3.655	0.152	0.360	0.158	16.990	18.9
8-82-MB	172.73	5	4.3	1.389	71.1	1.957	0.148	0.308	0.104	3.596	18.9
8-82-MC	172.73	10	10.1	1.449	71.2	7.829	0.158	0.277	0.073	1.104	18.9
8-82-MD	172.73	13	5.6	1.329	67.3	7.829	0.155	0.250	0.067	1.246	18.9
8-83-MA	133.09	0	4.0	1.758	91.4	3.655	0.143	0.280	0.113	6.513	19.4
8-83-MB	133.09	5	4.2	1.300	66.5	1.957	0.145	0.229	0.094	1.897	19.4
8-83-MC	133.09	10	8.5	1.320	64.9	7.829	0.148	0.204	0.067	0.850	19.4
8-83-MD	133.09	13	9.9	1.335	67.6	7.829	0.146	0.177	0.052	0.453	19.4
8-84-MA	300.16	0	4.0	1.758	91.4	3.655	0.155	0.680	0.274	63.996	20.0
8-84-MB	300.16	5	6.2	1.289	66.0	1.957	0.151	0.591	0.262	32.989	20.0
8-84-MC	300.16	10	11.3	1.193	58.7	7.829	0.151	0.533	0.152	16.990	20.0
8-84-MD	300.16	13	9.8	1.286	65.1	7.829	0.149	0.454	0.165	19.001	20.0

Note:
Duration of experiments varied between 12 to 16 hours.

Table 32. Results of Kaolinite clay experiments in the 2.44-m wide flume, with 0.22-m abutment width.

Run ID	Flow Discharge Q (l/s)	Percent Clay Content CC (%)	Initial Water Content IWC (%)	Dry Density (ρ_{dry}) (t/m^3)	Compaction C (%)	Torvane Shear Strength S (kPa)	Flow Depth Y (m)	Approach Velocity V (m/s)	Scour Depth D_{sc} (m)	Scour Volume V_{sc} (l)	Flow Temp. T (^oC)
8-71-MA	157.16	30	14.8	1.661	84.1	30.337	0.177	0.308	0.015	0.453	19.4
8-71-MB	157.16	30	13.4	1.672	84.7	41.101	0.173	0.262	0.000	0.000	19.4
8-71-MC	157.16	30	13.3	1.684	85.3	42.080	0.168	0.238	0.055	1.303	19.4
8-72-MA	421.92	30	15.4	1.707	86.4	23.487	0.191	0.811	0.030	0.793	19.4
8-72-MB	421.92	30	14.7	1.758	89.0	41.101	0.183	0.820	0.037	0.963	19.4
8-72-MC	421.92	30	15.4	1.707	86.4	16.636	0.175	0.960	0.070	1.897	19.4
8-73-MA	286.00	30	20.1	1.741	88.2	7.829	0.159	0.637	0.021	0.651	18.9
8-73-MB	286.00	30	26.5	1.621	82.1	3.914	0.157	0.527	0.040	1.048	18.9
8-73-MC	286.00	30	29.7	1.523	77.1	1.957	0.165	0.457	0.037	0.991	18.9
8-74-MA	351.13	30	18.8	1.732	87.7	10.765	0.165	0.719	0.030	0.850	20.0
8-74-MB	351.13	30	23.4	1.641	83.1	4.893	0.155	0.686	0.046	1.189	20.0
8-74-MC	351.13	30	27.5	1.541	78.0	2.936	0.139	0.777	0.058	1.388	20.0
8-75-MA	237.86	30	21.8	1.695	85.8	4.893	0.158	0.512	0.000	0.000	20.0
8-75-MB	237.86	30	25.1	1.641	83.1	1.957	0.161	0.460	0.000	0.000	20.0
8-75-MC	237.86	30	29.7	1.532	77.6	0.979	0.170	0.439	0.000	0.000	20.0
8-76-MA	489.88	30	21.8	1.695	85.8	4.893	0.193	0.817	0.037	0.963	20.0
8-76-MB	489.88	30	25.1	1.641	83.1	1.957	0.177	0.808	0.067	1.812	20.0
8-76-MC	489.88	30	29.7	1.532	77.5	0.979	0.167	1.201	0.158	9.486	20.0
8-77-MA	170.75	10	15.5	1.695	85.8	2.936	0.152	0.030	0.146	8.014	19.4
8-77-MB	170.75	20	17.1	1.741	84.5	3.914	0.158	0.223	0.012	0.396	19.4
8-77-MC	170.75	50	16.6	1.552	85.2	45.016	0.173	0.195	0.094	3.511	19.4
8-77-MD	170.75	50	27.1	1.478	81.1	2.936	0.174	0.171	0.000	0.000	19.4
8-78-MA	235.03	10	13.5	1.692	85.6	2.936	0.155	0.512	0.229	13.989	19.4
8-78-MB	235.03	20	14.7	1.518	73.6	3.914	0.155	0.460	0.046	0.481	19.4
8-78-MC	235.03	50	15.7	1.335	73.3	45.016	0.168	0.439	0.192	6.513	19.4
8-78-MD	235.03	50	25.8	1.586	87.0	2.936	0.171	0.372	0.000	0.000	19.4
8-79-MA	288.83	10	16.2	1.841	93.2	2.936	0.162	0.582	0.256	21.011	20.0
8-79-MB	288.83	20	16.8	1.775	86.1	3.914	0.161	0.479	0.052	1.359	20.0
8-79-MC	288.83	50	15.7	1.335	73.3	45.016	0.174	0.424	0.177	12.006	20.0
8-79-MD	288.83	50	30.9	1.455	79.9	2.936	0.174	0.357	0.000	0.000	20.0
8-80-MB	356.79	20	16.8	1.775	86.1	3.914	0.170	0.607	0.152	10.987	20.0
8-80-MC	356.79	50	15.7	1.335	73.3	45.016	0.176	0.539	0.226	18.010	20.0
8-80-MD	356.79	50	30.9	1.455	79.9	2.936	0.168	0.472	0.000	0.000	20.0

Note:
Duration of experiments varied between 12 to 16 hours.

6.4 ANALYSIS

The functional relationship between the maximum depth of abutment scour and the parameters defining the soil, fluid, and the geometry of the abutment is derived through dimensional analysis. The depth of abutment scour in cohesive material (D_{sc}) is expressed as a function of the following independent variables:

$$D_{sc} = f(D_s, Y, a, L, V, IWC, C, CC, S, Mn, T, t, g, \alpha, \phi, \rho, \upsilon) \quad (36)$$

in which D_s = depth of abutment scour in noncohesive material for conditions corresponding to D_{sc}; Y = depth of approach flow; a = abutment protrusion length; L = length of abutment in the direction of flow; V = velocity of approach flow; IWC = initial water content; C = compaction related to the optimum compaction; CC = clay content; S = Torvane shear stress, Mn = type of clay (e.g., Kaolinite, Illite, Montmorillonite); T = water temperature; t = duration of experiment; g = gravitational acceleration, α = angle of attack; ϕ = abutment shape factor; ρ = fluid density; and υ = kinematic viscosity of fluid.

Applying the dimensional analysis using D_s, V, and ρ as repeating variables, and using appropriate simplifications, the following set of dimensionless parameters can be obtained:

$$\frac{D_{sc}}{D_s} = f\left(IWC, \frac{S}{\rho V^2}, C, Mn\right) \quad (37)$$

In the derivation of equation 37, the CC was eliminated as a variable since, as shown in Chapter 4, the effects of this parameter was found to be an independent factor up to 12 percent clay content. In the cohesive abutment scour experiments, the clay content was kept above 30 percent. In abutment scour experiments the variation of scour with time was measured. This relationship was shown by Molinas and Reiad to be an asymptotic function with a sharp initial scour development followed by a gradual increase[5]. The initial rate of scour hole development is generally controlled by the nature of the clay mineral and other cohesive material parameters such as compaction, initial water content, etc. Experimental and theoretical studies have shown that the velocity at the nose region of a vertical wall abutment is amplified by a factor of 1.2 to 1.8 times the approach V. According to Molinas, Khereldin, and Wu, bottom shear stresses that are related to V^2 are also amplified (by up to 11 times) and cause local scour in the affected zone[26]. If approach velocities are increased beyond a threshold value defined as critical velocity, the entire approach channel bottom becomes subject to general scour in addition to the local scour. Under these conditions, the scour hole development process continues until equilibrium slopes are attained for the entire reach and may last indefinitely. The experimental study presented in this report limited itself to conditions in which the oncoming flows do not scour the approach reach (clear water conditions). Under these conditions, as soon as the scour hole reaches a depth where the shear stress within the base becomes equal to the critical shear stress of the cohesive material, local scouring ceases. The duration of experiments in the study were long enough to maintain the equilibrium condition for at least 4 hours. The final scour depth values obtained under

these conditions are independent of time, and therefore in deriving equation 37 the time parameter, *t*, is eliminated. Additionally, the dimensionless *S* can be related to *C* and *IWC*, further reducing the number of parameters.

The local abutment scour analysis in this study was conducted separately for the two clay types. This distinction is made since the type of clay mineral (*Mn*) was found to have a dominant effect on the scourability of bed material.

MONTMORILLONITE SCOUR

The measured values of (D_{sc} /D_s) were regressed against the remaining dimensionless groups in equation 37 using nonlinear multiple regression analysis. The best-fit regression equations resulting from the statistical analysis of experimental data were reported earlier by Molinas, Reiad, and Jones[27] and are given below.

For **unsaturated** clays with initial water content less than 25 percent:

$$\frac{D_{sc}}{D_s} = (2.186 - 0.05342\ IWC)\ (15.407 - 0.522C + 0.006087C^2 - 0.0000235\ C^3) \qquad (38)$$

where the *IWC* and *C* are in percent.

For **saturated** clays with initial water content in the range of 28 to 45 percent:

$$\frac{D_{sc}}{D_s} = (4.76 - 0.451\ IWC + 0.01361\ IWC^2 - 0.000126\ IWC^3)\ (0.339 + 0.01744\ C) \qquad (39)$$

In deriving equations 38 and 39, *IWC* ranged from 12 to 45 percent, and *C* ranged from 58 to 89 percent. Equations 38 and 39 were developed based on laboratory tests in which Froude numbers ranged from 0.1 to 0.6 and soil shear strength values ranged from 0.1 to 0.63 kg/cm^2. The plot of equations 38 and 39 with observed data is presented in figure 36.

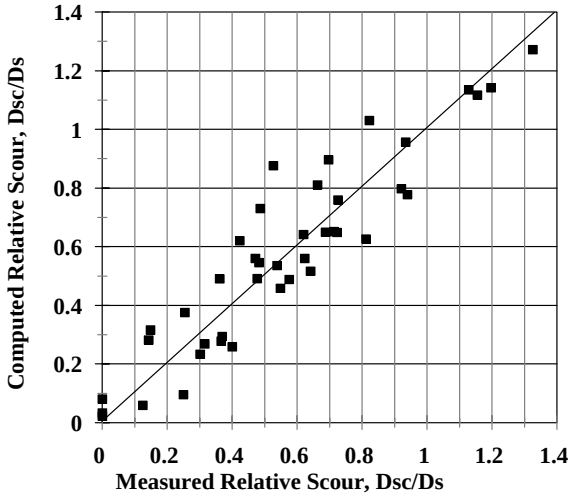

Figure 36. Computed and measured relative abutment scour for Montmorillonite clay.

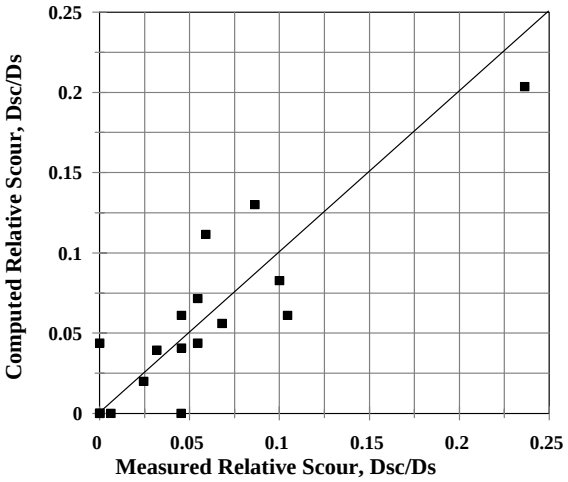

Figure 37. Computed and measured relative abutment scour for Kaolinite clay.

KAOLINITE SCOUR

For unsaturated Kaolinite clay soils, the basic form of equation 37 was retained. For the cohesive soil consisting of 30 percent Kaolinite clay and 70 percent medium sand with a median diameter of 0.81 mm, the best-fit regression equation from the statistical analysis of experimental data is:

$$\frac{D_{sc}}{D_s} = (0.12 + 0.014\ IWC - 0.00205\ IWC^2 - 0.000057\ IWC^3)\ (0.4 + 0.017\ C) \qquad (40)$$

Scour initiating velocities for the Kaolinite clay mixture were experimentally determined to be 0.6 m/s. For velocities smaller than this value, the scour ratio is zero. The plot of equation 40 with observed data is presented in figure 37.

6.5 CONCLUSIONS

Abutment scour in cohesive soils shows a wide range of variability depending on the properties of soils. In the experiments, under the same geometric and flow conditions, measured scour in cohesive materials varied anywhere from 7 percent to 140 percent of that measured in medium sand. This is due to initial water content, soil shear strength, degree of compaction, and type of clay mineral present in the soil. For Montmorillonitic soils, the relative scour depth is expressed in terms of initial water content and degree of compaction. For unsaturated Montmorillonitic mixtures, abutment scour depth decreases as the compaction and initial water content increases. For saturated cohesive soils, however, the scour depth is mainly a function of initial water content and is inversely proportional to initial water content. For unsaturated Kaolinitic mixtures the initiation of scour takes place under higher flow intensities, and under same flow conditions, the total scour may be up to 80 percent smaller than the corresponding scour encountered in noncohesive material.

REFERENCES

1. Molinas, A., and Abdou, M. I. (1998). *Effects of Gradation and Cohesion on Bridge Scour, Vol. 1, Effect of Sediment Gradation and Coarse Material Fraction on Clear Water Scour Around Bridge Piers*, Federal Highway Administration, FHWA-RD-99-183.

2. Molinas, A., and Noshi, M. H. (1998). *Effects of Gradation and Cohesion on Bridge Scour, Vol. 2, Experimental Study of Sediment Gradation and Flow Hydrograph Effects on Clear Water Scour Around Circular Piers*, Federal Highway Administration, FHWA-RD-99-184.

3. Molinas, A., and Abdeldayem. A. W. (1998). *Effects of Gradation and Cohesion on Bridge Scour*, *Vol. 3, Abutment Scour for Nonuniform Mixtures*, Federal Highway Administration, FHWA-RD-99-185.

4. Molinas, A., and Hosny, M. (1998). *Effects of Gradation and Cohesion on Bridge Scour, Vol. 4, Experimental Study of Scour Around Circular Piers in Cohesive Soils*, Federal Highway Administration, FHWA-RD-99-186.

5. Molinas, A., and Reiad, N. Y. (1998). *Effects of Gradation and Cohesion on Bridge Scour, Vol. 5, Effect of Cohesion on Bridge Scour*, Federal Highway Administration, FHWA-RD-99-187.

6. Molinas, A., and Noshi, M. H. (1998). *Effects of Gradation and Cohesion on Bridge Scour, Vol. 6, Abutment Scour in Uniform and Stratified Sand Mixtures*, Federal Highway Administration, FHWA-RD-99-188.

7. Abdou, M. I. (1994). *Effect of Sediment Gradation and Coarse Material Fraction on Clear Water Scour Around Bridge Piers*, Ph.D. Dissertation, Department of Civil Engineering, Colorado State University, Fort Collins, CO, 205 pp.

8. Gessler, J. (1967). *The Beginning of Bed Load Movement of Mixtures Investigated as Natural Armoring in Channels*, Translated by E. A. Prych, Translation T-5, W. M. Keck Laboratory of Hydraulics and Water Research, California Institute of Technology, Pasadena, CA.

9. Little, W. C., and Mayer, P. G. (1972). *The Role of Sediment Gradation on Channel Armoring*, Georgia Institute of Technology, Environmental Research Center, Report ERC-0672.

10. Davies, B. E. (1971). *The Armoring of Alluvial Channel Beds*, Unpublished M.Sc. Thesis, University of Canterbury, Christchurch.

11. Proffitt, G. T. (1980). *Selective Transport and Armoring of Nonuniform Alluvial Sediments*, Ph.D. Dissertation, Civil Engineering Department, University of Canterbury, Christchurch, New Zealand.

12. Day, T. J. (1976). *Preliminary Results of Flume Studies into the Armoring of a Coarse Sediment Mixture*, Report of Activities, Part C, Geological Survey, Canada, Paper 76-1C, pp 277-287.

13. Richardson, E. V. and Davis, S. (1995). *Evaluating Scour at Bridges*, Hydraulic Engineering Circular No. 18, Federal Highway Administration, FHWA-IP-90-017, 3rd Edition, 129 pp.

14. Einstein, H. A., and Chien, N. (1953). *Transport of Sediment Mixtures with Large Ranges of Grain Sizes*, MRD Sediment Series No. 2, U.S. Army Engineer Division, Missouri River, U.S. Army Corps of Engineers, Omaha, NE.

15. Ackers, P., and White, W. R. (1973). *Sediment Transport: New Approach and Analysis*, Journal of Hydraulic Engineering Division, American Society of Civil Engineers, Vol. 99, HY11, pp. 2041-2060.

16. Chabert, J., and Engeldinger, P. (1956). *Étude des Affouillements Autour des Piles de Ponts, (Study of Scour Around Bridge Piers),* Laboratoire National D'Hydraulique, 6 Quai Watier, Chatou, Oct. 1956.

17. Shen, H. W., Schneider, V. R., and Karaki, S. S. (1966). *Mechanics of Local Scour, Data Supplement*, Prepared for Bureau of Public Roads, Office of Research and Development, Civil Engineering Department, Colorado State University, Fort Collins, CO, Report CER66-67HWS27.

18. Shen, H. W., Schneider, V. R., and Karaki, S. S. (1969). *Local Scour Around Bridge Piers*, Journal of Hydraulic Engineering Division, American Society of Civil Engineers, Vol. 95, HY6, pp 1919-1940.

19. Neill, C. R. (1968). *Note on Initial Movement of Coarse Uniform Bed Material*, Journal of Hydraulic Research, International Association of Hydraulic Engineering and Research, Vol. 17, No. 2, pp. 247-249.

20. Abdeldayem, A. W. (1996). *Abutment Scour for Nonuniform Mixtures*, Ph.D. Dissertation, Department of Civil Engineering, Colorado State University, Fort Collins, CO, 310 pp.

21. Hosny, M. (1995). *Experimental Study of Scour Around Circular Piers in Cohesive Soils*, Ph.D. Dissertation, Civil Engineering Department, Colorado State University, Fort Collins, CO, 177 pp.

22. Yakoub, N. G. Reiad. (1995). *Effect of Cohesion on Bridge Abutment Scour*, Ph.D. Dissertation, Civil Engineering Department, Colorado State University, Fort Collins, CO, 231 pp.

23. Molinas, A. and Abdeldayem, A. (1998). *Effect of Clay Content on Bridge Scour*, Proceedings of the 1998 International Water Resources Engineering Conference, American Society of Civil Engineers, Vol. 1, pp 280-285.

24. Molinas, A., Hosny, M., and Jones, S. (1998). *Pier Scour in Montmorillonite Clay Soils*, Proceedings of the 1998 International Water Resources Engineering Conference, American Society of Civil Engineers, Vol. 1, pp 292-297.

25. Molinas, A., Jones, S. and Hosny, M. (1999). *Effects of Cohesive Material Properties on Local Scour Around Piers,* Journal of the Transportation Research Board, Transportation Research Record, No. 1690, National Academy Press, pp. 164-175.

26. Molinas, A., Kheireldin, K., and Wu, B. (1998). *Shear Stress Around Vertical Wall Abutments*, Journal of Hydraulic Engineering, American Society of Civil Engineers, Vol. 124, No. 8, pp 822-830.

27. Molinas, A., Reiad, N. G. Y., and Jones, S. (1998). *Effect of Cohesion on Abutment Scour*, Proceedings of the 1998 International Water Resources Engineering Conference, American Society of Civil Engineers, Vol. 1, pp 252-257.